

CALIFORNIA
INSTITUTE OF
TECHNOLOGY

DOE CONTRACT DE-FC36-04GO14276
Dr. William A. Goddard III
Principal Investigator
CALTECH

Using Ionic Liquids in Selective Hydrocarbon
Conversion Processes

- **Covering the Period** July, 2004 – June, 2009
- **Date of Report** – September 28th, 2009
- **Award Number** – DE-FC36-04GO14276
- **Project Title** – Using Ionic Liquids in Selective Hydrocarbon Conversion Processes
- **Project Period** – from 07/01/2004 through 06/30/2009
- **Recipient Organization** – California Institute of Technology
- **Partners**
 1. Power, Energy, and Environmental Research Center (PEER)
California Institute of Technology
 2. Material and Process Simulation Center (MSC)
California Institute of Technology
 3. Loker Hydrocarbon Institute, University of Southern California
 4. ChevronTexaco Corp (15% cost-sharing)
 5. Sachem Inc (15% cost sharing)
- **Team Members**

PI:	William A. Goddard III
Co-PI's:	Yongchun Tang, Roy Periana
Staff Members:	Weiqun Chen, Adri van Duin, Robert Nielsen, Patrick Shuler, Qisheng Ma, Mario Blanco, Zaiwei Li, Jonas Oxgaard,
Postdoctoral Scholars:	Jihong Cheng,
Graduate Students:	Sam Cheung, Sanja Pudar
Senior Technician:	Mark Haught

CONTACT INFORMATION

- **Technical Contact:**

- **Yongchun Tang**

- Mailing Address: 738 Arrow Grand Circle, Covina, CA 91722
(626) 858 5077 (Tel.) (626) 858-9250 (Fax.), tang@peer.caltech.edu

- **William A. Goddard III**

- Mailing Address: 321 Beckman Institute, Mail Code: Chemistry 139-74, California Institute of Technology, Pasadena, CA 91125
(626) 395-2731 (Tel.) (626) 585-0918 (Fax.), wag@wag.caltech.edu

- **Business Contact: Richard P. Seligman**

- Mailing Address: 1200 E. California Blvd. Mail Code: 201-15, California Institute of Technology, Pasadena, CA 91125
(626) 395-6357 (Tel.) (626) 395-4571 (Fax), Richard.seligman@caltech.edu

- **DOE Project Officer: Bill Prymak**

- Mailing Address: Golden Field Office, 1617 Cole Blvd., Golden, CO 80401
(303) 275-4931 (Tel.) (303) 275-4753 (Fax), bill.prymak@go.doe.gov

- **DOE Project Monitor:**

- **DOE HQ contactor:**

- **DOE Contract Specialist: Beth H. Dwyer**

- Mailing Address: Golden Field Office, 1617 Cole Blvd. Golden, CO 80401
(303) 275-4719 (Tel.) (303) 275-4788 (Fax.), beth.dwyer@go.doe.gov

Disclaimer

This report was prepared as an account of work sponsored by an agency of the United States Government. Neither the United States Government nor any agency thereof, nor any of their employees, makes any warranty, express or implied, or assumes any legal liability or responsibility for the accuracy, completeness, or usefulness of any information, apparatus, product, or process disclosed, or represents that its use would not infringe privately owned rights. Reference herein to any specific commercial product, process, or service by trade name, trademark, manufacturer, or otherwise does not necessarily constitute or imply its endorsement, recommendation, or favoring by the United States Government or any agency thereof. The views and opinions of authors expressed herein do not necessarily state or reflect those of the United States Government or any agency thereof.

ABSTRACT

This is the Final Report of the five-year project “Using Ionic Liquids in Selective Hydrocarbon Conversion Processes” (DE-FC36-04GO14276, July 1, 2004-June 30, 2009), in which we present our major accomplishments with detailed descriptions of our experimental and theoretical efforts.

Upon the successful conduction of this project, we have followed our proposed breakdown work structure completing most of the technical tasks. Finally, we have developed and demonstrated several optimized homogenously catalytic methane conversion systems involving applications of novel ionic liquids, which present much more superior performance than the Catalytica system (the best-to-date system) in terms of three times higher reaction rates and longer catalysts lifetime and much stronger resistance to water deactivation. We have developed in-depth mechanistic understandings on the complicated chemistry involved in homogenously catalytic methane oxidation as well as developed the unique yet effective experimental protocols (reactors, analytical tools and screening methodologies) for achieving a highly efficient yet economically feasible and environmentally friendly catalytic methane conversion system.

The most important findings have been published, patented as well as reported to DOE in this Final Report and our 20 Quarterly Reports.

TABLE OF CONTENTS

ABSTRACT.....	3
CHAPTER ONE: PROJECT INTRODUCTION.....	14
1.1 EXECUTIVE SUMMARY	14
1.2 BACKGROUND INFORMATION	14
1.3 TASKS AND SCHEDULES	15
1.4 ACOMPLISHMENTS LIST	17
CHAPTER TWO: REACTORS AND ANALYTICAL TOOLS.....	19
2.1 SUMMARY	19
2.2 LOW PRESSURE REACTORS.....	19
2.3 HIGH PROESSURE REACTORS.....	24
2.4 CHARACTERIZATIONS AND QUANTIFICATIONS.....	27
CHAPTER THREE: IONIC LIQUIDS FOR HYDROCARBON CONVERSION.....	32
3.1 SUMMARY	32
3.2 MOLECULAR MODELING OF IONIC LIQUID DATABASE	32
3.3 PEER SYNTHESIZED IONIC LIQUIDS.....	34
3.4 IONIC LIQUIDS SCREENING	36
3.4.1 Solubility and Stability Tests.....	36
3.4.2 Compatibility Tests.....	42
3.5 STABLE IONIC LIQUIDS FOR CATALYTIC METHANE CONVERSION.....	45
CHAPTER FOUR: Pt-CATALYST/IL/H ₂ SO ₄ SYSTEMS	48
4.1 SUMMARY	48
4.2 C-H ACTIVATION	48
4.3 METHANE OXIDATION TO METHANOL.....	50

4.4 ROLES OF IONIC LIQUIDS IN METHANE ACTIVATION & OXIDATION..	54
CHAPTER FIVE: CATALYTIC SYSTEMS FOR METHANE CONVERSION.....	57
5.1 SUMMARY	57
5.2 OXIDANTS	58
5.3 SOLVENTS	61
5.3.1 Acetic Acid	62
5.3.2 Triflic Acid.....	65
5.3.3 Melting Salts (eg. NH_4HSO_4)	67
5.4 TRANSITION METAL CATALYSTS.....	67
CHAPTER SIX: HIGH-TEMPERATURE SHILOV-LIKE SYSTEM	74
6.1 SUMMARY	74
6.2 C-H ACTIVATION IN THE SHILOV SYSTEM.....	75
6.3 KINETICS STUDY ON THE H/D EXCHANGE REACTION IN HIGH-TEMPERATURE SHILOV SYSTEM [K_2PTCL (5 MM) + CD_3COOD (30%) + DCL (9M WITH D_2O) + CH_4]	79
6.4 STABILITIES OF VARIOUS PARTIAL OXIDATION PRODUCTS OF METHANE	83
6.5 OPTIMIZATION OF THE HT-SHILOV-LIKE SYSTEM	87
CHAPTER SEVEN: REAXFF METHOD AND VRP METHOD	92
7.1 A BRIEF SUMMARY ON CALIBRATING THE REAXFF METHOD WITH DFT CALCULATIONS	92
7.2 THE REAXFF POTENTIAL FOR IONIC LIQUIDS AND QM STUDIES OF CATALYST STABILITY	95
7.2.1 Development of a ReaxFF potential for imidazolium/anion ionic liquids	95
7.2.2 Development of a ReaxFF potential for Pt-complexes.....	95
7.2.3 Molecular modeling and calibration of the ReaxFF method on methane activation in ionic liquids.....	96
7.2.4 ReaxFF simulation for the Pt complexes in H_2SO_4 with ionic liquids	102

7.3 A VIRTUAL RAPID PROTOTYPING (VRP) METHOD FOR FAST-SCREENINGS OF APPROPRIATE IONIC LIQUIDS.....	105
CHAPTER EIGHT: MECHANISTIC INVESTIGATION	110
8.1 TYPICAL QUANTUM MECHANICAL METHODS UTILIZED	110
8.2 REACTION MECHANISM OF C-H ACTIVATION CATALYZED BY PtCl_4^{2-} IN IONIC LIQUID SOLUTIONS	110
8.3 MECHANISTIC UNDERSTANDING ON SHILOV CHEMISTRY	112
8.4 EFFECTIVE OXIDATION STATE OF PT-CATALYST IN HOT CONCENTRATED SULFURIC ACID FOR CATALYTIC METHANE CONVERSION.....	122
8.5 THE OXIDATION STEP OF SHILOV CHEMISTRY WITH HIGHLY-CONCENTRATED $[\text{Cl}^-]$	129
CHAPTER NINE: PROPOSED FUTURE WORK	133

LIST OF TABLES

Table 1.1: Task To be Performed (Original Schedule for the Four-Year Duration)	16
Table 1.2: Task To be Performed (Revised Schedule for the Last Two Quarters of Year Four and the Extended One-Year)	16
Table 1.3: Status of updated task performance (with the expanded tasks 6.1 and 6.2 for the extended project period).....	16
Table 2.1: Compatibility between ionic liquids and concentrated sulfuric acid at room temperature and at elevated temperatures.....	20
Table 2.2: Compatibility of Pt-based catalysts in concentrated sulfuric acid at room temperature and at elevated temperatures.....	21
Table 2.3: Compatibility of Pt-based catalysts in ionic liquids, primarily dependent on the type of anion.	21
Table 2.4: Stability of ternary systems of H ₂ SO ₄ /Catalyst/Ionic Liquid at 200 °C.	22
Table 2.5: Oxidation rate study of H ₂ SO ₄ /Catalyst/[bmim][Cl] ternary system at 200 °C. [bmim] was used as a model compound for oxidation. Rates were determined based on ¹ H NMR in D ₂ SO ₄ using acetic acid as the internal standard.	22
Table 2.6: Summary of high-pressure reactor designs and applications.	24
Table 3.1: Molecular Calculations of Selected Monosubstituted Imidazolium Derivatives	34
Table 3.2: Index of ionic liquids synthesized at PEER.....	34
Table 3.3: Compatibility between ionic liquids and concentrated sulfuric acid at room temperature and at elevated temperatures.....	37
Table 3.4: Compatibility of Pt-based catalysts in concentrated sulfuric acid at room temperature and at elevated temperatures.....	41
Table 3.5: Compatibility of Pt-based catalysts in ionic liquids, primarily dependent on the type of anion.	41
Table 3.6: Stability of ternary systems of H ₂ SO ₄ /Catalyst/Ionic Liquid at 200 °C.	42
Table 3.7: Compatibility studies of ionic liquids in ternary systems. Three steps are developed (1) stability in Periana's system (H ₂ SO ₄ + [bpym]PtCl ₂) at 200 °C; (2) solubility of PtCl ₂ in ionic liquids upon heating; (3) compatibility of PtCl ₂ +ILs in sulfuric acid upon heating.....	43
Table 3.8: Compatibility of Pt-based catalysts (both Pt(II) and Pt(IV) species) in ionic liquids.....	44
Table 3.9: Summary of studied ionic liquids (ILs) in the application of catalytic conversion of methane to methanol.....	45
Table 4.1: Methane C-H activation in Pt/IL/ D ₂ SO ₄ ternary systems monitored by H/D exchange at 150 °C for 2 hr in the 10 mL short reactor (Entries 1-13) and in the mini gold tube reactor (Entries 14-21)	48

Table 4.2: Catalytic oxidation of methane to methanol in 96% H ₂ SO ₄ ^a	52
Table 4.3: Effects of water concentration in difference catalyst systems on methane C-H activation and oxidation to methanol	53
Table 5.1: Summary of candidates for each component of the catalytic system for direct methane conversion tested with the systems with optimized performance shaded in yellow	57
Table 5.2: Compatibility tests for new oxidants potentially used for partial oxidation of methane to methanol	59
Table 5.3: Compatibility studies of Pt/ILs/AcOH systems. The concentration of Pt species was 12.5 mM. AcOH was added as 1 mL	62
Table 5.4: C-H bond activation of the butyl group in [bmim] ionic liquid via H/D exchange in Pt/IL/AcOH-d ₄ systems at 250 °C	65
Table 5.5: Solubility tests on several potential transition metal catalysts with NH ₄ HSO ₄ as dissolution media or solvent	67
Table 5.6: Methane C-H activation catalyzed by selected Re- and Ru-based catalysts, in comparison with Os-based catalysts monitored by H/D exchange in gold tube reactors at 250 °C for 4 h	68
Table 5.7: Preliminary results of methane C-H activation in selected Os-based systems monitored by H/D exchange in gold tube reactors	69
Table 5.8: Effects of ionic liquids on C-H activation of methane catalyzed by Os-04 and Os-05 in sulfuric acid (98 and 85%) at 250 °C for 4 h	71
Table 5.9: H/D exchange at different C-H sites of [bmim]- ionic liquid in Os/[bmim]Cl/D ₂ SO ₄ (98%) quantified by ¹ H NMR with D ₂ SO ₄ (98%) as solvent and CH ₃ COOH as internal standard	72
Table 6.1: H/D Exchange Experiments at 140 °C in Shilov's System	75
Table 6.2; H/D Exchange Experiments at 185 °C in Shilov's System	76
Table 6.3: H/D Exchange Experiments at 185 °C with Varied Cl ⁻ Concentration (K ₂ PtCl ₄ (20mM) + 30% CD ₃ COOD)	77
Table 6.4: H/D Exchange in High-Temperature-Shilov system [K ₂ PtCl (5 mM) + CD ₃ COOD (30%) + DCl (9M with D ₂ O) + CH ₄] at 200 °C for varied reaction time	79
Table 6.5: Definition of reactions occurred in methane H/D exchange experiments for kinetics fitting and the preliminary fitting results	82
Table 6.6: Gold-tube experiments on methanol stability tests under various reaction conditions	84
Table 6.7: Gold-tube experiments on methlychloride stability tests under various reaction conditions	86
Table 6.8: Fast heating gold-tube experiments investigating the effect of reaction temperature and time on product selectivity of high-temperature Shilov-like system.	

(Experimental conditions: K_2PtCl_4 (5mM) + $CuCl_2$ (300 mM) + HCl (8.4 M) + CH_4 (~50 PSi) + Hydraulic Pressure (~ 3400 PSi))	90
Table 7.1: Coordination energies for imidazole- $PtCl_2(NH_3)$ complexes at various position on the imidazole ring. All complexes with Pt were calculated using B3LYP/LACV3P ^{**++} otherwise B3LYP/6311G ^{**++} . Diffuse functions were excluded in solvation-phase calculation	99
Table 7.2: Relative energies of amidazole (mim), Cl^- and H_2O for $PtCl_2$ in imidazole. All complexes with Pt were calculated using B3LYP/LACV3P ^{**++} otherwise B3LYP/6311G ^{**++} . Diffuse functions were excluded in solvation-phase calculation.	100
Table 7.3: Coordination energies for imidazole- $PtCl_2(NH_3)$ complexes at various position on the imidazole ring. All complexes with Pt were calculated using B3LYP/LACV3P ^{**++} otherwise B3LYP/6311G ^{**++} . Diffuse functions were excluded in solvation-phase calculations.	100
Table 7.4: Relative energies of L- $PtCl(IM)$ complexes and ligands. All complexes with Pt were calculated using B3LYP/LACV3P ^{**++} otherwise B3LYP/6311G ^{**++} . Diffuse functions were excluded in solvation-phase calculations.	101
Table 7.5: Relative stabilities of selected Pt(II) complexes in H_2SO_4 solutions.	102
Table 7.6: QM results for selected Pt(II) complexes react with methane.....	103
Table 7.7: QM results for replacing a chloride ligand in complexes 2 and 3 with a water molecule.....	104
Table 7.8: Calculated C-N Bond Rupture Energies of Imidazolium and their Derivatives.	106
Table 7.9: Calculated C-N Bond Rupture Energies of Diazine and their Derivatives. ..	107
Table 8.1: Free energies, relative to $PtCl_4^{2-}$ in $kcal\ mol^{-1}$, for substituted Pt^{II} species... ..	113
Table 8.2: Free energies, relative to $PtCl_4^{2-}$ in $kcal\ mol^{-1}$, for dissociative methane uptake intermediates.	114
Table 8.3: Free energies, relative to $PtCl_4^{2-}$ in $kcal\ mol^{-1}$, for the methane uptake products.....	115
Table 8.4: Free energies, relative to $PtCl_4^{2-}$ in $kcal\ mol^{-1}$, for the deprotonated oxidative addition products.....	117
Table 8.5; Free energies, relative to $PtCl_4^{2-}$ in $kcal\ mol^{-1}$, for the deprotonated oxidative addition products.....	118
Table 8.6: Comparison of the performance of the standard Los Alamos pseudopotentials and valence basis functions with a valence basis augmented with additional p- and f-functions.....	121
Table 8.7: Comparison of two pseudopotentials (by Los Alamos and Ermler, et al.)... ..	121
Table 8.8: Evaluation chlorine thermodynamics with and without d- and f-angular momentum polarization functions	122

LIST OF FIGURES

Figure 2.1: ¹ H NMR spectra of the liquid of H ₂ SO ₄ /[bpym]PtCl ₂ /[bmim][Cl] ternary system after rate tests using the low pressure reactor. (a) room temperature, as reference; (b) 200 °C, 2 hr; and (c) 200 °C, 27 hr.	24
Figure 2.2: ¹ H NMR spectra of the liquid of H ₂ SO ₄ /Pt(IV) Catalyst/CH ₄ ternary system after methane oxidation tests using the high-pressure reactor. (a) PtCl ₄ + IL-003 system; (b) PtO ₂ + IL006 system. Acetic acid was used as the internal standard.....	28
Figure 2.3: Gas chromatograph of methane after partially exchanged with deuterated solvent of (a) the Periana system, (bpym)PtCl ₂ in 98% D ₂ SO ₄ ; and (b) PtCl ₂ + IL-004-d ₅ in 98% D ₂ SO ₄ . Fig. 1(c) is an overlaid chromatograph for mass ions of methane isotopes of system (b).	30
Figure 2.4: GC-MS spectra of the liquid of H ₂ SO ₄ /Catalyst/CH ₄ ternary system after methane oxidation tests using the high-pressure reactor. (a) system #1, using [bpym]PtCl ₂ as the catalyst; and (b) system #2, using PtCl ₂ -IL003 as the catalyst. About 0.2 mL liquid after each reaction run was hydrolyzed in 5 mL H ₂ O solution and then neutralized with NaOH. They differ in the total peak area integrated.....	31
Figure 3.1: 9 Basic classes of cations (a) Monosubstituted imidazolium; (b) Disubstituted Imidazolium; (c) Trisubstituted Imidazolium; (d) Pyridinium; (e) Phosphonium; Ammonium; (f) Pyrrolidinium; (g) Guanidinium; (i) Isouronium	33
Figure 3.2: Typical Anions (a) Monoatom, Cl, Br, I; (b) Borates; (c) Phosphates and Antimonates; (d) Sulfates; (e) Sulfonates; (f) Tosylates; (g) Amides (CN) ₂ N ⁻ ; (h) Imides; (i) Methanes [HC(SO ₂ CF ₃) ₂] ⁻ ; (j) Cobalt-tetracarbonyl Co-(CO) ₄ ⁻ ; (k) Trifluoroacetate CF ₃ COO ⁻	33
Figure 3.3: ¹ H-NMR spectra of [bmim][BF ₄] in D ₂ SO ₄ at 25 °C for (a) 5 hr, (b) 30 hr, and (c) 60 hr, respectively.....	38
Figure 3.4: ¹ H-NMR spectra for [bmim][BF ₄] solution in D ₂ SO ₄ (a) at room temperature, (b) at 100 °C, and (c) 150 °C for 3 hr each.	39
Figure 3.5: ¹ H-NMR spectra for (a) [bmim][BF ₄] solution in D ₂ O resulting from neutralization of D ₂ SO ₄ with NaOD, and (b) [bmim][BF ₄] dissolved in D ₂ O directly.	40
Figure 4.1: ¹ H NMR spectra from the liquid of Carbon-13 methane oxidation test using PtCl ₂ and IL-004.	51
Figure 4.2: Methanol yield as a function of the concentration of H ₂ SO ₄ (reaction conditions: 200 °C, 2.5 hr). The methanol concentration from the Catalytica reaction in 2% oleum was 600 mM and was not indicated in the plot.	54
Figure 5.1: Temperature dependence of the calculated amounts (in mole) of SO ₃ in 100 mg of sulfuric acid solutions with different concentrations.....	58
Figure 5.2: ¹ H NMR spectra of the liquids from methane oxidation tests using 10 wt% PEER-6 type ionic liquids at 200 °C for 2.5 hrs. (a) PtCl ₂ + IL-050 only as a blank; (b) PtCl ₂ + IL-050 + K ₂ SeO ₄ ; and (3)PtCl ₂ + IL-050 + V ₂ O ₅ . Acetic acid was used as the internal standard.....	61

Figure 5.3: Possible sites in an ionic liquid containing [bmim] as the cation for C-H activation that are similar to methane C-H bonds. (a) Schematic structure; and (b) ^1H NMR spectrum.....	64
Figure 5.4: ^1H NMR spectra of the liquids from mini gold tube reactors at 200 °C for 4 hrs. (a) 50 mM (bpym)PtCl ₂ in 1 mL 96% H ₂ SO ₄ ; and (b) 50 mM (bpym)PtCl ₂ in 0.5 mL 96% H ₂ SO ₄ + 0.5 mL CF ₃ SO ₃ H. Acetic acid was used as the internal standard.....	66
Figure 5.5: Ratios of different methane isotopomers to the original methane after H/D exchange experiments in Os-03/D ₂ SO ₄ (98%) at 220 and 250 °C, respectively.	70
Figure 6.1: Comparison of the C-H activation products of the PEER, Shilov and Periana-Catalytica system.	74
Figure 6.2: CD _x H _{4-x} isotopomer distribution of methane H/D exchange experiments in [K ₂ PtCl (5 mM) + CD ₃ COOD (30%) + DCl (9M with D ₂ O) + CH ₄] at 200 °C (a) exchange ratio v.s. time and (b) relative isotopomer distribution.....	80
Figure 6.3: Comparison of the experimental data and the calculated data from empirical fitting for H/D exchange experiments in the HT-Shilov-like system.	83
Figure 6.4: GC-MS chromatogram and spectrum for liquid products of reaction [0.3 mL D ₂ O (with 8.4 M DCl, 5mM K ₂ PtCl ₄ and 300mM FeCl ₃) + 100 μmole CH ₄] in gold tube reactor with ~3700 PSi hydraulic external pressure at ~320 °C for 4 h. (a) Chromatogram, (b) Spectrum of the HCOOD peak, and (c) standard spectrum of HCOOH.....	89
Figure 7.1: ReaxFF and QM (Mulliken) charge distributions for an imidazole cation/HTFS anion dimer.....	93
Figure 7.2: ReaxFF and QM-energies for an imidazole dimer as a function of intermolecular N-H distance.	93
Figure 7.3: Snapshot from a ReaxFF MD/NVT simulation on a trifluorimidazole cation/HTFS anion/trifluorimidazole mixture, showing a concerted hydrogen transfer event. Hydrogens involved in the transfer event are bright green (for clarity), other hydrogens are white. Note that in the simulations ReaxFF uses the same atom type for all hydrogens.....	94
Figure 7.4 Total and vehicular diffusion obtained from ReaxFF MD/NVT (400K) simulations on 8% and 30% trifluorimidazole cation/trifluorimidazole/HTFS anion mixtures.....	94
Figure 7.5: DFT singlet (black) /triplet (red) and ReaxFF (green) energies for Pt-X bond dissociation in PtClX(NH ₃) ₂ -clusters.....	96
Figure 7.6: Imidazole/pyrazine cations, anions, and Pt-complexes obtained from DFT simulations and included in the ReaxFF training set. (White, gray, blue, green and purple balls represent H, C, N, Cl, and Pt atoms respectively.).....	97
Figure 7.7: Various bonding configurations of a PtCl ₂ (NH ₃) complex to a) 1-methylimidazole cation [mim] ⁺ through the b) N1 atom, c) C2 atom, d) N3 atom, e) C4 atom, and the f) C5 atom. Blue, gray and white balls represent N, C and H atoms, respectively.	99

Figure 7.8: Optimized molecular geometry of the stable and ring-opened imidazole and their derivatives for different C-N bond ruptures.	105
Figure 7.9: Optimized molecular geometry of the stable and ring-opened diazine and their derivatives for different C-N bond ruptures.....	106
Figure 7.10: Development and applications of the Virtual Rapid Prototyping (VRP) to identify stable ionic liquids in the presence of the Pt catalyst. that the reaction $[\text{PtCl}_4][\text{HIm}]_2 \rightarrow [\text{PtCl}_3\text{-Im}][\text{HIm}] + \text{HCl}$ is exothermic by -0.1 kcal/mol, while calculations on the ionic liquid $[\text{H-Pyrazolium}][\text{Cl}]$ ($[\text{HPz}][\text{Cl}]$) show that the reaction $[\text{PtCl}_4][\text{HPz}]_2 \rightarrow [\text{PtCl}_3\text{-Pz}][\text{HPz}] + \text{HCl}$ is endothermic by 8.9 or 12.1 kcal/mol.....	108
Figure 8.1: Reaction energy profile of C-H activation catalyzed by PtCl_4^{2-} in acidic condition (relative energies are in kcal/mol)	111
Figure 8.2: Reaction energy profile of C-H activation catalyzed by PtCl_4^{2-} in pyrazolium based ionic liquid solution (relative energies are in kcal/mol)	111
Figure 8.3: Key structures and relative stabilities (kcal/mol) along a possible hydrogen exchange pathway	112
Figure 8.4: Schematics and free energies, relative to PtCl_4^{2-} in kcal mol ⁻¹ , for four methane uptake transition states.	114
Figure 8.5: Reaction schematic for oxidative addition transition state and pyramidal product for the 5 possible cases. Free energies are in kcal mol ⁻¹ , bond distances in Angstroms and angles in degrees.....	116
Figure 8.6: Free energy schematic for lowest energy mechanism to form activated $\text{Pt}^{\text{II}}\text{-CH}_3$. All free energies are in kcal mol ⁻¹	117
Figure 8.7: Free energy diagram, relative to PtCl_4^{2-} in kcal mol ⁻¹ , for methane activation using the lowest energy single acetate species, $\text{PtCl}_3\text{OAc}^{2-}$	119
Figure 8.8: Free energy diagram, relative to PtCl_4^{2-} in kcal mol ⁻¹ , for methane activation using the <i>cis</i> and <i>trans</i> bis-acetate species, $\text{PtCl}_2\text{OAc}_2^{2-}$	120
Figure 8.9: Oxidation of the Pt^{II} complex 1 to the Pt^{IV} complex	124
Figure 8.10: Methane activation by Pt^{IV} and Pt^{II} . Pt^{IV} is found to have an inaccessible reaction barrier in agreement with experimental results, hence oxidation of the catalyst inactivates it towards reaction with methane. Relative G(500) in italics.	125
Figure 8.11: Inner-sphere electron transfer between non-methylated Pt^{IV} and methylated Pt^{II} . Relative G(500) in italics.	128
Figure 8.12: Nucleophilic functionalization of the methylated Pt^{IV} generates the methyl bisulphate product and regenerates the active Pt^{II} catalyst. Relative G(500) in italics... ..	128
Figure 8.13: Free Energies of variously substituted reactant complexes in Shilov system	130
Figure 8.14: Energy barrier for formation of encounter complex $\text{Pt}^{\text{II}}(\text{CH}_3)(\text{Cl})_2(\text{H}_2\text{O}) \cdot \text{Pt}^{\text{IV}}(\text{Cl})_4(\text{H}_2\text{O})_2^{1-}$	130

Figure 8.15: Energy barrier for formation of encounter complex $\text{Pt}^{\text{II}}(\text{CH}_3)(\text{Cl})_2(\text{H}_2\text{O}) \cdot \text{Pt}^{\text{IV}}(\text{Cl})_5(\text{H}_2\text{O})^{2-}$	131
Figure 8.16: Energy barrier for formation of encounter complex $\text{Pt}^{\text{II}}(\text{CH}_3)(\text{Cl})_2(\text{H}_2\text{O}) \cdot \text{Pt}^{\text{IV}}(\text{Cl})_6^{2-}$	131
Figure 9.1: Schematic Diagram of <i>in situ</i> UV-vis spectroscopy to monitor the oxidation state change of Pt^{II} and Pt^{IV}	136

CHAPTER ONE: PROJECT INTRODUCTION

1.1 EXECUTIVE SUMMARY

The final objective of this project is to improve catalytic systems for methane oxidation by using ionic liquids as the reaction media. In particular, the plan is to develop a low-temperature, cost-effective, environmental-friendly catalytic oxidation process for methane conversion to methanol with Pt-based catalysts using selected ionic liquids as reaction media in place of sulfuric acid. Our approach is based on a strongly integrated theoretical/experimental/industrial investigation to develop and optimize a catalyst/oxidant/solvent system that would be ready to work towards commercialization. In Phase I our experimental programs were focused on determining compatibility and performance of various combined systems of catalysts, oxidants, and ionic liquids; and to obtain information to calibrate our computational methods and validate theoretical findings. At the theoretical aspect, we have successfully use molecular modeling techniques to establish a database of various ionic liquids prototypes and to calibrate the developing ReaxFF method. In Phase II, we combined the experimental and theoretical knowledge from phase I to more deeply understand the roles of ILs in C-H activation reaction and to evaluate using ILs as solvent for methane conversion. We successfully developed several Pt/IL/H₂SO₄ systems (PEER system) for methane to methanol conversion, some of which present higher water tolerance, higher reaction rates and longer lifetime compared to the Periana-Catalytica system. Mechanistic studies were conducted as well to provide fundamental understanding on the methane to methanol conversion process in the PEER system. In addition, a Virtual Rapid Prototyping (VRP) method was established for fast-screenings of appropriate ionic liquids. In Phase III, we continued to optimize the selected solvent/catalyst/oxidant catalytic system based on the experimental and theoretical achievements during Phase I and II. We have demonstrated the optimized catalytic system, which potentially can be commercialized for low temperature methane functionalization. Efforts have also been taken into scaling-up reactor design and modification so that we will be able to further advance our work toward larger scale investigations providing necessary data and information for the potential industrial applications. The ultimate goal of this project is to develop an efficient yet economically feasible as well as environmentally friendly technology to utilize the abundant yet mostly untapped natural gas resources of the U.S. and the whole world.

1.2 BACKGROUND INFORMATION

The direct oxidative conversion of methane to an easily transportable liquid such as methanol has been extensively investigated for decades. However, the most current available technologies rely on the initial conversion of methane to syn-gas (CO/H₂) which is carried out at high temperature (> 500 °C) using gas-phase tubes and shell reactors that require expensive and energy-consuming processors. An improvement on this process is our recently developed homogeneously catalytic systems, which can directly convert methane to methanol in an unprecedented, high one-pass yield (40~70% based on the added methane) with a high selectivity (> 90%) at temperature below 220 °C. However, this promising direct methane to methanol conversion process involves

using highly concentrated sulfuric acid as the reaction media. This substantially increases the capital costs due to the requirement to separate the produced methanol from the sulfuric acid.

Searching for the ideal reaction media to replace or limit the use of the sulfuric acid has been an on-going effort, with ionic liquids emerging as most promising. Recognized as “green” and “designer” reaction solvents, ionic liquids have demonstrated advantages as replacements over conventional solvents in selective hydrocarbon conversion processes. In order to rationalize the potential usage of ionic liquids in direct methane oxidation reactions and in other selective hydrocarbon conversion processes, we proposed a strong integration of theoretical and experimental program to develop a fast-screening method to identify the best ionic liquids for an optimized catalyst/ oxidant/ solvent system, that can be operated at low-temperature, that is highly product selective, that is product friendly for easier separation, and that is cost-effective.

The success of utilizing ionic liquids as reaction media to improve current methane conversion processes as well as developing new chemical processes relies on our fundamental understanding of the functionality of ionic liquids. Since the physical and chemical properties of ionic liquids are very sensitive to molecular structures of composing ionic species, understanding their influences in chemical reactions should be done at the atomic level. Advances of molecular modeling in the last decade provide an important computational tool for this task. Throughout this project, we will combine the modern quantum mechanics (QM) calculations with our newly developed Reactive Force Field (ReaxFF) method, in conjunction with our extensive experimental efforts to develop an optimized homogeneously catalyzed partial methane oxidation process mediated by proper ionic liquids as a replacement for at least part of the sulfuric acid.

1.3 TASKS AND SCHEDULES

Tests of compatibility

Task 1.1 – Stability of ionic liquids to sulfuric acid

Task 1.2 – Stability of methanol in ionic liquid containing sulfuric

Novel reactor designs

Task 2.1 – Low-pressure reactor for testing methane conversion

Task 2.2 – High-pressure reactor for methane conversion to methanol

Quantitative Analyses

Task 3.1 – Quantitative gas analysis of methane isotopomers and other gases

Task 3.2 – Quantitative analysis of methanol formation rates

Theoretical Programs

Task 4.1 – Establishing a database of the molecular structural information ionic liquid prototypes

Task 4.2 – Calibrating the ReaxFF method with DFT calculations

PHASE II

Task 5.1 – Development of the fundamental understanding on roles of ionic liquids to the chemical reactions, in particular the C-H activation reaction

Task 5.2 – Evaluation of the utility of ionic liquids as solvent for methane conversion

Task 5.3 – Development of a Virtual Rapid Prototyping (VRP) method fast-screenings of appropriate ionic liquids

PHASE III

Task 6.1 – Optimizing the selected solvent/acid/oxidant catalytic system

Task 6.2 – Demonstrating the optimized solvent/acid/oxidant catalytic system

Table 1.1: Task To be Performed (Original Schedule for the Four-Year Duration)

Task	Duration (Quarter)															
	1	2	3	4	5	6	7	8	9	10	11	12	13	14	15	16
Task 1.1	■	■	■	■												
Task 1.2	■	■	■	■												
Task 2.1	■	■	■	■	■	■										
Task 2.2			■	■	■	■	■	■								
Task 3.1			■	■	■	■	■	■								
Task 3.2			■	■	■	■	■	■								
Task 4.1	■	■	■	■	■	■	■									
Task 4.2			■	■	■	■	■	■	■	■						
Task 5.1					■	■	■	■	■	■	■	■				
Task 5.2							■	■	■	■	■	■				
Task 5.3									■	■	■	■				
Task 6.1									■	■	■	■	■	■		
Task 6.2													■	■	■	■

Table 1.2: Task To be Performed (Revised Schedule for the Last Two Quarters of Year Four and the Extended One-Year)

Task	DESCRIPTION	Duration (Quarter)					
		15	16	17	18	19	20
Task 6.1.1	Reaction media selection	■	■	■			
Task 6.1.2	Solvent/Acid/Oxidant catalytic system optimization	■	■	■	■		
Task 6.2.1	Bench-scale reactor design			■	■	■	■
Task 6.2.2	System demonstration with catalyst deactivation evaluation					■	■

Table 1.3: Status of updated task performance (with the expanded tasks 6.1 and 6.2 for the extended project period)

Task Number	Title or Brief Task Description	Task Completion Date				Progress Notes
		Original Planned	Revised Planned	Actual	Percent Complete	
1.1	Stability of IL in H2SO4	07/01/04 - 06/30/05	NA	NA	100	

1.2	Stability of CH ₃ OH in IL	07/01/20 - 06/30/05	NA	NA	100	
2.1	Low-pressure Reactor	07/01/04 - 12/31/05	NA	NA	100	
2.2	High-pressure Reactor	01/01/04 - 06/30/06	NA	NA	100	
3.1	Gas Analysis	01/01/04 - 06/30/06	NA	NA	100	
3.2	CH ₃ OH Formation Rate	07/01/05 - 06/30/06	NA	NA	100	
4.1	Database of IL	07/01/04 - 12/31/05	NA	NA	100	
4.2	Calibration of ReaxFF	01/01/05 - 12/31/06	NA	NA	100	
5.1	Roles of IL	07/01/05 - 06/30/07	NA	NA	100	
5.2	Evaluation of IL as Solvent	07/01/06 - 06/30/07	NA	NA	100	
5.3	VRP Method	07/01/06 - 06/30/07	NA	NA	100	
6.1	Optimization	07/01/06 - 12/31/07	NA	NA	100	
6.2	Demonstration	07/01/07 - 06/30/08	NA	NA	100	
6.1.1	Reaction Media Selection	01/01/08-09/30/08	NA	NA	100	
6.1.2	System Optimization	01/01/08-12/31/08	NA	NA	100	
6.2.1	Bench Scale Reactor	07/01/08-06/30/09	NA	NA	100	
6.2.2	Demonstration	01/01/09-06/30/09	NA	NA	100	

1.4 ACOMPLISHMENTS LIST

During this 5-year project, we have achieved enormous accomplishments on developing the efficient low temperature catalytic methane conversion technology. In addition, our critical findings on C-H activation/oxidation processes and the innovated roles of ionic liquids in hydrocarbon chemical reactions can also be applied to other valuable chemical processes and thus bring enormous impacts to the nation's chemical industrial and energy strategy. Below listed are the major accomplishments during this project, and in the following chapters we will present our work in details.

- (1) We have identified and patented 6 types of stable ionic liquids under harsh conditions involving strong acid, strong oxidant, powerful catalyst and relatively high temperature (<250 °C). (*“Stable Ionic Liquids as Media Using at High Temperature, Highly Oxidative and Strong Acidic Conditions”*, Z. Li, Y. Tang and J. Cheng, U.S. Provisional Patent Application 60/673509, 2006)

- (2) We have developed several PEER catalytic systems (Pt-Catalyst/Concentrated Sulfuric Acid/ILs) with significant improvements compared to the Catalytica system in terms of 3 times of reaction rate, longer catalyst lifetime and enhanced water resistance. **The PEER systems have been reported in *Chemical Communication* of Royal Chemical Society and won the honor of the most downloaded paper.**
- (3) We have developed the Reactive Force Field (ReaxFF) method and the Virtual Rapid Prototyping (VRP) method as our theoretical tools for mechanism understanding and catalytic system fast screening. Effectively integrating the experimental and theoretical efforts has provided us indepth mechanistic understandings on the ionic liquids affiliated catalytic methane conversion process. (***“The mechanism by which ionic liquids enable Shilov-type CH activation in an oxidizing medium”***, Xu Z., Oxgaard J. and Goddard III, W.A *Organometallics*, 2008, 27 (15), 3770)
- (4) We have achieved many fundamental understandings on the various functions of ionic liquids in chemical reactions, especially in catalytic methane converting reactions. Such knowledge can be applied to further work on discovering efficient direct methane oxidation chemistry as well as many other important chemical industrial applications where the innovated coordination chemistry introduced by ionic liquid participation might lead to breakthrough improvements.
- (5) We have successfully designed and established **experimental protocols, reactors, characterization tools** for developing and optimizing efficient catalytic methane conversion systems.
- (6) Preliminary efforts have been taken to extend the possible catalytic systems in terms of the reaction medias (H_2SO_4 , CF_3COOH , CH_3COOH , H_2O etc), catalysts (various of Pt, Os, Ru based compounds), oxidants (H_2SO_4 , Pt(IV), Fe(III), Cu(II)), with the application of suitable (stability, reactivity, solubility of catalyst/oxidant) ionic liquids. (***“Use of Ionic Liquids as Coordination Ligands for Organometallic Catalysis”***, Z. Li, Y. Tang and J. Cheng, U.S. Patent Application 20060069169, 2006)
- (7) We have also developed a High-Temperature- Shilov-like system for low temperature homogenous methane oxidation. With application of appropriate stabilizer (mineral acids, ionic liquids, benzene, etc) we have been able to stabilize the Pt-catalyst to up to 300 °C resulting in significantly increased methane conversion. In addition, cheaper oxidants such as FeCl_3 , CuCl_2 were found to present similar efficiency to the expensive Pt(IV) oxidant making this system further attractive in terms of production costs. (***“Novel Concept of Methane Oxidation”*** Y. Tang, Z. Li, and Chen, W. Provisional Patent application, CIT-4892-P, 2007)

CHAPTER TWO: REACTORS AND ANALYTICAL TOOLS

2.1 SUMMARY

This highly challenging project is successfully completed through a strongly integrated theoretical-experimental approach. Our experimental experts have taken intensive efforts on experimental protocol design, novel reactor build-up and modification, and suitable analytical tools selection to carry out various tasks in effective yet cost/time efficient ways. This part of work has been conducted throughout the whole project and served as the fundamental of this study. On the other hand, our achievements on reactors and analytical methodologies themselves are of great significance to the researches of low temperature homogeneously catalytic methane conversion and can be potentially applied (with necessary modifications) to other laboratory chemistry studies.

Specifically designed for various experiments (ionic liquid stability and solubility tests, ionic liquids, catalysts, oxidants and reaction media binary or ternary compatibility tests, C-H bond activation probed by model compounds (suitable ionic liquids, such as [bmim]-ionic liquids), kinetics study of H/D exchange in methane activation and direct oxidation of methane), we have developed low pressure reactors, which are low cost and easy to operate and four types of high pressure reactors. We would like to proudly emphasize that our custom-made mini gold reactors combined with the high pressure autoclave can provide experimental conditions assuring 100% mass balance, 3700 PSi external hydraulic pressure and highly reproducible heating profiles. The experimental results can be analyzed and quantified by GC with FID, TCD, FPD and MSD detectors, ¹H NMR spectroscopy as well as HPLC-UV method.

Detailed information of these experimental protocols, reactors and analytical tools are introduced in the following sections.

2.2 LOW PRESSURE REACTORS

The low pressure reactors utilized in this project are easy to build, operate control with low cost. They are mainly used in ionic liquid solubility and stability tests and catalytic system compatibility tests which are designed to efficiently screen the huge variety of ionic liquids for developing effective IL/Catalyst/Oxidant/Media catalytic systems for methane conversion.

During an experiment with a low pressure reactor, solid/liquid components are added into liquid phase media where a magnetic stir bar is applied to assist the dissolution and mixing. The test is open to atmosphere and does not involve gas phase reactants. Heating is realized by oil bath or heating tape. The liquid products are easy to collect and ready for characterization. Table 2.1,

Table 2.2, Table 2.3, and Table 2.4 presents some compatibility testing results for binary systems (ionic liquid/concentrated sulfuric acid, Pt-catalyst/concentrated sulfuric acid, Pt-catalyst/ionic liquid) and ternary systems (Pt-catalyst/ionic liquid/concentrated sulfuric acid) at room temperature and elevated temperature (above 200 °C, which is the target reaction temperature range of the proposed methane catalytic systems), respectively. In fact a huge amount of such tests have been conducted on over 285 types of commercial ionic liquids and 55 types of custom-synthesized ionic liquids at our lab. We have been able to efficiently screen out several types of extremely stable ionic liquids which can survive under the harsh conditions (high temperature, strong acid and oxidant, powerful catalyst) of catalytic methane conversion.

Table 2.5 lists the results of another type of test with our low pressure reactor. [bmim][Cl] was used as the model compound to probe the oxidation rate of H₂SO₄/Catalyst/[bmim][Cl] ternary system at 200 °C. Typical experimental conditions were 0.05 mmol Pt-based catalyst and 0.73 mmol ionic liquid in 1 mL 96% H₂SO₄ at atmospheric pressure using oil bath (200 °C) and magnetic stirring. The rates were all normalized to reference ternary systems that were prepared at room temperature. The conversion rate is arbitrarily defined from NMR as the intensity decrease of the –CH₃ on the butyl group, but in fact the intensities of CH₂ groups also decreased. When the butyl group changes, the electronic environment of the methyl group also changes, which leads to a new –CH₃ peak right next to the old one. As expected, the total intensity remains almost the same. The oxidation rate is thus defined as the newly formed –CH₃ peak intensity relative to the total. As seen from Table 2.5, oxidation rate is fastest in the [bpym]PtCl₂ system and decreases in the order of [bpym]PtCl₂, K₂PtCl₄, and PtCl₂. The ¹H NMR spectra for the [bpym]PtCl₂ system for different reaction times are plotted in Figure 2.1.

Table 2.1: Compatibility between ionic liquids and concentrated sulfuric acid at room temperature and at elevated temperatures

Ionic Liquid	Solubility in H ₂ SO ₄ at R. T.	Stability in H ₂ SO ₄ up to 200 °C	
		Cation	Anion
Ammonium-based			
(CH ₃) ₃ N(C ₁₄ H ₂₉)Br	Soluble	Stable	HBr released
(CH ₃) ₄ NCl	Soluble	Stable	HCl released
Phosphonium-based			
(CH ₃) ₃ P(C ₁₆ H ₃₃)Br	Soluble	Stable	HBr released
Pyridinium-based			
[bpy][Cl]	Soluble	Stable	HCl released
Imidazolium-based			
[bmim][PF ₆]	Slow and small		
[mmim][CH ₃ SO ₄]	Soluble	Stable	Decomposes

[bmim][Cl]	Soluble	Stable	HCl released
[bmim][BF ₄]	Soluble	Stable	HF/BF ₃ released
[emim][CF ₃ SO ₃]	Soluble	Stable	Stable

Table 2.2: Compatibility of Pt-based catalysts in concentrated sulfuric acid at room temperature and at elevated temperatures.

Pt-based Catalyst	Solubility and Stability in H ₂ SO ₄	
	Room Temp.	High Temp., up to 220 °C
[bpym]PtCl ₂	Yes	Free ligand bpym is observed by NMR at > 110 °C.
[NH ₃] ₂ PtCl ₂	Yes	Decomposes at > 180 °C and PtCl ₂ precipitates.
K ₂ PtCl ₄	No, decomposes to PtCl ₂	No
PtCl ₂	No	No

Table 2.3: Compatibility of Pt-based catalysts in ionic liquids, primarily dependent on the type of anion.

Ionic Liquid	Pt-based Catalyst Solubility in IL, up to 220 °C			
	[bpym]PtCl ₂	[NH ₃] ₂ PtCl ₂	K ₂ PtCl ₄	PtCl ₂
[bmim][BF ₄]	No	No	No	No
[emim][CF ₃ SO ₃]	No	No	No	No
[bmim][Cl]	Yes at 200 °C; free bpym is seen	Yes upon melting	Yes at 200 °C	Yes upon melting

[bmim][HSO ₄]	Yes at 200 °C; free bpym is seen	Yes at 200 °C	Yes at 200 °C	Yes at 200 °C
---------------------------	-------------------------------------	---------------	---------------	---------------

Table 2.4: Stability of ternary systems of H₂SO₄/Catalyst/Ionic Liquid at 200 °C.

Ionic Liquid	Pt-based Catalyst ^a		
	[bpym]PtCl ₂ system	K ₂ PtCl ₄ system	PtCl ₂ system
[mmim][HSO ₄]	Cation stable; Anion decomposed	(Insoluble)	(Insoluble)
[emim][CF ₃ SO ₃]	Ethyl oxidized; Anion stable	(Insoluble)	(Insoluble)
[bmim][BF ₄]	Butyl oxidized; BF ₄ decomposed	(Insoluble)	(Insoluble)
[bmim][Cl]/[HSO ₄]	Butyl oxidized	Butyl oxidized	Butyl oxidized
IL-003 to IL-009 ^b	Compatible	Compatible	Compatible

^a Pt-based catalysts were either dissolved in H₂SO₄ first or in ionic liquid first at elevated temperature.

^b Ionic liquids (IL-003 to IL-009) are home designed and synthesized and meet the compatibility requirement in the ternary system up to 220 °C.

Table 2.5: Oxidation rate study of H₂SO₄/Catalyst/[bmim][Cl] ternary system at 200 °C. [bmim] was used as a model compound for oxidation. Rates were determined based on 1H NMR in D₂SO₄ using acetic acid as the internal standard.

Time at 200 °C	[bpym]PtCl ₂ system		K ₂ PtCl ₄ system		PtCl ₂ system	
	Conversion ^a	Yield ^a	Conversion	Yield	Conversion	Yield
R.T. (ref.)	0	0	0	0	0	0
70 min	37%	37%	47%	20%	24%	12%
2 hr	65%	55%	~60%	24%	~40%	21%

27 hr	100%	100%	80%	72%	50%	50%
-------	------	------	-----	-----	-----	-----

^a See the definitions of conversion and yield in the text.

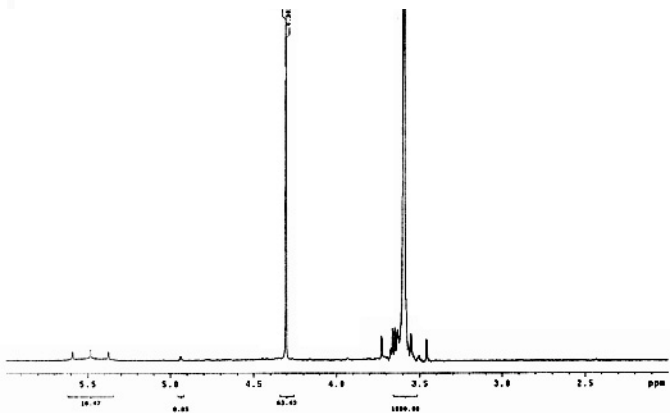
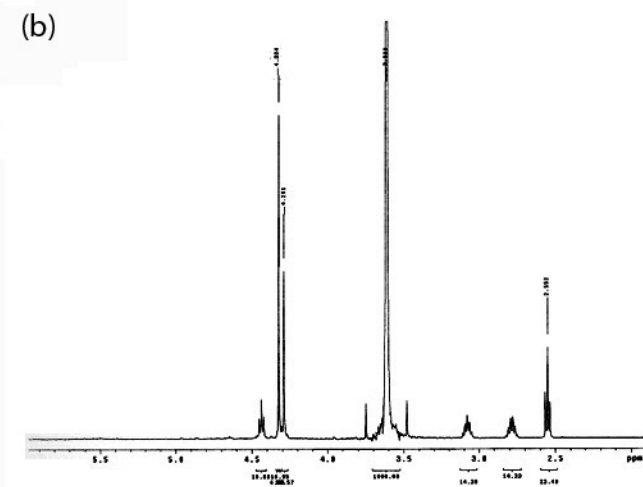
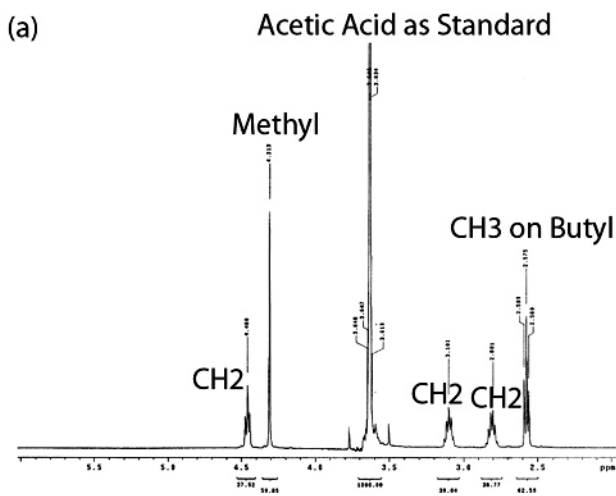


Figure 2.1: ^1H NMR spectra of the liquid of $\text{H}_2\text{SO}_4/[\text{bpym}]\text{PtCl}_2/[\text{bmim}][\text{Cl}]$ ternary system after rate tests using the low pressure reactor. (a) room temperature, as reference; (b) 200 °C, 2 hr; and (c) 200 °C, 27 hr.

2.3 HIGH PROESSURE REACTORS

Due to the poor solubility of methane gas in the reaction liquid, effective contact between the methane and other reactants in the liquid phase requires high pressure and efficient mixing/stirring. In addition, the reaction media is very corrosive, so that the high pressure reactor design is much more challenging. Table 2.6 summarizes the four types of major high pressure reactors designed/built/modified and utilized during this project, which are resulted from our unique and world leading expertise on experimental investigations on homogenous catalysis especially on selective hydrocarbon conversion. The progresses we have made on these high pressure reactors are valuable for not only future work on the development of efficient homogenously catalytic methane conversion systems but also can be applied for other innovated studies in catalytic inorganic/organic chemistry.

Table 2.6: Summary of high-pressure reactor designs and applications.

Reactor Name	Volume (mL)	Physical Description	Gas/Liquid Mixing	Application & Conditions	Pros and Cons
Big Reactor	~ 69	Lab-built, from stainless steel tube, 5 in. long	Magnetic stir bar spinning	Oxidation, 1 mL liquid + 500 psi CH_4	Easy to operate Low conversion Poor T/P control
Short Reactor	~ 6	Lab-built, from stainless steel tube, 2 in. long	Magnetic stir bar spinning	Activation, 1 mL liquid + 500 psi CH_4	Easy to operate Low mixing speed Poor T/P control
Mini Reactor	~ 1	Gold tube, 4 in. long, sealing by arc welding	External hydraulic pressure up to 3700 psi	Activation & Oxidation, 0.3 mL liquid + 50 psi CH_4	High conversion High yield Difficult to operate
Parr Reactor	25	Purchased but gold coated inside and with modified baffle	Rotation of axle and baffle up to 1500 rpm	Activation & Oxidation, 10 mL liquid + 500 psi CH_4	High conversion High yield High cost for a run Difficult to operate

A home-built stainless steel high-pressure reactor was initially used for the methane oxidation tests. There are some drawbacks associated with this reactor design. (1)

Large dead volume. The total capacity of the reactor is about 69 mL but we usually only load 1 mL reaction liquid. It is not surprising to see a low conversion rate and a low yield thereafter. Thus this reactor is not in an optimized condition for methane oxidation. (2) Poor temperature control for the reaction zone. The lower part of the cylindrical reactor was submerged into an oil bath whose temperature can be well controlled. However, the liquid inside is hard to reach a stable desired temperature. (3) Low mixing speed for gas-liquid phases. A magnetic stir bar driven by the stirring plate can only provide a gas/liquid surface reaction, thus a low yield is expected. Overall, these several factors result in a relatively large uncertainty for the yield determination. Later, this big stainless steel reactor was mainly used for semi-quantitative tests on new catalytic systems and for some tests requiring high pressure gas mixture ($\text{CH}_4 + \text{O}_2$) in the reaction system. This reactor has excellent gas evacuation/refill system and convenient gas sampling part for GC analysis.

A modified stainless steel high-pressure reactor with much shrunk size (10 mL, later to 6 mL), the Short Reactor was designed and built for methane activation study at 150 °C or below. The smaller size reduces the total amount of methane loaded and ensures an observable H/D exchange. One milliliter of reaction liquid is added into the reactor and the gas/liquid is mixed by a magnetic stir bar spinning. Similarly, this Short Reactor bears the advantages and disadvantages of the Big Reactor.

We would like to emphasize our innovated reactor design – the mini gold tube reactor which assures 100% mass balance, uniform temperature control and 3700 Psi external hydraulic pressure and thus efficient contact between the gas phase methane and the liquid phase reaction media with catalysts, ionic liquids and oxidants. The mini gold tube has a total volume of about 1 mL, 30% of which is loaded with reaction liquid and the remaining space can be filled by methane gas (usually 50 – 100 psi). Arc welding is used for sealing at both ends. Sealed tubes are placed in a stainless autoclave to which an external hydraulic pressure of up to 3700 psi will be applied. Then the autoclave is heated in a box furnace at desired temperature. The weight of each gold tube is recorded before and after reaction and usually the mass difference is no more than 0.1 mg. Gas phases are analyzed using GC and liquid phase is by ^1H NMR. In addition, multiple mini gold tube reactors can be placed into one autoclave for heating and our box oven has multiple heating slots with very close temperature to each other upon heating. Therefore, parallel experiments with different variables (catalytic system compositions, heating temperature, heating time etc) can be conducted with good reproducibility and good T/P control. With the mini gold tube reactors, high conversion and high yield can be achieved at the price of difficult operation and relatively high costs, for example, the cost for manufacturing/recycling the gold tubes.

Most of the gold tube experiments were conducted in the big box oven where heating was achieved through hot air circulation oven. The temperature is controlled by a thermocouple sitting inside of the oven. Such a heating system is not able to provide precise temperature control. More important, the time required for reaching system equilibrium, i.e. heating the reactor to desired temperatures (200°C~350°C) and reach equilibrium can take as long as couple hours. Even if we place the autoclave into the

oven after it reaches the desired temperature, it still takes 30 minutes or one hour for the thermocouple sitting directly on the autoclave to stabilize. During this slow heating process, we are afraid that some reactions, i.e. slow oxidation of methanol, could also finish after methanol conversion. We built a heating system with an autoclave that could still hold gold tube reactor yet could reach equilibrium temperature (200°C~350°C) within a couple of minutes. This short heating process allowed us to stop the reaction and analyze the final products in a very short time.

The old autoclave is made of steel, and has a dimension of 1.5” hexagonal cross-section and 14” long. Although sturdy, it is slow in conducting heat and reaching temperature equilibrium. The circulating air in the oven is quite slow in passing the heat to the autoclave. In addition, the inside space is much larger than necessary for holding one mini-gold-tube reactor so that relatively large amount of water will fill out that space to provide the over 3000 PSi hydraulic external pressure for the reaction. Therefore the heating response is very slow in this system. We first redesigned the autoclave that holds the gold tube reactor. The material is changed from Steel to Aluminum (Al6061T), and the designs still allow the autoclave and connectors to hold water at high pressure (over 3,000 PSi) and high temperature (up to 350°C). In this way the reaction conditions, i.e. temperature ranging from 200°C~350°C and pressure up to 3,000 PSi, are still available to the gold tube reactor, much the same as the large steel autoclave. The size of the aluminum autoclave is reduced to 1” hexagonal cross-section and only 5” long when assembled. The reduced size and mass of the aluminum autoclave directly translate into reduced heat capacity; while the aluminum material could allow heat to transfer from the outside to the inside of the autoclave at a much faster rate, i.e. Aluminum has heat conductivity almost 5 times as that of steel. These changes allowed temperature to go up at much faster rate compared to the old steel system if the heating system could provide strong enough heat flow for transfer.

The heating system was also changed from the large hot air circulating oven, much like a roast turkey in an oven, to a flux solder tin pot where the Aluminum autoclave is dipped into the pot, much like a chicken drum dipped into a hot frying pot. The latter heating system obviously could provide much stronger heat flow for transferring into the autoclave. The newly purchased solder tin pot (Model C161, Made in China) uses 3 kg of Tin (70%)-Cu (30%) alloy and could provide a pot of melt solder tin at controlled temperature from 180°C to 450°C. The dimension of the Titanium pot is 140 mm×70 mm×43 mm, which is suitable for the newly designed small Al autoclave. Preliminary results show that we could reach a temperature stability of ±4°C at 300°C within 3 minutes.

Upon developing some promising catalytic systems for efficient methane conversion with the stainless steel reactors and the mini gold tube reactors, we advanced our efforts on developing a bench scale reactor ---modification of the commercially purchased Parr Reactor. This commercial product is superior at providing high pressure (up to 1000 Psi), high gas-liquid mixing (rotating baffles at 3000 rpm) and in-situ temperature and pressure control. However, this reactor is not applicable for our catalytic methane conversion system mainly due to its poor corrosion resistance. On the other

hand, the heating rate for this reactor is too slow, which is not desired for the repeatability and quantification of our experiments. Creative yet minor modifications have been applied. For example, we increased the reaction vessel size from 25 mL to 50 mL for larger reaction volume and larger space for the rotating baffle. Besides gold-coating all exposed surfaces, we also inserted a liner inside of the reaction vessel to avoid damage/precipitates on the wall of the reaction vessel. While, our preliminary tests showed that such minor modifications still could not meet the requirements for our harsh experimental conditions. Because of the inevitable vibration caused by the high-speed baffle-rotation, frictions between the rotation baffle, the reaction vessel and the thermocouple will wear off the protecting gold coating and then corrode the parts leading to serious damage to the reactor. In addition, gold coating can not reach some tunnels in the reactor where the corrosive acid vapor can reach. It is also possible to damage other electronic components of the reactor. In short, cost for test with the modified Parr Reactor can be very high with potential damage to the gold coating, quartz liner or other components. Therefore, to completely solve the corrosion problem requires major modification of the reactor such as replacing some of the exposed components by Tantalum material. However, such major modification will be very costive and require a long proceeding time which can not be realized within the time-frame and the budget of the current project.

Based on our experience with the Parr Reactor Modification and development of various custom-made small scale reactors (stainless steel reactor, gold tube reactor, fast heating system), we have propose to build up a new bench scale reactor which is capable to operate under highly corrosive condition, to provide in-situ temperature/pressure control (including heating rate), and to enable in-line result analysis (GC, GC/MS measurements on the reaction gases).

2.4 CHARACTERIZATIONS AND QUANTIFICATIONS

The major analytic tools utilized in this project are ^1H NMR (Proton Nuclear Magnetic Resonance) and GC (Gas Chromatography) coupled with FID (Flame Ionization Detector), TCD (Thermal Conductivity Detector) or MSD (Mass Selective Detector). Also utilized are HPLC (High Performance Liquid Chromatography) with a UV (Ultraviolet) and Elemental Analysis.

^1H NMR is heavily employed in various compatibility tests and methanol/methyl bisulfate production quantification. It is worth to be pointed out that we have developed a suitable protocol for analyzing our concentrated sulfuric acid containing reaction liquids. Instead of those normally utilized deuterated solvents, we are using 98% D_2SO_4 as the solvent and CH_3COOH as the internal standard for most NMR measurements. A Varian Mercury 300 MHz NMR spectrometer was utilized to conduct all NMR measurements. Table 2.5 and Figure 2.1 show one example of the NMR analysis, i.e. using NMR to quantify the oxidation rate of $\text{H}_2\text{SO}_4/\text{Catalyst}/[\text{bmim}][\text{Cl}]$ ternary system at 200 $^\circ\text{C}$. While, Figure 2.2 show typical NMR spectra for the liquid of $\text{H}_2\text{SO}_4/\text{Pt(IV) Catalyst}/\text{CH}_4$ ternary system after methane oxidation tests using the high-pressure reactor.

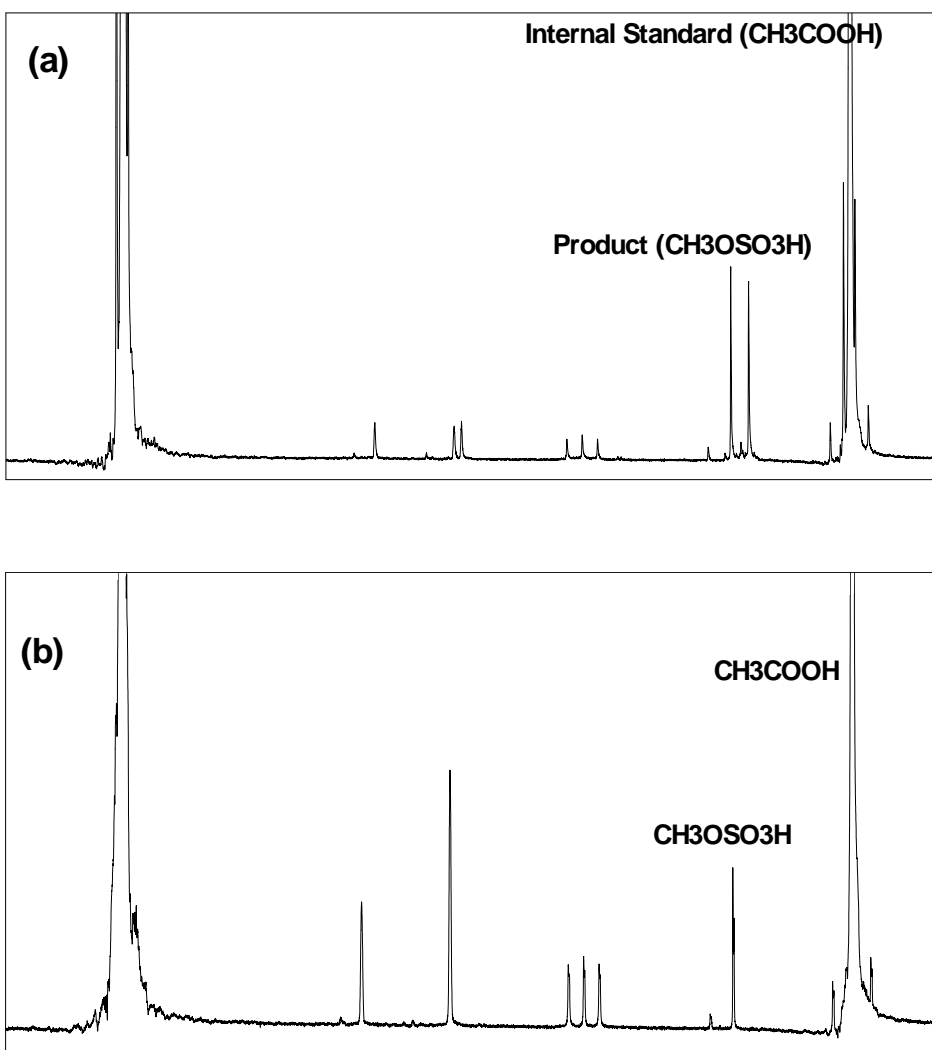
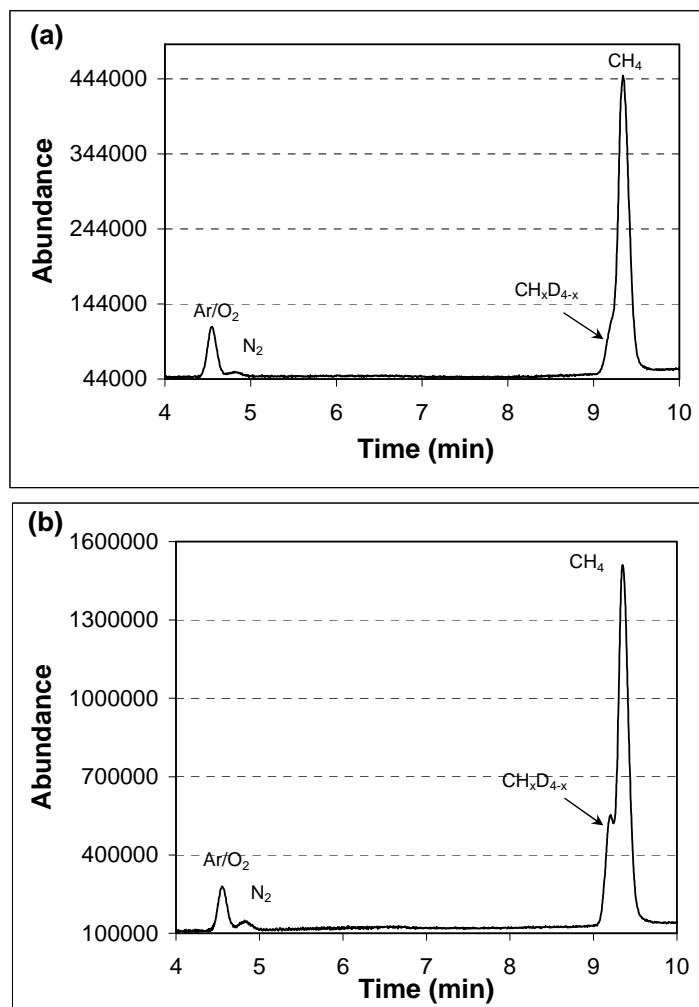


Figure 2.2: ¹H NMR spectra of the liquid of H₂SO₄/Pt(IV) Catalyst/CH₄ ternary system after methane oxidation tests using the high-pressure reactor. (a) PtCl₄ + IL-003 system; (b) PtO₂ + IL006 system. Acetic acid was used as the internal standard.

An HP 6890 GC with MSD detector and specially designed sample holder was used for the quantification of the deuterated methane isotopomers produced from the H/D exchange experiments designed for investigating the C-H activation of methane. Figure 2.3 shows the gas chromatographs of methane after partially exchanged with deuterated solvent of (a) the Periana system, (bpym)PtCl₂ in 98% D₂SO₄; and (b) PtCl₂ + IL-004-d₅ in 98% D₂SO₄; (c) is an overlaid chromatograph for mass ions of methane isotopes of system (b).

Two types of reactors, the mini gold tube and the short stainless steel reactor, were used for the H/D exchange experiments. The results from each reactor provide an internal check about the validity of the data. The Pt catalyst concentration was kept at 50 mM. The dilution of sulfuric acid is achieved by adding D₂O or deuterated ionic liquids. Two deuterated imidazolium-based ionic liquids, IL-004-d₅ (alkylated) and IL-007-d₅, were synthesized through H/D exchange between the regular ones and D₂SO₄. The gold

tube was loaded with 0.3 mL reaction liquid and 50 psi CH₄ (with 3% Ar as the internal standard). The short reactor was loaded with 1 mL reaction liquid and 500 psi CH₄. Both were heated at 150 °C for 2 hours. The gold tube was in an oven and the short reactor was in an oil bath. The gas phases after reaction were introduced into the HP 6890 GC-MS system. The total amount of methane was deduced from the internal standard Ar integration. The methane isotopes were identified from their characteristic ion masses such as 20 for CD₄, 19 for CHD₃, 18 for CH₂D₂, and 17 for CH₃D.



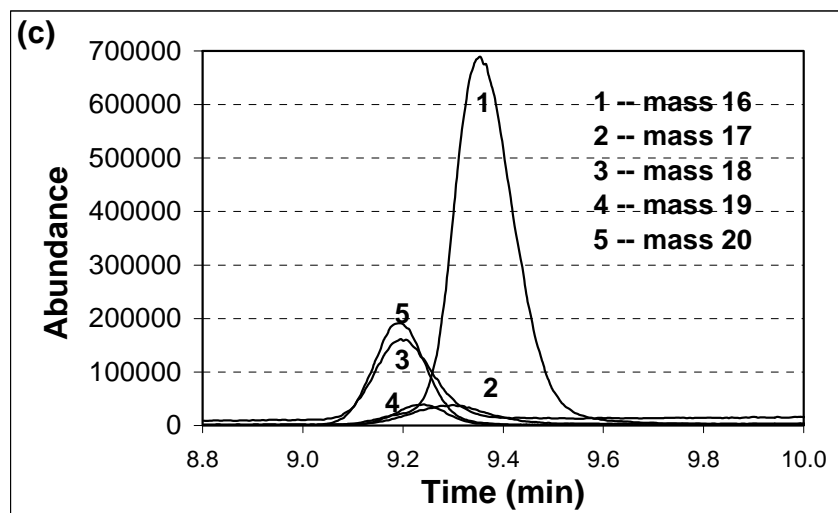
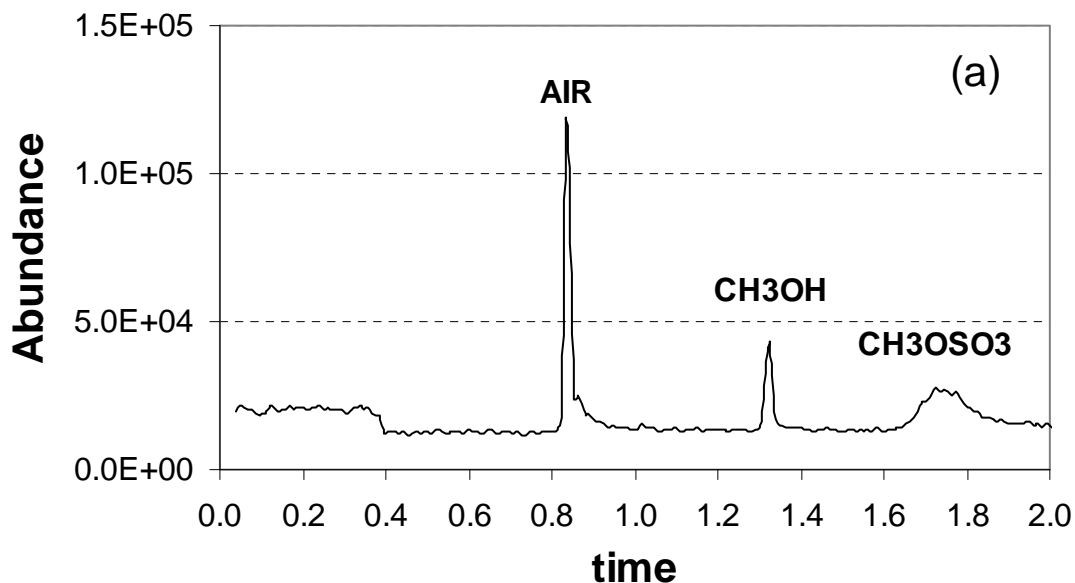


Figure 2.3: Gas chromatograph of methane after partially exchanged with deuterated solvent of (a) the Periana system, (b) $(\text{bpy})\text{PtCl}_2$ in 98% D_2SO_4 ; and (c) $\text{PtCl}_2 + \text{IL-004-d}_5$ in 98% D_2SO_4 . Fig. 1(c) is an overlaid chromatograph for mass ions of methane isotopes of system (b).

An HP 5890 GC with MSD detector can also be used to quantify the methanol (and methyl bisulfate) production. The liquid after reaction was hydrolyzed and neutralized with NaOH to a PH ~ 7 for the GC-MS measurements. Figure 2.4 shows the GC-MS spectra of the liquid of $\text{H}_2\text{SO}_4/\text{Catalyst}/\text{CH}_4$ ternary system after methane oxidation tests highlighting both the free CH_3OH peak and the CH_3HSO_4 peak.



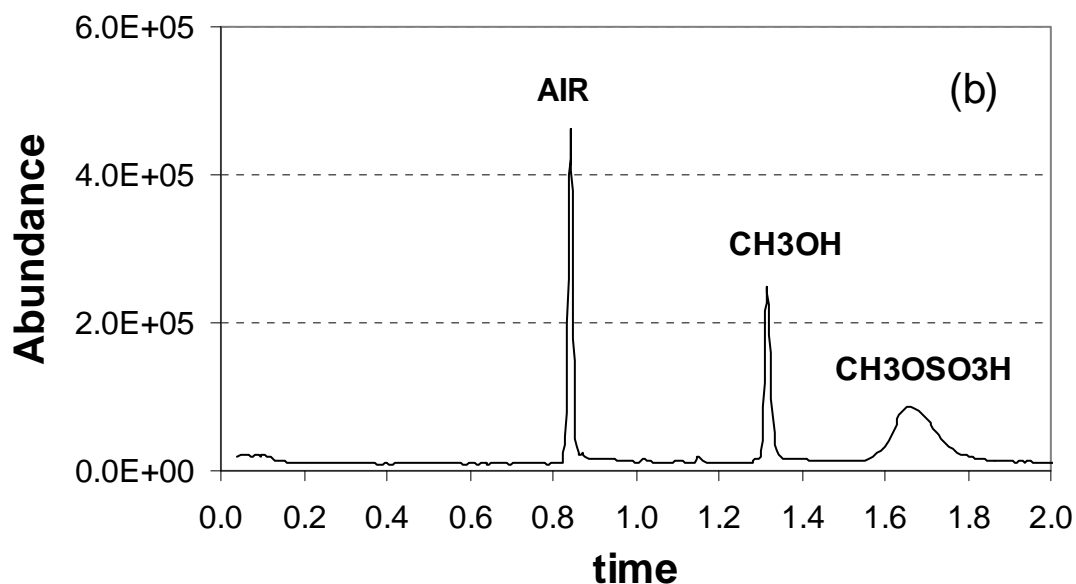


Figure 2.4: GC-MS spectra of the liquid of $\text{H}_2\text{SO}_4/\text{Catalyst}/\text{CH}_4$ ternary system after methane oxidation tests using the high-pressure reactor. (a) system #1, using $[\text{bpym}]\text{PtCl}_2$ as the catalyst; and (b) system #2, using $\text{PtCl}_2\text{-IL003}$ as the catalyst. About 0.2 mL liquid after each reaction run was hydrolyzed in 5 mL H_2O solution and then neutralized with NaOH . They differ in the total peak area integrated

The gas phase products from the methane oxidation experiments were transferred, quantified and analyzed with an HP 6890 GC with FID, TCD and FPD (Flame Photometric Detector) detectors. The methane gas reactant contains 3% or 15% He as internal standard. Through this analytical protocol, we were able to characterize/quantify the total amounts of methane loaded and remained, CH_3Cl , CO_2 and SO_2 generation, which gave us the conversion and selectivity data.

CHAPTER THREE: IONIC LIQUIDS FOR HYDROCARBON CONVERSION

3.1 SUMMARY

During this five-year project, totally 285 commercial ionic liquids and 55 PEER-synthesized ionic liquids have been tested and screened for application in homogeneously catalytic conversion of methane. One of our powerful tools for describing/predicting the major physical and chemical properties of the huge amount of varieties of ionic liquids is the molecular modeling based on the DFT calculations. Combined the molecular modeling results and the experimental observations on eight major types of ionic liquids, we have been able to not only identify/synthesize several classes of super stable ionic liquids under the harsh conditions (high temperature ~ 250 °C, highly acidic and oxidative of concentrated sulfuric acid, and powerful catalysts Pt or other transition metal compounds) for catalytic methane oxidation reaction, but also achieve mechanistic understandings of the functions of ionic liquids in catalytic methane conversion systems or other catalytic chemical reactions.

Our findings on innovated applications of ionic liquids in chemical reactions are of critical significance to open some new chemistry in some chemical industries. Enormous beneficial impacts can be expected from such innovated applications of ionic liquids given their “green” and “designer” nature.

3.2 MOLECULAR MODELING OF IONIC LIQUID DATABASE

The potential combinations of different ionic liquids are enormous. A simple statistical estimation of currently-known cation/anion combinations results in a 10^{14} different ionic liquid prototypes. A comprehensive list of various ionic liquid candidates is essential for the screening purpose. Currently, we have identified nearly 300 different types of ionic liquids that are commercially available. These ionic liquid compounds serve as basic components of our ionic liquid database. Upon collections of their physical and chemical properties from vast literature search and from direct input from Sachem, molecular modeling based on the Density Functional Theory (DFT) calculations was initiated.

To examine the molecular properties of ionic liquid compounds, and to obtain their geometry, chemical bonding and energetic relations as important inputs for the calibrations of the ReaxFF method, an ion-pair formation of the ionic liquid is computed. Geometry of the ion-pair is fully optimized in gas-phase, and in various organic solvents using the continuous solvation model. Structural information, such as H-bonding, can then be obtained. Other structural related properties such as dipole moment, highest occupied molecular orbital (HOMO), lowest unoccupied molecular orbital (LUMO), as well as molecular weight, surface, and volume, can also be determined.

Basically, there are 9 major cation classes that are most commonly used to form ionic liquids; and the variation of their molecular structure such as different alkyl chain length and attached positions, have great impact to the ionic liquid physical properties

such as melting point and stability. Figure 3.1 illustrates these cation classes. On the other hand, the molecular compositions of the anion are more various. In general, the influence of the anion species is more relevant to the ionic liquid chemical properties, such as acidity and chemical reactivity. Figure 3.2 are some common anion species of ionic liquids. In Table 3.1, we list a few calculated molecular properties of the monosubstituted Imidazolium Derivatives.

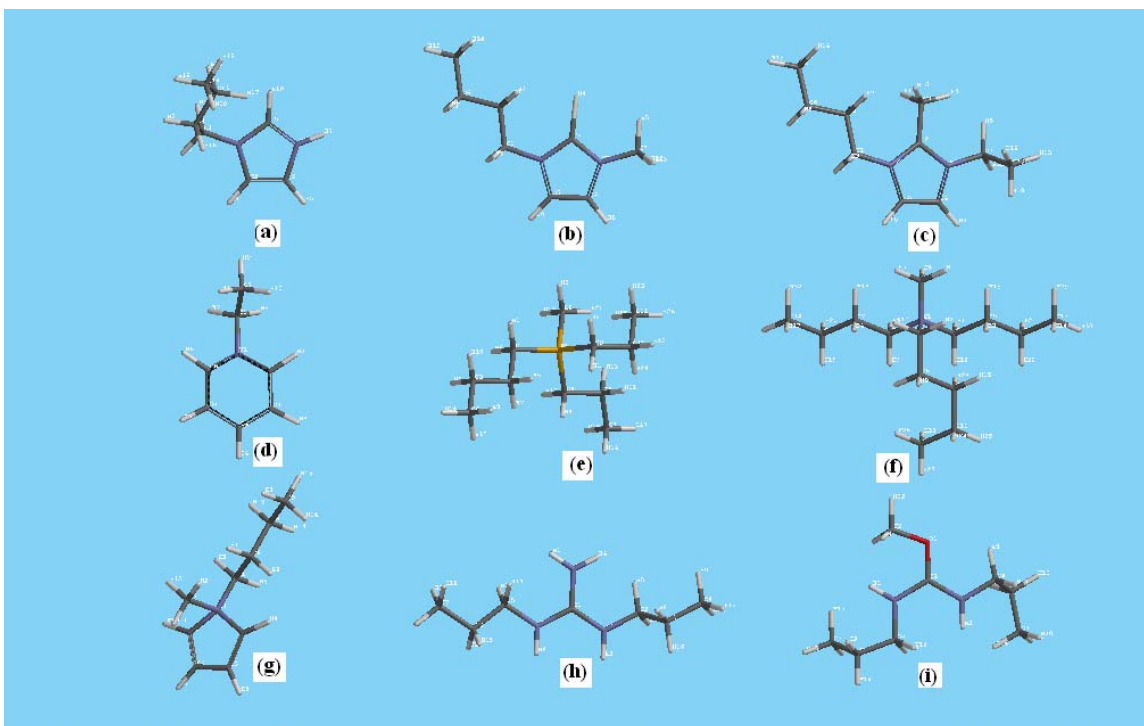


Figure 3.1: 9 Basic classes of cations (a) Monosubstituted imidazolium; (b) Disubstituted Imidazolium; (c) Trisubstituted Imidazolium; (d) Pyridinium; (e) Phosphonium; Ammonium; Pyrrolidinium; (g) Guanidinium; (i) Isouronium

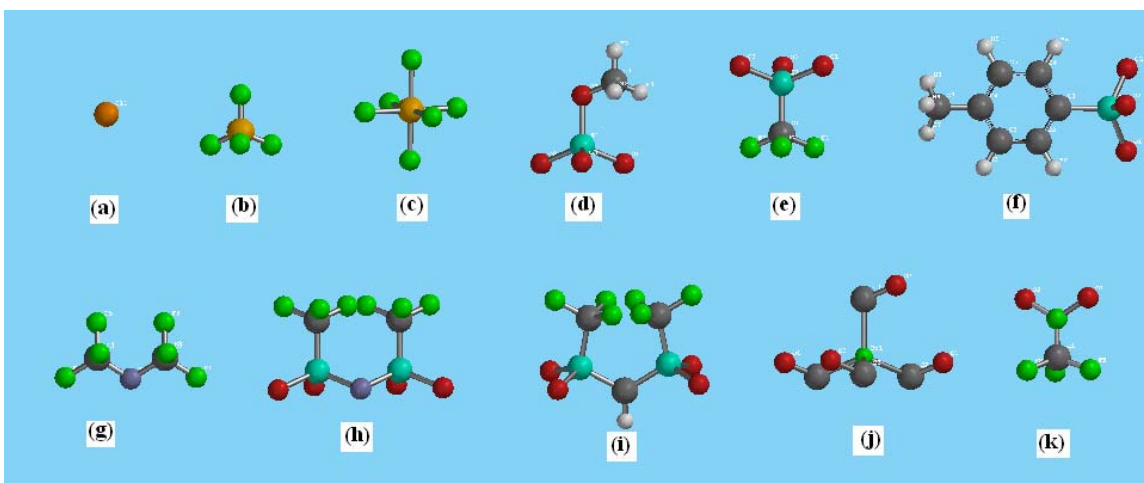


Figure 3.2: Typical Anions (a) Monoatom, Cl, Br, I; (b) Borates; (c) Phosphates and Antimonates; (d) Sulfates; (e) Sulfonates; (f) Tosylates; (g) Amides $(CN)_2N^-$; (h) Imides; (i) Methanes $[HC(SO_2CF_3)_2]^-$; (j) Cobalt-tetracarbonyl $Co-(CO)_4^-$; (k) Trifluoroacetate CF_3COO^- .

Table 3.1: Molecular Calculations of Selected Monosubstituted Imidazolium Derivatives

Name	E (kcal/mol)	E LUMO (kcal/mol)	E HOMO (kcal/mol)	Dipole (debye)	CPK Area (Å ²)	CPK Volume (Å ³)	Molecular Wt.(amu)
BuIM-PF6	-407.365502	-27.9160612	-262.510724	17.5133907	259.800966	222.379222	270.157
MIM-PF6	-386.986348	-30.3499635	-265.059038	17.3223922	201.724106	167.361035	228.076
BuIM-BF4	-303.604583	-24.0957444	-252.201981	15.1715128	234.085348	203.385083	211.998
MIM-BF4	-287.737826	-25.0096852	-256.243402	15.1686695	175.292662	147.621564	169.917
BuIM-CF3SO3	-235.447322	-24.9744165	-226.134191	15.0997478	270.381686	235.584331	274.263
MIM-CF3SO4	-214.714862	-27.6667009	-225.935397	15.6620077	217.530773	181.046419	232.182
BuIM-Tosylate	-52.8853165	-12.8444881	-209.308256	8.37428936	333.214469	302.236697	296.391
MIM-Tosylate	-32.8452996	-14.3166646	-209.670742	8.50752999	272.966536	246.868164	254.31

3.3 PEER SYNTHESIZED IONIC LIQUIDS

Guided by our molecular modeling calculations and experimental observations, we have synthesized about 54 types of new ionic liquids as listed in Table 3.2. Therefore, our ionic liquid pool includes not only those commercially available products but also some types that can be synthesized at our facilities. Expertise on design, synthesis and characterization of ionic liquids has brought us great advantages on achieving the desired ionic liquids with tailored structure (and thus properties) for applications in catalytic methane conversion.

Table 3.2: Index of ionic liquids synthesized at PEER

IL No.	Name
IL-001	1-neopentyl-3-methylimidazolium chloride [npmim][Cl]
IL-002	1-isopropyl-3-methylimidazolium bromide [ipmim][Br]
IL-003	1-methylimidazolium chloride, [1-mim][Cl]
IL-004	1-methylimidazolium bisulfate, [1-mim][HSO ₄]
IL-005	1-methylimidazolium triflate, [1-mim][CF ₃ SO ₃]
IL-006	Imidazolium chloride, [im][Cl]
IL-007	Imidazolium bisulfate, [im][HSO ₄]
IL-008	1,3-dimethylimidazolium iodide, [mmim][I]
IL-009	1,3-dimethylimidazolium bisulfate, [mmim][HSO ₄]
IL-010	Tetramethylammonium trifluoroacetate

IL-011	2-methylimidazolium bisulfate, [2-mim][HSO ₄]
IL-012	4-methylimidazolium bisulfate, [4-mim][HSO ₄]
IL-013	1,2-dimethylimidazolium bisulfate, [1,2-dimim][HSO ₄]
IL-014	1,4-dimethylimidazolium bisulfate, [1,4-dimim][HSO ₄]
IL-015	1,2,3-trimethylimidazolium methanesulfate, [1,2,3-trimim][CH ₃ SO ₄]
IL-016	2,4,5-trimethyloxazolium bisulfate, [2,4,5-trimox][HSO ₄]
IL-017	1-trifluoroacetylimidazolium bisulfate
IL-018	1-methylbenzimidazolium bisulfate
IL-019	1,3-dimethylbenzimidazolium bisulfate
IL-020	Pyridinium bisulfate, [pyr][HSO ₄]
IL-021	1,4-dimethylpyridinium bisulfate
IL-022	2,6-lutidinium bisulfate
IL-023	3,5-lutidinium bisulfate
IL-024	Pyrazinium bisulfate, [pyz][HSO ₄]
IL-025	1-methylpyrazinium bisulfate
IL-026	2-methylpyrazinium bisulfate
IL-027	2,3-dimethylpyrazinium bisulfate
IL-028	2,3,5-trimethylpyrazinium bisulfate
IL-029	2,3,5,6-tetramethylpyrazinium bisulfate
IL-030	1,2,3,5,6-pentamethylpyrazinium bisulfate
IL-031	Quinoxalinium bisulfate
IL-032	Quinoxalinium chloride
IL-033	Pyrimidinium bisulfate
IL-034	1-methylpyrimidinium bisulfate
IL-035	4,6-dimethylpyrimidinium bisulfate
IL-036	Triazinium bisulfate
IL-037	Bipyrimidinium bisulfate

IL-038	1-methylbipyrimidinium bisulfate
IL-039	Aminopyrazinium bisulfate
IL-040	Pyrazinecarbonitrile bisulfate
IL-041	2,3-pyrazinedicarbonitrile bisulfate
IL-042	2-Methoxypyrazinium Bisulfate
IL-043	Chloropyrazinium Bisulfate
IL-044	1,2,4-triazolium bisulfate
IL-045	1H-1,2,3-triazolium bisulfate
IL-046	1,2,4-triazolo(1,5-a)pyrimidine in H ₂ SO ₄
IL-047	2-aminoimidazolium bisulfate
IL-048	Pyrazolium Bisulfate
IL-049	Pyrazolium Chloride
IL-050	1-MethylPyrazolium Bisulfate
IL-051	1-MethylPyrazolium Chloride
IL-052	1,2-diMethylPyrazolium Bisulfate
IL-053	1,2-diMethylPyrazolium Chloride
IL-054	4-MethylPyrazolium Bisulfate

3.4 IONIC LIQUIDS SCREENING

3.4.1 Solubility and Stability Tests

Our experimental screening started from the solubility and stability tests on commercial ionic liquids. Table 3.3 presents the testing results of the four main categories of ionic liquids distinguished by their cations, namely ammonium-based, phosphonium-based, pyridinium-based, and imidazolium-based. Solubility and stability of ionic liquids in concentrated sulfuric acid were tested at room temperature and elevated temperature (up to 200 °C) for varied periods of time. The stabilities of the cations and anions were evaluated respectively.

Table 3.3: Compatibility between ionic liquids and concentrated sulfuric acid at room temperature and at elevated temperatures.

Ionic Liquid	Solubility in H ₂ SO ₄ at R. T.	Stability in H ₂ SO ₄ up to 200 °C	
		Cation	Anion
Ammonium-based			
(CH ₃) ₃ N(C ₁₄ H ₂₉)Br	Soluble	Stable	HBr released
(CH ₃) ₄ NCl	Soluble	Stable	HCl released
Phosphonium-based			
(CH ₃) ₃ P(C ₁₆ H ₃₃)Br	Soluble	Stable	HBr released
Pyridinium-based			
[bpy][Cl]	Soluble	Stable	HCl released
Imidazolium-based			
[bmim][PF ₆]	Slow and small		
[mmim][CH ₃ SO ₄]	Soluble	Stable	Decomposes
[bmim][Cl]	Soluble	Stable	HCl released
[bmim][BF ₄]	Soluble	Stable	HF/BF ₃ released
[emim][CF ₃ SO ₃]	Soluble	Stable	Stable

¹H NMR was the main analytic tool for these stability tests. Prepared solutions were analyzed at different time intervals at room temperature (Figure 3.3). No obvious changes (chemical shifts or peak integral) were observed for this IL. Then the solutions were heated at different temperatures for a certain time followed by NMR analysis (Figure 3.4). It is clear to see the intensity of the peaks next to the D₂SO₄ peak (left side) decreased with increasing temperature while others stayed almost unchanged. Does decomposition occur during heating? Comparison among the NMR spectra for the starting materials 1-methylimidazole, chlorobutane, their mixture at the ratio of 1:1, and the product [bmim][Cl] that is the precursor of [bmim][BF₄] allows an easy assignment of those peaks to the protons on the imidazolium ring. It is unreasonable to justify that protons on the ring lose while protons in alkyl groups are still stable. Instead, it is more likely that those protons on the ring have exchanged with deuterium in D₂SO₄. Heating accelerated this process, resulting in a dramatic drop in proton concentration. So, it is possible that the drop in proton concentration is associated with an exchange process instead of thermal decomposition.

To make sure that [bmim][BF₄] did not decompose right after it was added to D₂SO₄ and before subjected to NMR, the acid solution was neutralized with NaOD-saturated solution in D₂O. The NMR spectrum after neutralization is shown in Figure 3.5 (a), together with Figure 3.5 (b) for comparison, the one for [bmim][BF₄] dissolved in D₂O directly. All characteristic peaks were reproducible. This strongly suggests that [bmim][BF₄] not only dissolves well in sulfuric acid, but also is stable for a prolonged time.

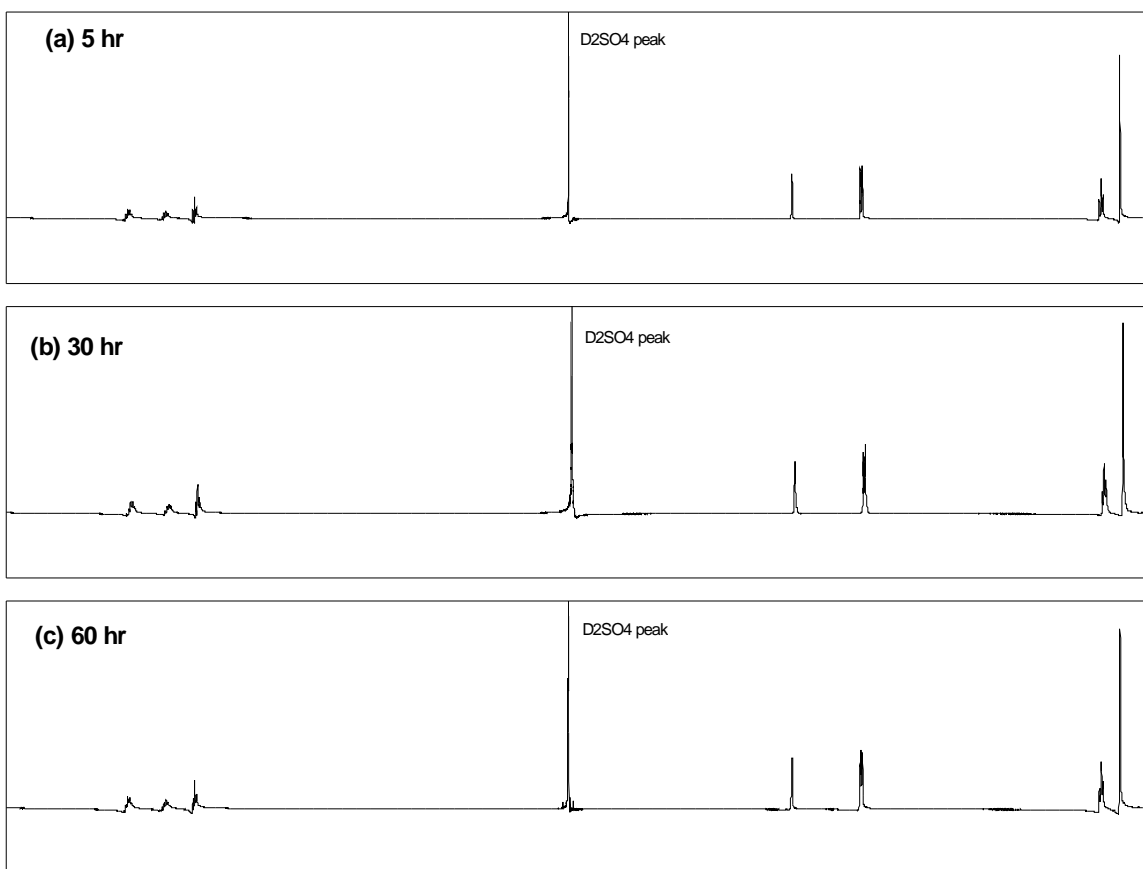


Figure 3.3: ¹H-NMR spectra of [bmim][BF₄] in D₂SO₄ at 25 °C for (a) 5 hr, (b) 30 hr, and (c) 60 hr, respectively.

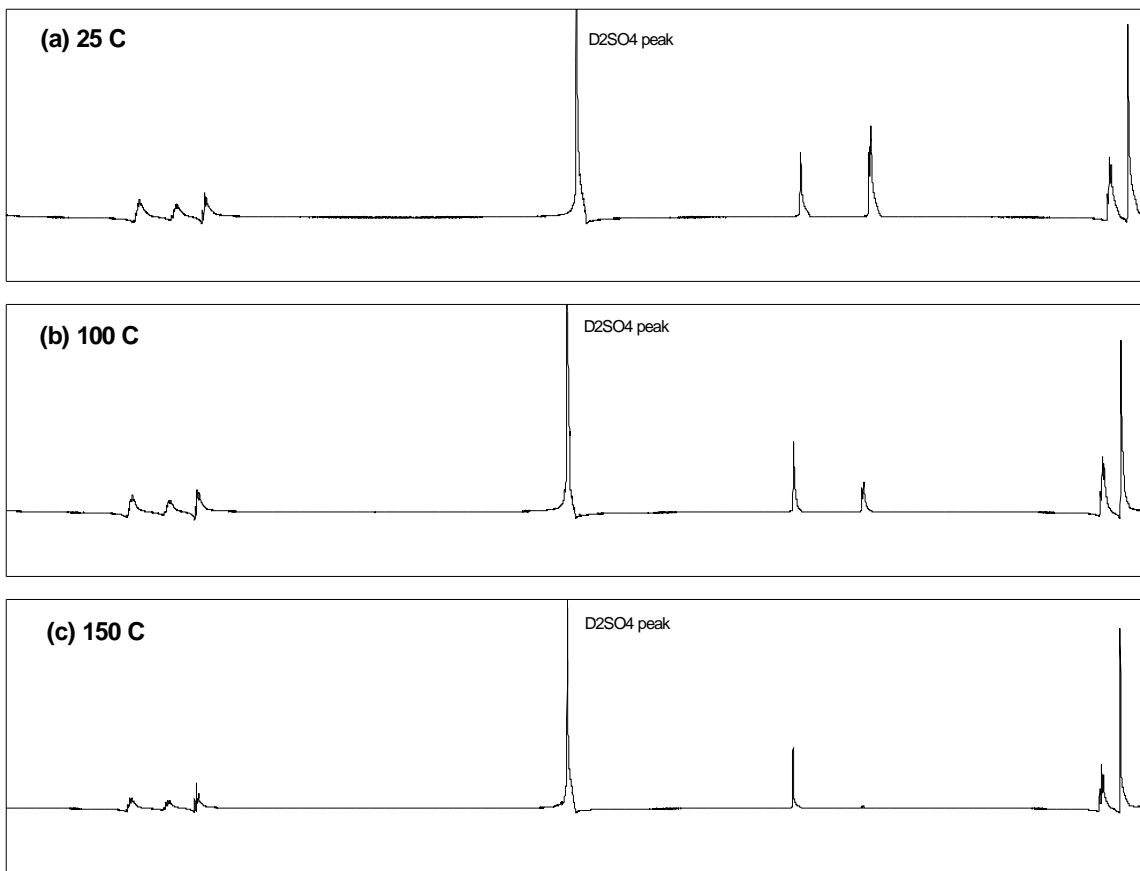


Figure 3.4: ¹H-NMR spectra for [bmim][BF₄] solution in D₂SO₄ (a) at room temperature, (b) at 100 °C, and (c) 150 °C for 3 hr each.

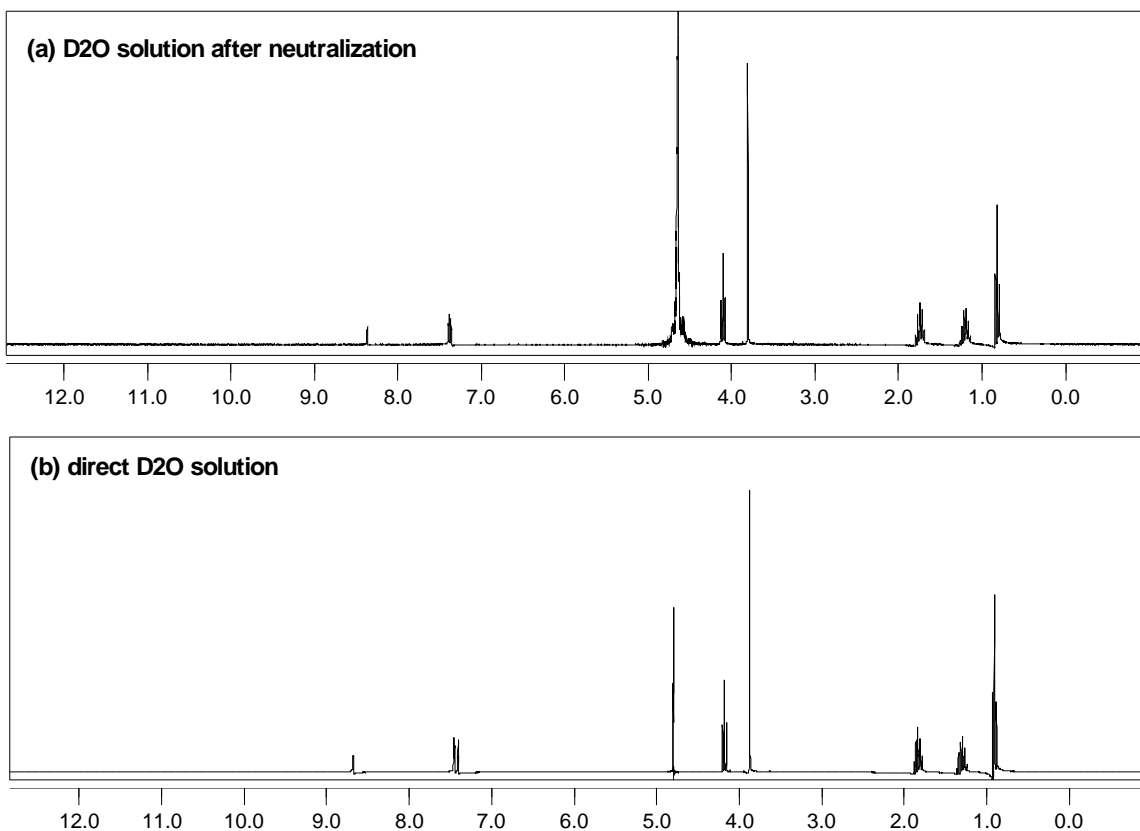


Figure 3.5: ¹H-NMR spectra for (a) [bmim][BF₄] solution in D₂O resulting from neutralization of D₂SO₄ with NaOD, and (b) [bmim][BF₄] dissolved in D₂O directly.

The solubility and stability tests of ionic liquids in concentrated sulfuric acid have covered all four major types (ammonium-based, phosphonium-based, pyridinium-based, and imidazolium-based). All the cations are found to be stable but for anions only triflate (CF₃SO₃⁻) and bisulfate (HSO₄⁻) are stable. The anion decomposition was indicated by gas release in the form of HX gas (X = Cl⁻ or Br⁻). For [bmim][BF₄], the anion (BF₄⁻) decomposed to HF and BF₃ in H₂SO₄ at elevated temperatures. Because ionic liquids with triflate as the anion do not dissolve platinum-based catalysts very well, we use most ionic liquids with a bisulfate anion. From the cation side, we decide to continue focusing on the imidazolium-based and start to develop new heterocyclic cation-based ionic liquids. The reasons are (1) ammonium and phosphonium-based ionic liquids are poor solvents for Pt-based catalysts (such as PtCl₂) probably due to their poor coordination capability; (2) pyridinium-based ionic liquids can dissolve Pt-based catalysts but the ternary system almost did not show any catalytic activity for methane oxidation; and (3) imidazolium-based ionic liquids have demonstrated excellent performance in methane to methanol conversion tests.

Table 3.4 shows the solubility and stability of several Pt-catalysts ([bpym]PtCl₂, [NH₃]₂PtCl₂, K₂PtCl₄ and PtCl₂). It is already known that [bpym]PtCl₂, the so-called Catalytica catalyst dissolves well and is stable in concentrated sulfuric acid at room temperature. [NH₃]₂PtCl₂ shows better catalytic activity at 180 °C than [bpym]PtCl₂,

however, it decomposes within a short time and produces PtCl_2 which is insoluble in H_2SO_4 . K_2PtCl_4 is the starting material for the synthesis of $[\text{bpym}]\text{PtCl}_2$.¹ It is worth noting that ^1H NMR observations revealed the free ligand, bipyrimidine (bpym), from $[\text{bpym}]\text{PtCl}_2$ after being heated at elevated temperatures, but no PtCl_2 precipitated.

Table 3.4: Compatibility of Pt-based catalysts in concentrated sulfuric acid at room temperature and at elevated temperatures.

Pt-based Catalyst	Solubility and Stability in H_2SO_4	
	Room Temp.	High Temp., up to 220 °C
$[\text{bpym}]\text{PtCl}_2$	Yes	Free ligand bpym is observed by NMR at > 110 °C.
$[\text{NH}_3]_2\text{PtCl}_2$	Yes	Decomposes at > 180 °C and PtCl_2 precipitates.
K_2PtCl_4	No, decomposes to PtCl_2	No
PtCl_2	No	No

Here comes the first major function of ionic liquid applied in catalytic methane conversion systems: to assist the dissolution of potential transition metal based catalysts which are otherwise insoluble in most reaction media. Table 3.5 shows the solubility tests of Pt-based catalysts in a variety of imidazolium-based ionic liquids. The molar ratio of ionic liquid to Pt-compound was at least 4:1 to ensure a complete dissolution. As seen in the table, the catalyst dissolution is greatly facilitated with heating, and it is strongly influenced by select anions. Chloride and bisulfate ionic liquids readily dissolve all Pt-based catalysts after heating at 200 °C for several minutes, while tetrafluoroborate and triflate are not effective at all. On the other hand, the cations, e.g., [bmim] vs. [emim], seem not to significantly affect the solubility. Since dialkylimidazolium chloroplatinates (both II and IV) have been synthesized at similar conditions, we propose the dissolution during heating is actually a chelating process in which the anions of the ionic liquid coordinate to the Pt center to form a new anion. Remarkably, the new compound (with excess ionic liquid) dissolves well in concentrated H_2SO_4 , presumably due to the replacement of Cl^- by HSO_4^- .

Table 3.5: Compatibility of Pt-based catalysts in ionic liquids, primarily dependent on the type of anion.

Ionic Liquid	Pt-based Catalyst Solubility in IL, up to 220 °C			
	$[\text{bpym}]\text{PtCl}_2$	$[\text{NH}_3]_2\text{PtCl}_2$	K_2PtCl_4	PtCl_2
$[\text{bmim}][\text{BF}_4]$	No	No	No	No
$[\text{emim}][\text{CF}_3\text{SO}_3]$	No	No	No	No

[bmim][Cl]	Yes at 200 °C; free bpym is seen	Yes upon melting	Yes at 200 °C	Yes upon melting
[bmim][HSO ₄]	Yes at 200 °C; free bpym is seen	Yes at 200 °C	Yes at 200 °C	Yes at 200 °C

After the binary systems, we advanced to the stability test of ternary systems at elevated temperatures. [bpym]PtCl₂ was used as the primary catalyst but PtCl₂ and K₂PtCl₄ were also studied for comparison. The results are summarized in

Table 3.6. Commercially available ionic liquids are usually with dialkyl groups on the imidazolium ring.

Table 3.6 shows that the alkyl groups longer than methyl are not stable in the presence of Pt-based catalysts in hot sulfuric acid. It is not surprising to see that the butyl group was oxidized, considering the power of [bpym]PtCl₂ for methane oxidation in such conditions. One important point is that K₂PtCl₄ and PtCl₂ have similar catalytic capability when dissolved in ionic liquids. Furthermore, development of stable ternary systems for methane oxidation, with consideration to avoid potentially oxidizable ionic liquids, has led to the development of new ionic liquids designed and synthesized in our laboratory.

Table 3.6: Stability of ternary systems of H₂SO₄/Catalyst/Ionic Liquid at 200 °C.

Ionic Liquid	Pt-based Catalyst ^a		
	[bpym]PtCl ₂ system	K ₂ PtCl ₄ system	PtCl ₂ system
[mmim][HSO ₄]	Cation stable; Anion decomposed	(Insoluble)	(Insoluble)
[emim][CF ₃ SO ₃]	Ethyl oxidized; Anion stable	(Insoluble)	(Insoluble)
[bmim][BF ₄]	Butyl oxidized; BF ₄ decomposed	(Insoluble)	(Insoluble)
[bmim][Cl]/[HSO ₄]	Butyl oxidized	Butyl oxidized	Butyl oxidized

^a Pt-based catalysts were either dissolved in H₂SO₄ first or in ionic liquid first at elevated temperature.

^b Ionic liquids (IL-003 to IL-009) are home designed and synthesized and meet the compatibility requirement in the ternary system up to 220 °C.

3.4.2 Compatibility Tests

Compatibility here means the combination of solubility, stability as well as catalytic reactivity for C-H activation/oxidation. After the initial screening upon solubility and stability tests, the potential ionic liquids for methane conversion

applications have been greatly narrowed down. Therefore, our efforts on synthesizing new ionic liquids have been focused on imidazolium-based and related ionic liquids. Table 3.7 shows the compatibility test results for part of ionic liquids synthesized at our laboratory.

Table 3.7: Compatibility studies of ionic liquids in ternary systems. Three steps are developed (1) stability in Periana's system ($\text{H}_2\text{SO}_4 + [\text{bpym}]\text{PtCl}_2$) at 200 °C; (2) solubility of PtCl_2 in ionic liquids upon heating; (3) compatibility of PtCl_2 +ILs in sulfuric acid upon heating

Ionic Liquid (default anion = HSO_4^-)	STEP 1	STEP 2	STEP 3
	IL's Stability in Periana System	Solubility of PtCl_2 in IL	Compatibility of PtCl_2 +IL in H_2SO_4
Five-member Ring			
IL-011 to IL-015 ^a (alkylated imidazolium)	Unstable	Soluble	Soluble but unstable
IL-016 (alkylated oxazolium)	Unstable		
IL-017 (1- CF_3CO -imidazolium)	Unstable		
IL-018 and IL-019 (fused benzimidazolium)	Imidazole ring is stable	Soluble	Soluble & imidazole ring is stable
Six-member Ring			
IL-020 (pyridinium)	Unstable	Soluble	Soluble but unstable
IL-021 to IL-023 (alkylated pyridinium)	Unstable	Tested IL-023 Soluble	Soluble but unstable
IL-024 (heterocyclic cation)	Stable	Soluble	Soluble and stable
IL-025 to IL-030 (alkylated IL-024)	Unstable		
IL-031 and IL-032 ^b (fused aromatic IL-024)	Stable	Soluble	Soluble but unstable
IL-033 (heterocyclic cation)	Unstable	Soluble	Soluble but unstable
IL-034 and IL-035 (alkylated IL-033)	Unstable	Soluble	Soluble but unstable
IL-036 (heterocyclic cation)	Unstable		
Bi Six-member Ring			
IL-037 (bipyrimidinium)	Stable	Soluble	Soluble and stable
IL-038	Stable	Low solubility	

A set of procedures for fast screening of stable ionic liquids have been established. The stability of ionic liquids in sulfuric acid is not a major concern here as most ionic liquids contain the stable anion, bisulfate. Our emphasis is on the solubility of platinum salts in ionic liquids and then the solubility and stability of the ionic liquids in a ternary system containing sulfuric acid. To oxidize methane, the ionic liquids themselves should be stable in a catalytic system. The procedures of fast screening of ionic liquids can be described as follows. First, some amount of ionic liquids (bisulfate) is added into the Periana system at room temperature which is homogenous and catalytic. The solution was heated at 200 -220 °C for 2.5 hours and then checked by ¹H NMR. Any chemical shift change or peak intensity change give information for the ionic liquid's structure change. Particularly, the triple peak (NH₄⁺) is a characteristic indication for ring opening. If we observe that the ionic liquid is stable, we proceed to the next step. Table 3.7 shows that alkylated imidazolium-based, alkylated pyridinium-based, and alkylated other heterocyclic (containing carbon and nitrogen) six member ring cation-based ionic liquids are all unstable in the Periana system. However, we are still able to identify a few truly stable ionic liquids, for examples, fused heterocyclic imidazolium-based IL-018 and IL-019, heterocyclic IL-024 and IL-037. The second step is to test the solubility of PtCl₂ (and other Pt species if applicable) in those ionic liquids that have passed the first step screening. Not surprising, most ionic liquids are powerful solvents for platinum salts such as PtCl₂ after heating at 200 °C for a certain period. The third and key step is to test the solubility and stability of PtCl₂-ionic liquid solution in concentrated sulfuric acid at elevated temperatures. IL-024 and IL-037 have showed good solubility and stability. The common features of these two ionic liquids include highly symmetric structure and possessing lone electron pair of nitrogen on the heterocyclic rings.

With certain selected ionic liquids, compatibility tests can be advanced to searching for new platinum catalysts. Table 3.8 lists some Pt species' solubility in a number of representative ionic liquids. These findings are important because they make many homogeneous catalysis processes in ionic liquids possible, including our current methane to methanol oxidation project. Selected Pt(IV) salts dissolved in imidazolium-based ionic liquids and then in sulfuric acid have also shown high catalytic reactivity for methane oxidation.

Table 3.8: Compatibility of Pt-based catalysts (both Pt(II) and Pt(IV) species) in ionic liquids.

Ionic Liquid	Pt-based Catalyst Solubility in IL, up to 220 °C			
	PtCl ₂	PtCl ₄	H ₂ PtCl ₆	PtO ₂
IL-003 (imidazolium-based chloride)	Yes at 200 °C	Yes at 200 °C	Yes at 200 °C	Yes at 200 °C
IL-004 (imidazolium-based bisulfate)	Yes at 200 °C	Yes at 200 °C	Yes at 200 °C	Yes at 200 °C

IL-006 (imidazolium-based chloride)	Yes at 200 °C	Yes at 200 °C	Yes at 200 °C	Yes at 200 °C
IL-020 (pyridinium-based bisulfate)	Yes at 200 °C	Yes at 200 °C		No
IL-024 (heterocyclic cation-based bisulfate)	Yes at 200 °C	Yes at 200 °C		No
IL-037 (bipyrimidinium-based bisulfate)	Yes at 230 °C			

3.5 STABLE IONIC LIQUIDS FOR CATALYTIC METHANE CONVERSION

As one of the major accomplishments achieved during this project, we have synthesized/identified several classes of ionic liquids which are super stable under the typical harsh conditions for catalytic methane conversion. Table 3.9 summarizes the compatibility tests of the eight major classes of ionic liquids (including six PEER types). More valuable is that we have achieved some fundamental understandings on tailoring the compatibility of methane catalytic systems with ionic liquids, which has critical significance to developing the target low temperature efficient catalytic methane conversion systems.

Table 3.9: Summary of studied ionic liquids (ILs) in the application of catalytic conversion of methane to methanol

Type of IL	Source	Typical Example	Pt-catalyst Solubility	IL Stability in Pt/IL/H ₂ SO ₄ system	Applicable in CH ₄ conversion
Ammonium-based					
	Purchased	(CH ₃) ₃ N(C ₁₄ H ₂₉)Br	Insoluble		No
Phosphonium-based					
	Purchased	(CH ₃) ₃ P(C ₁₆ H ₃₃)Br	Insoluble		No
Imidazolium-based (PEER-1)					
	Purchased & Synthesized	IL-003 IL-004	Soluble	Good for a short time	Yes
Pyridinium-based (PEER-2)					
	Purchased & Synthesized	IL-020	Soluble	Good for a short time	Not effective
Bipyrimidinium-based (PEER-3)					
	Synthesized	IL-037	Soluble	Good for a short time	Yes

Pyrazinium-based (PEER-4):	Synthesized	IL-024	Soluble	Stable below 200 °C	Not effective
Triazolium-based (PEER-5)	Synthesized	IL-044	Soluble	Stable up to 220 °C	No reactivity
Pyrazolium-based (PEER-6)	Synthesized	IL-048 to IL-053	Soluble	Stable up to 220 °C	Yes

The major results from the compatibility tests can be summarized as below:

1) The compatibility (solubility and stability) of eight types of ionic liquids (ammonium-based, phosphonium-based, pyridinium-based, imidazolium-based, bipyridinium-based, pyrazinium-based, triazolium-based and pyrazolium-based) with concentrated sulfuric acid has been tested. All the cations are found to be stable but for anions (such as BF_4^- , PF_6^- , CF_3SO_3^- , HSO_4^- , CH_3SO_4^- and halide) only triflate (CF_3SO_3^-), bisulfate (HSO_4^-) and chloride (Cl^-) are stable.

2) Most inorganic Pt compounds (such as PtCl_2 , PtCl_4 , K_2PtCl_4 , H_2PtCl_6 and PtO_2) can be dissolved in PEER1 through PEER6 ionic liquids with HSO_4^- or Cl^- as their anion. Heating facilitates the dissolution process. Ammonium and phosphonium-based ionic liquids are poor solvents for Pt catalysts probably due to their poor coordination capability. These inorganic Pt compounds usually are insoluble or decompose in concentrated H_2SO_4 .

3) Pre-treated Pt species in ionic liquids can be dissolved in concentrated H_2SO_4 at room temperature to give a homogeneous ternary solution. Stability of ionic liquids themselves was tested in a low-pressure reactor. In the case of imidazolium-based ionic liquids, side chains (on 1 and 3 position) longer than methyl will be catalytically oxidized in the ternary systems. On the other side, this also indicated that these ternary systems are catalytically active in alkane oxidation.

4) Compatible ternary systems were applied to direct methane oxidation tests using high-pressure reactors. Though, pyridinium-based, pyrazinium-based and triazolium-based ionic liquids can dissolve Pt-based catalysts, the ternary systems in H_2SO_4 only showed negligible activity for methane conversion to methanol. Imidazolium-based ionic liquids have demonstrated excellent performance. However, imidazolium ring is not stable enough in the harsh environment for a long time. Ring opening (deep oxidation) was observed at the same time of methane oxidation to methanol. Pyrazolium-based ionic liquids turn out to be the most promising candidates for catalytic methane conversion since they possess not only excellent stability but also form catalytically active systems for methane conversion. .

6) Most ionic liquids, including those commercially available and home made, are miscible with methanol (CH_3OH) and are stable. Methanol in concentrated sulfuric acid exists as a mixture of free methanol (small part) and methyl bisulfate (CH_3OHSO_3) (large part), as determined from ^1H NMR in D_2SO_4 .

CHAPTER FOUR: Pt-CATALYST/IL/H₂SO₄ SYSTEMS

4.1 SUMMARY

So far, the most successful system for direct methane conversion is the Catalytic system discovered by Dr. Roy Periana et al. in late 90s, in which a platinum-based catalyst ((bpym)PtCl₂) enabled a high one-pass yield (>70%) and high selectivity (> 80%) of methane conversion at low temperatures (< 250 °C) in concentrated sulfuric acid. However, this technology suffers from several severe obstacles, including insufficient reaction rate, catalyst poisoning by water, high cost for product separation, high cost for the regeneration of concentrated sulfuric acid, and the environmental concerns for using concentrated sulfuric acid.

Our initial efforts on developing an efficient catalytic methane conversion system started from the Catalytica system. Upon addition of certain ionic liquids, we were not only able to dissolve most of Pt-catalysts to form homogenously catalytic system but also potentially modified/optimized the catalytic methane conversion chemistry through certain coordination introduced by ionic liquids. Several PEER systems (Pt-catalysts/ILs/Sulfuric Acid ternary systems) we have developed during this project presented much more superior performance compared to the Catalytica system in terms of higher reaction rate, longer catalysts lifetime and stronger resistance to water.

While developing the PEER systems, we have also investigated the possible functions of ionic liquids in these systems which will serve as the basis for our further discovering effective homogenously catalytic system for methane conversion with other transition metal catalysts, oxidants and reaction media.

4.2 C-H ACTIVATION

It has been generally accepted that the first step of the direct partial oxidation of methane to methanol is C-H bond activation. Periana *et al.* has showed that in deuterated sulfuric acid solution at 150 °C, the regular methane, CH₄, will exchange the protons with deuterium in the solvent to generate methane isotopes, CH_xD_{4-x} (x = 0 -3). Those systems presenting excellent performance in solubility and stability tests were further subjected to H/D exchange experiments, which served as a very important step for developing and optimizing the catalytic systems for methane conversion.

Table 4.1: Methane C-H activation in Pt/IL/ D₂SO₄ ternary systems monitored by H/D exchange at 150 °C for 2 hr in the 10 mL short reactor (Entries 1-13) and in the mini gold tube reactor (Entries 14-21)

Entry	Pt Catalyst	Ionic Liquid	Acid	[acid] (wt%)	Diluent (wt%)	Exchange Rate ([CH _x D _{4-x}]/[CH ₄])
1	(bpym)PtCl ₂	--	D ₂ SO ₄	98%	2% D ₂ O	3.6%
2	PtCl ₂	007-d ₅	D ₂ SO ₄	98%	2% D ₂ O	2.6%

3	PtCl ₂	004-d ₅	D ₂ SO ₄	98%	2% D ₂ O	4.0%
4	PtCl ₂	009-d ₄	D ₂ SO ₄	98%	2% D ₂ O	3.5%
5	PtCl ₄	004-d ₅	D ₂ SO ₄	98%	2% D ₂ O	3.9%
6	(bpym)PtCl ₂	--	D ₂ SO ₄	94%	6% D ₂ O	3.1%
7	PtCl ₂	007-d ₅	D ₂ SO ₄	94%	6% D ₂ O	2.3%
8	PtCl ₂	004-d ₅	D ₂ SO ₄	94%	6% D ₂ O	3.7%
9	PtCl ₂	024-d ₆	D ₂ SO ₄	70%	2% D ₂ O 28% IL	Non-detectable
10	PtCl ₂	043-d ₅	D ₂ SO ₄	70%	2% D ₂ O 28% IL	Non-detectable
11	PtCl ₂	004-d ₅	D ₂ SO ₄	50%	2% D ₂ O 48% IL	Detectable but small
12	(NH ₃) ₂ PtCl ₂	004-d ₅	D ₂ SO ₄	50%	2% D ₂ O 48% IL	Detectable but small
13	(bpym)PtCl ₂	004-d ₅	D ₂ SO ₄	50%	2% D ₂ O 48% IL	Detectable but small
14	(bpym)PtCl ₂	--	D ₂ SO ₄	98%	2% D ₂ O	19.9%
15	PtCl ₂	007-d ₅	D ₂ SO ₄	98%	2% D ₂ O	17.1%
16	PtCl ₂	004-d ₅	D ₂ SO ₄	98%	2% D ₂ O	26.0%
17	(bpym)PtCl ₂	--	D ₂ SO ₄	94%	6% D ₂ O	23.6%
18	PtCl ₂	007-d ₅	D ₂ SO ₄	94%	6% D ₂ O	8.8%
19	PtCl ₂	007-d ₅	D ₂ SO ₄	90%	2% D ₂ O + 8% IL	9.3%
20	(NH ₃) ₂ PtCl ₂	007-d ₅	D ₂ SO ₄	90%	2% D ₂ O + 8% IL	16.4%
21	PtCl ₂	007-d ₅	D ₂ SO ₄	70%	2% D ₂ O + 28% IL	8.3%

Table 4.1 presents some methane C-H activation experiments on different Pt species, e.g., PtCl₂, PtCl₄, (NH₃)₂PtCl₂ and (bpym)PtCl₂ and varied D₂SO₄ concentration (98% and 94%) as well as on diluting D₂SO₄ with large amount of ionic liquids, say, 50 wt%. Pt catalyst concentration was about 50 mM. The dilution of acid is achieved by adding D₂O or deuterated ionic liquids. Deuterated ionic liquids were synthesized through H/D exchange between the regular ones and D₂SO₄. The short reactor was loaded

with 1 mL reaction liquid and 500 psi CH₄, followed by heating at 150 °C for 2 hours. The gold tube was loaded with 0.3 mL reaction liquid and 50 psi CH₄ (with 3% Ar as the internal standard). The gas phases after reaction were introduced into a HP 6890+ GC system with a mass selective detector (MSD). The total amount of methane was deduced from the internal standard Ar integration. The methane isotopomers were identified from their characteristic ion masses such as 20 for CD₄, 19 for CHD₃, 18 for CH₂D₂, and 17 for CH₃D.

The different exchange rates achieved from the similar experiments conducted with the Short reactor and the mini gold tube reactor were mainly caused by the different amounts of total methane gas loaded. However, the trends on C-H activation variations corresponding to different system compositions are the same indicated by experiments with the two types of reactors. Basically all systems exhibited a similar or higher H/D exchange rate and water content increasing from 2% to 6% seemed not to severely affect the rate. When using ionic liquids to dilute the sulfuric acid, we gradually increased the amount of ionic liquids in sulfuric acid from 6% to 28% to 50%. The overall trend for Pt reactivity in methane activation is quite clear: decrease with adding more ionic liquids.

A few other phenomena are also worth discussing. First is the C-H activation through a Pt(IV) metal center. Though the Periana paper indicated that Pt(II) was the species to activate methane and Pt(IV) to oxidize, we demonstrated that Pt(IV)/IL/D₂SO₄ system was highly active at 150 °C. Second, PEER-4 type ionic liquid systems resulted in non-detectable H/D exchange. Instead, appreciable amount of CO₂ and SO₂ was observed which was a strong sign of deep methane oxidation.

4.3 METHANE OXIDATION TO METHANOL

Methane oxidation to methanol is our target reaction for this project. The oxidation experiments were conducted with systems having good compatibility. We have successfully developed several Pt-catalyst/IL/H₂SO₄ ternary catalytic systems, the so-called PEER systems which present superior performance to the Catalytica system in terms of reaction rates, catalysts lifetime and water tolerance.

Upon observations of methanol/ methyl bisulfate from GC and NMR analysis, we first confirmed that the products were indeed generated from methane, not the ionic liquids added in the system. In cases of using methylated imidazolium-based ionic liquids as the solvent for platinum catalysts, one may argue that the product methylbisulfate is possibly from the dissociation of the methyl group from the imidazole ring. So we conducted the methane oxidation test using a pure ¹³CH₄ instead of the normal ¹²CH₄ with PtCl₂ and IL-004. Figure 4.1 clearly showed that the majority of methylbisulfate was ¹³CH₃HSO₄ (> 95%). This proves that the product is almost exclusively from the oxidation of the methane gas.

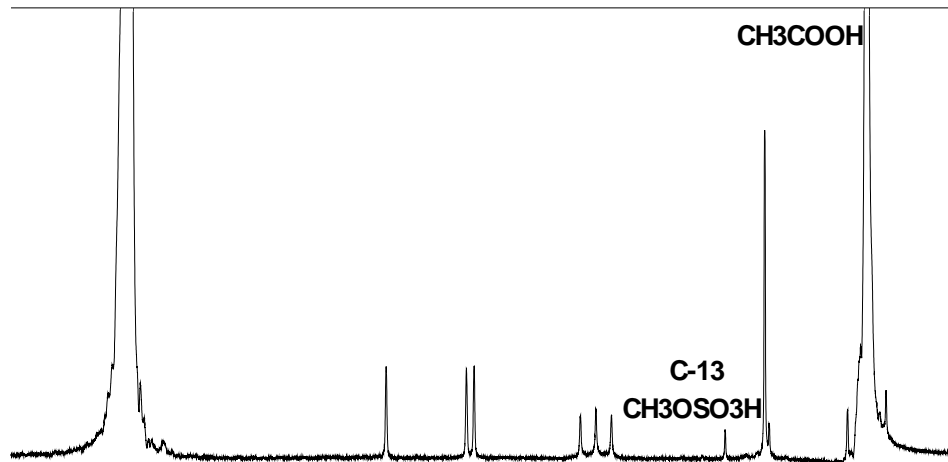


Figure 4.1: ^1H NMR spectra from the liquid of Carbon-13 methane oxidation test using PtCl_2 and IL-004.

Extensive methane oxidation experiments have been conducted with some highlighted results listed in

Table 4.2,

Table 4.3 and Figure 4.2. These results can be briefly summarized as below:

1) Almost all Pt-compounds tested ($(\text{bpym})\text{PtCl}_2$, PtCl_2 , K_2PtCl_4 , PtCl_4 , PtO_2 , and H_2PtCl_6) can be dissolved in concentrated H_2SO_4 and present some activity on methane oxidation given the appropriate ionic liquid addition.

2) Among those stable ionic liquids synthesized at PEER, the pyridinium-based, pyrizinium-based and triazolium-based ionic liquids did not make active systems for direct methane oxidation to methanol, but the imidazolium-based ionic liquids have demonstrated excellent performance.

3) Systems containing no Cl^- were found not active, which might be attributed to the coordination chemistry between Pt and Cl^- during the methane conversion process.

4) In 96% H_2SO_4 , several PEER (Pt/IL/ H_2SO_4) systems showed comparable or much better reactivity than the Catalytica system.

5) Although, dilution of H₂SO₄ lowered the reactivity on C-H activation and methane to methanol conversion of both the PEER systems and the Catalytica system, the application of ionic liquids significantly improved the water tolerance of the PEER systems.

Table 4.2: Catalytic oxidation of methane to methanol in 96% H₂SO₄^a.

Entry	Catalyst	Ionic Liquid ^b	Temp. (°C)	CH ₃ OH (mM) ^c	TON
1	(bpym)PtCl ₂		220	31	0.6
2	(bpym)PtCl ₂	[im][Cl]	220	26	0.5
3	PtCl ₂	[1-mim][Cl]	220	173	3.5
4	PtCl ₂	[im][Cl]	220	100	2.0
5	PtCl ₂	[mmim][HSO ₄]	220	73	1.5
6	K ₂ PtCl ₄	[1-mim][Cl]	220	105	2.1
7	PtCl ₄	[1-mim][Cl]	220	89	1.8
8	PtO ₂	[im][Cl]	220	52	1.0
9	PtO ₂	[1-mim][HSO ₄]	220	0	0
10	H ₂ PtCl ₆	[1-mim][Cl]	220	157	3.1
11	PtCl ₂	[pyrid][HSO ₄]	220	1	~ 0
12	PtCl ₂	[pyraz][HSO ₄]	200	42	0.8
13	PtCl ₂	[1-mpyraz][HSO ₄]	200	79	1.6
14	PtCl ₂	[mmpyraz][HSO ₄]	200	94	1.9
15	PtCl ₂	[triaz][HSO ₄]	200	0	0

^a Reaction conditions: 0.05 mmol Pt species + 0.3 mmol IL + 1 mL 96% H₂SO₄ + 3.4 MPa CH₄ in a 69 mL reactor at a temperature for 2.5 hr. ^b IL: im = imidazolium; 1-mim = 1-methylimidazolium; mmim = 1,3-dimethylimidazolium; pyrid = pyridinium; pyraz = pyrazolium; 1-mpyraz = 1-methylpyrazolium; mmpyraz = 1,2-dimethylpyrazolium; triaz = 1,2,4-triazolium. ^c The methanol concentration was determined from ¹H NMR, which was the sum of free or protonated methanol, and

the ester (CH₃OSO₃H).

Table 4.3: Effects of water concentration in different catalyst systems on methane C-H activation and oxidation to methanol

Entry	System	Activation at 150 °C ^a		Oxidation at 200 °C ^b	
		[CH _x D _{4-x}] (mmol)	TON	[CH ₃ OH] (mmol)	TON
1	(bpym)PtCl ₂ + 2% water	0.367	7.35	0.047	0.94
2	(bpym)PtCl ₂ + 6% water	0.276	5.51	0.016	0.31
3	PtCl ₂ + [1-mim][HSO ₄] + 2% water	0.480	9.60	0.065	1.31
4	PtCl ₂ + [1-mim][HSO ₄] + 6% water	0.420	8.39	0.037	0.73

^a H/D exchange occurred between CH₄ and deuterated liquid media D₂SO₄, D₂O and [1-mim-d₄][DSO₄]. TON was determined from the gas analysis for methane isotopomers by GC-MS. Reaction conditions: 0.05 mmol Pt(II) + 0.3 mmol IL + 1 mL D₂SO₄ + 3.4 MPa CH₄ in a 15 mL reactor; 150 °C, 2.0 hr. ^b Tests were performed using non-deuterated liquid media. Reaction conditions were the same as those in Table 1.

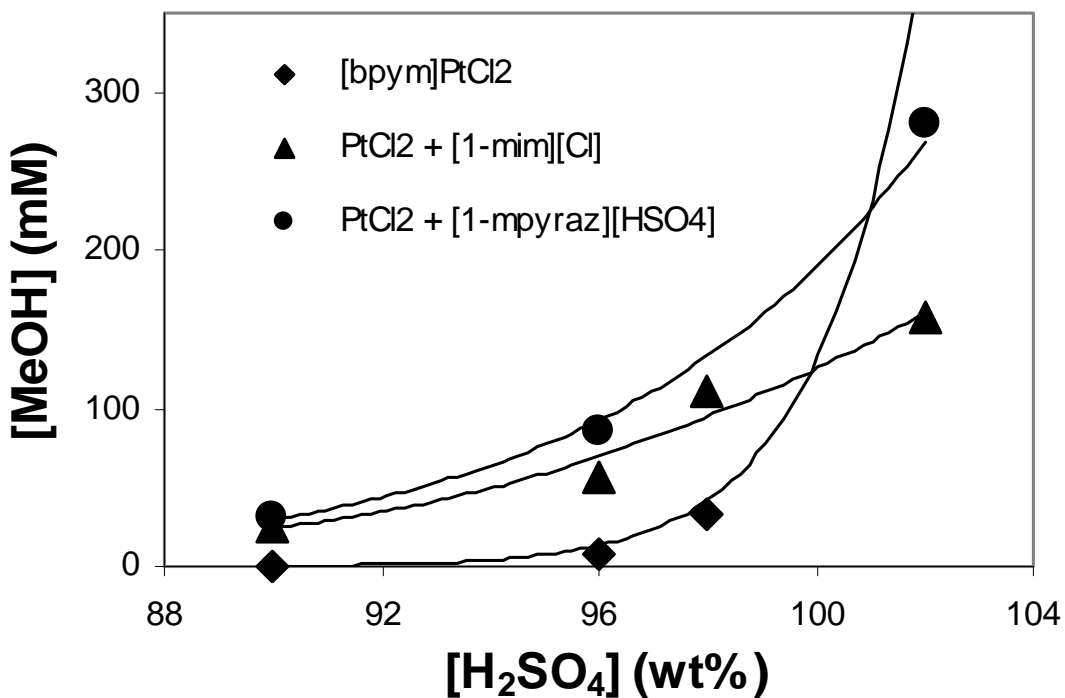


Figure 4.2: Methanol yield as a function of the concentration of H₂SO₄ (reaction conditions: 200 °C, 2.5 hr). The methanol concentration from the Catalytica reaction in 2% oleum was 600 mM and was not indicated in the plot.

4.4 ROLES OF IONIC LIQUIDS IN METHANE ACTIVATION & OXIDATION

During the process of developing PEER systems for efficient methane to methanol conversion, we have also built-up of our preliminary knowledge on the major roles of ionic liquids corresponding to the nature of the cations:

(1) **Dissolution media:** Six types of ionic liquids all can performance this function. Virtually any Pt compounds, as well as many other transition metal (e.g., Ru, Rh, Os, Ir, Au, etc.) compounds, can be dissolved in ionic liquids upon heating. The initial dissolution is believed to be via anion coordination.

(2) **Promotion of Pt reactivity in catalysis:** The Pt reactivity has been found to be very much related to the ionic liquids used. First, cation ring structure difference matters most. For example, imidazolium and pyrazolium-based ionic liquids can catalyze methane to methanol conversion at a higher rate than the Catalytica reaction in 96% H₂SO₄, while triazolium-based ionic liquids gave zero methanol production. Second, the variations on a same ring structure also modifies the Pt reactivity, which was verified by the no methyl, 1-methyl and 1,3-dimethyl imidazolium-based ionic liquid cases.

(3) **Co-solvent and interaction with other solvents:** Using ionic liquids dilutes sulfuric acid or any other solvent. This modifies the whole system's acidity and oxidizing

power. Furthermore, ionic liquids sometimes react with H_2SO_4 . For example, in the case of imidazolium-based ionic liquids, the ring structure can not sustain for a long time in the presence of Pt. Deep decomposition to CO_2 has been observed. In the case of pyrazolium-based ionic liquid, though there is no ring decomposition, structure modifications such as sulfonation or dimerization are proposed. We have found that ring structure changes had an adverse affect on the Pt reactivity. On the other hand, this gives us clues to design new stable ionic liquids, such as nitrated, sulfonated, or dimerized PEER-6 type ionic liquids.

(4) **Catalysis of other chemical reactions:** One good example is about the pyrazinium-based ionic liquids. Upon the formation of methyl bisulfate, it will be quickly converted to CO_2 due to the catalysis of this ionic liquid itself. A complete catalytic route can be described as: Step 1: C-H bond activation through the Pt(II) metal center; Step 2: oxidation through the Pt(IV) metal center; Step 3: functionalization of the methyl to methylbisulfate; Step 4: methylbisulfate was quickly converted to IL-025; Step 5: methyl group on IL-025 was quickly oxidized to CO_2 and IL-025 goes back to IL-024.

(5) **Probe for monitoring catalyst reactivity:** We have found for a long time that [bmim] cation are good substrate for studying the C-H bond activation by monitoring the H/D exchange between a regular butyl group ($-\text{CH}_2\text{CH}_2\text{CH}_2\text{CH}_3$) and deuterated solvent such as D_2SO_4 . It serves as dissolution media for Pt catalysts and is compatible with other solvents so there is no worry about solubility issue.

(6) **Reduction of product separation cost:** Methanol is miscible with most ionic liquids, so it is possible to use ionic liquids to extract methanol out from a specific system. But this procedure awaits a more powerful catalytic system.

Here we report a group of experiments using $(\text{NH}_3)_2\text{PtCl}_2$, imidazolium-based ionic liquids and concentrated acetic acid (with 10 wt% water), through which we can understand the multiple roles of ionic liquids in C-H activation.

Acetic acid vaporizes at temperatures above $120\text{ }^\circ\text{C}$ and severely corrodes steel parts. Stainless steel reactors even with gold plating were not convenient as gas/liquid mixing would be big challenge. We thus decided to use the mini gold tube reactor. The mini gold tube has a total volume of about 1 mL, 50% of which is loaded with reaction liquids and the remaining space can be filled with methane (CH_4 with 3% Ar) or flushed with Ar. Arc welding is used for sealing at both ends. Sealed tubes are placed in a stainless steel vessel to which an external hydraulic pressure of up to 3700 psi will be applied. Then the vessel is heated in a box furnace at $200 - 250\text{ }^\circ\text{C}$ for four hours. The weight of each gold tube is recorded before and after reaction and usually the mass difference is no more than 0.1 mg. Gas phases are analyzed using GC-MS and liquid phase is by ^1H NMR. Usually the Pt catalysts were used as 20 mM and first dissolved in 200 mM ionic liquid. Then the prepared Pt/IL mixture was dissolved in 1 mL deuterated acetic acid and D_2O solution at room temperature. As usual, H/D exchange rates were determined from ^1H NMR peak integration for [bmim] and from GC-MS for methane isotopomers.

Experiment 1: [bmim][CH₃COO] was used as the model compound. (NH₃)₂PtCl₂ was heated in this ionic liquid at 150 °C for 30 minutes and then was soluble in CD₃COOD-D₂O solution. H/D exchange occurred readily at 250 °C as evidenced by the butyl group peak intensity drop in ¹H NMR.

Experiment 2: [1-mim][Cl] was used as the dissolution media for (NH₃)₂PtCl₂ at 200 °C for 30 minutes. We tried to monitor the H/D exchange at 250 °C between CH₄ and deuterated solvents by GC-MS. Unfortunately, no measurable exchange was observed.

Experiment 3: [1-mim][HSO₄] was used as the dissolution media for (NH₃)₂PtCl₂ at 200 °C for 30 minutes. Once again, we did not see measurable amount of methane isotopomers.

A few conclusions can be drawn through this set of parallel experiments. (1) Ionic liquids serve as dissolution media for Pt catalysts, but the processing temperature largely depends on the length of the side chains, e.g., 1-butyl-3-methyl (150 °C) vs. 1-methyl (200 °C). (2) The coordination chemistry of ionic liquids plays a decisive role in catalysis. Here the acetate-ligated Pt seems to be active, while Cl or HSO₄-ligated Pt was inactive. (3) The inertness of butyl group might be quite different from that of methane.

One straightforward experiment for next step would be to test [1-mim][CH₃COO] ionic liquid.

CHAPTER FIVE: CATALYTIC SYSTEMS FOR METHANE CONVERSION

5.1 SUMMARY

One of the major functions of applying ionic liquids in homogeneously catalytic methane conversion systems is to employ their super dissolving power to greatly enlarge the candidate pool for each component: catalysts, oxidants and reaction media, because most of the transition-metal based compounds which are promising effective catalysts for methane conversion are insoluble to normal acid or base media. During this project, we have successfully developed several Pt-catalyst/ Concentrated sulfuric acid/ Ionic liquid catalytic systems for efficient and selective low temperature methane conversion, which present greatly improved performance compared to the Periana-Catalytica system in terms of reaction rate, catalyst lifetime and water tolerance. These optimized catalytic systems elaborate the success of this multi-year project and will serve as a promising start point for our future efforts on achieving a commercially viable methane utilization technique to solve the nation's energy crisis and to provide alternative hydrocarbon chemical feedstocks for the nation's chemical industry.

Table 5.1 summarizes the various candidates of the system component we have investigated. The combinations of the yellow-shaded ones are the currently optimal systems. In the following sections, we will explain in details of the optimization of each category.

Table 5.1: Summary of candidates for each component of the catalytic system for direct methane conversion tested with the systems with optimized performance shaded in yellow.

Catalyst	Ionic Liquid	Solvent	Oxidant
Pt-based	Imidazolium-based Pyrazolium-based (Bi)Pyridinium-based Pyrazinium-based	sulfuric acid (concentrated and diluted); hydrochloric acid, acetic acid (pure and concentrated)	sulfuric acid (concentrated) K ₂ PtCl ₆ FeCl ₃ CuCl ₂ V ₂ O ₅ CeO ₂ (NH ₄) ₂ Ce(NO ₃) ₆ H ₂ SeO ₄
Os-based	Bi-diazine-based		
Ru-based	1,2,4-triazolium-based		
Re-based	Ammonium-based	triflic acid	
Ir-based	Phosphonium-based with anion of HSO ₄ ⁻ , Cl ⁻ or Br ⁻ and NH ₄ HSO ₄	trifluoroacetic acid basic solution pure water	

5.2 OXIDANTS

Our experimental and theoretical work proposes that the effective oxidizing species in the Periana system and the PEER system is actually SO_3 instead of SO_4^{2-} which might be a possible reason for the sulfuric acid concentration dependence of the system performance. Figure 5.1 shows the calculated temperature dependence of the amounts (in mole) of SO_3 in 100 mg of sulfuric acid solutions with different concentrations. Clearly, at above 200 °C, the amount of SO_3 decreases dramatically upon the sulfuric acid concentration.

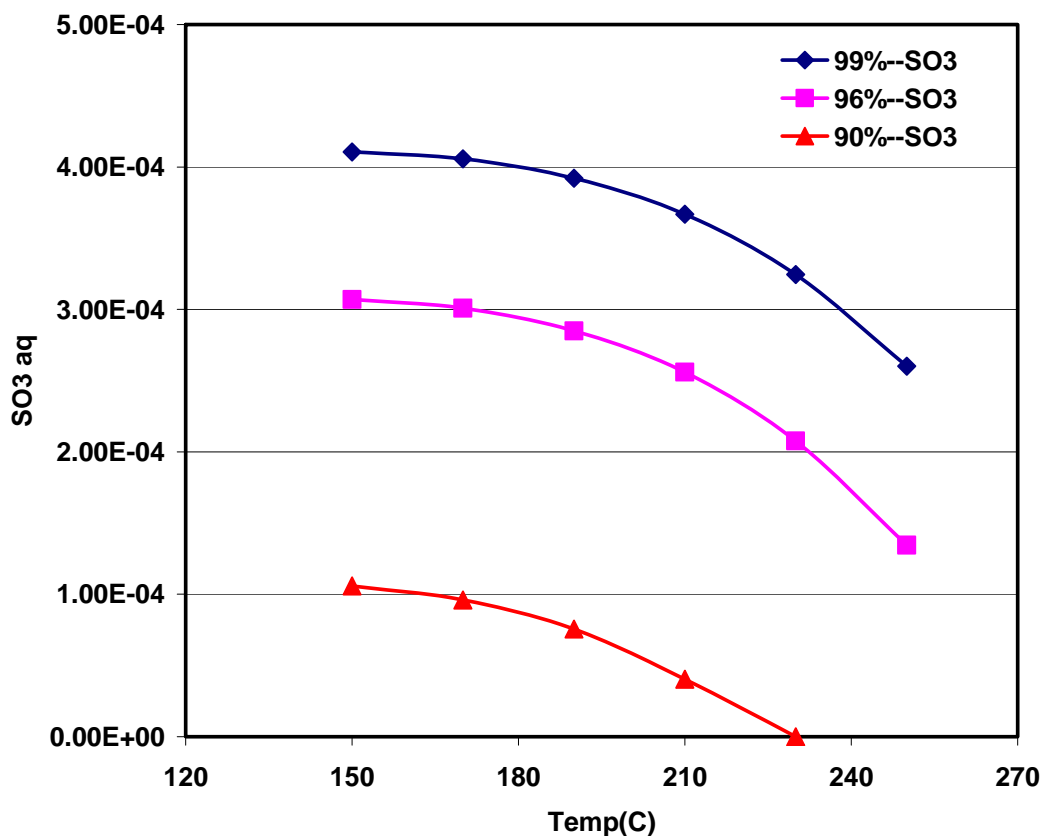


Figure 5.1: Temperature dependence of the calculated amounts (in mole) of SO_3 in 100 mg of sulfuric acid solutions with different concentrations.

Using concentrated sulfuric acid as the oxidant automatically assures the high selectivity of the methane oxidation, because the oxidized product methyl bisulfate is more stable than methane in this system. However, utilization of concentrated sulfuric acid also brings concerns on reactor cost and operation cost as well as environment damage. Search for alternative oxidants which are effective yet cheap has not been conducted intensively. Three criteria have been established for the screening: (1) the redox potential of the new oxidant is higher than sulfuric acid; (2) redox cycle of the new oxidant is relatively easy and inexpensive; and (3) new oxidants need to be compatible with ionic liquids, Pt-based catalysts and diluted sulfuric acid.

Table 5.2 summarized the compatibility tests we have conducted. Ce(IV), Cu(II) and V(V) seem to meet those criteria and the solubility of their compounds such as CeO₂, (NH₄)₂Ce(NO₃)₆, CuCl₂, and V₂O₅ was studied in both sulfuric acid and ionic liquids. Hydrogen peroxide is a strong oxidizer, but it is not compatible with Pt catalysts. In fact, we also tested selenic acid (H₂SeO₄), which turned out too strong so that over-oxidation occurred with a large amount of CO₂ generation.

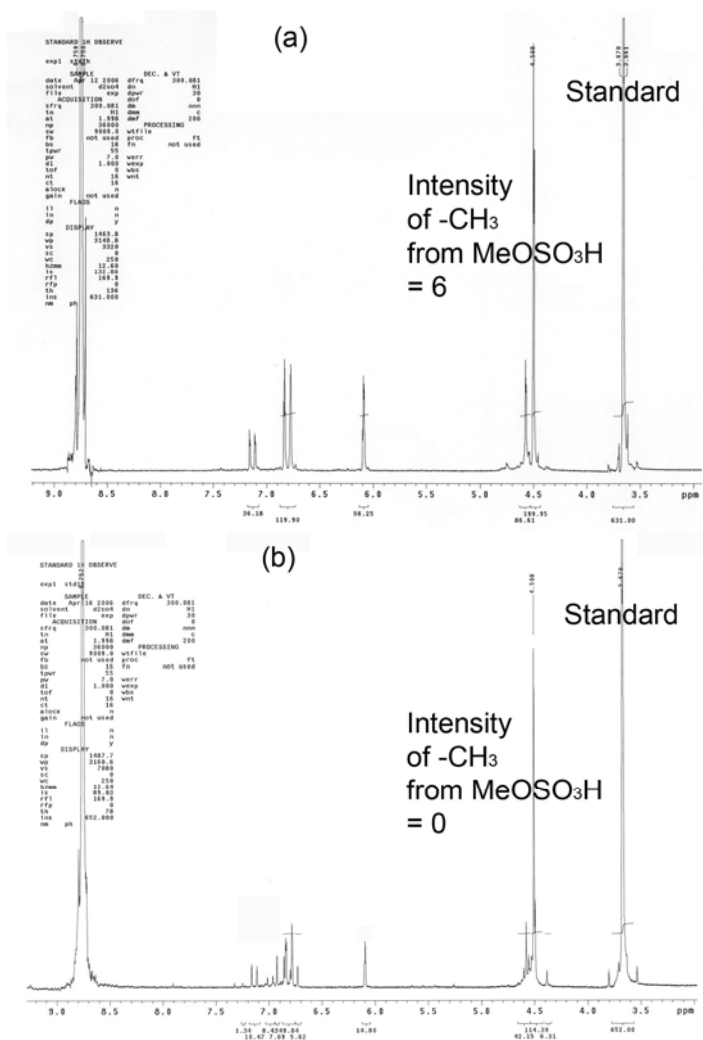
Table 5.2: Compatibility tests for new oxidants potentially used for partial oxidation of methane to methanol.

Oxidant	Solvent	Treatment Conditions	Solubility	Compatibility in a Catalytic system
CeO ₂	96% H ₂ SO ₄	90 °C 1 hr	Low, a lot of precipitates	Not compatible
CeO ₂	IL-024	95 °C 1 hr	Insoluble	Not compatible
(NH ₄) ₂ Ce(NO ₃) ₆	96% H ₂ SO ₄	90 °C 1 hr	Low, a lot of precipitates	Not compatible
(NH ₄) ₂ Ce(NO ₃) ₆	IL-024	100 °C 15 min	Soluble	Not compatible with H ₂ SO ₄
CuCl ₂ ·2H ₂ O	96% H ₂ SO ₄	90 °C 1 hr	Low, a lot of precipitates	Possibly compatible
CuCl ₂ ·2H ₂ O	IL-024	95 °C 1 hr	Soluble	Possibly compatible
CuO	[bmim][Cl]	Heating upon the IL melts	Soluble	Not compatible as [bmim] is not stable
CuO	IL-024	95 °C 1 hr	Insoluble	Not compatible
H ₂ O ₂	--	Pt black and PtCl ₂ and PtO ₂	Insoluble	Not compatible as H ₂ O ₂ is not stable
V ₂ O ₅	[bmim][Cl]	150 °C 30 min	Soluble	Not compatible as [bmim] is not stable
V ₂ O ₅	IL-004	150 °C 30 min	Soluble, dark red solution	Compatible with H ₂ SO ₄
V ₂ O ₅	96% H ₂ SO ₄	150 °C 15 min	Soluble, read solution	Compatible with IL and Pt catalysts

Vanadium oxide was both soluble in the acid and ionic liquids and thus was subjected to further study such as methane activation and oxidation. We started with PtCl₂, 10 wt% ionic liquid and 90 wt% H₂SO₄ (initial concentration 102%), which were processed to give a homogeneous solution. K₂SeO₄ and V₂O₅ were used as new oxidants to enhance the oxidizing power. The product yields, in the form of methylbisulfate, from these runs were determined from ¹H NMR (Figure 5.2).

The blank run (without new oxidant), Figure 5.2 (a), only resulted in less than 1 turnover number amount of methanol. K_2SeO_4 is a strong oxidant when it is dissolved in concentrated H_2SO_4 as selenic acid (H_2SeO_4) will be formed. Unfortunately, this oxidant seemed too strong. Figure 5.2 (b) showed that there was nearly zero methanol formed. On the other hand, gas analysis for this run indicated a large amount of CO_2 , implying methane was over-oxidized. V_2O_5 is also a strong oxidant and is soluble in concentrated sulfuric acid. This system was eventually successful in catalyzing methane up to 4 turnover numbers with negligible CO_2 emission (Figure 5.2 (c)).

Therefore, we have performed the proof-of-concept work. At least 10 wt% of PEER-6 type ionic liquids can be incorporated into concentrated sulfuric acid. With the aid of more powerful oxidants, the catalytic systems are able to efficiently convert methane to methanol (in the form of methylbisulfate) at a high selectivity. Nevertheless, there are still quite a few issues that need to be solved, such as how to recycle the oxidant, how to separate the methanol from the reaction media, and how to improve the efficiency.



have observed catalytic capability on C-H activation in all other solvents primarily catalyzed by certain Pt-based catalysts. However, other than using concentrated sulfuric acid as the oxidant, alternative oxidants are required for systems with other solvents. A partially oxidized product which can survive in the catalytic system without being further oxidized to CO₂ becomes the major concern if possessing enough oxidation power. Besides the systems relying on the utilization of concentrated sulfuric acid, another very promising methane conversion system developed is the High-Temperature Shilov system. In this system, the reaction media is milder (hydrochloric acid) and the oxidants can be cheap compounds of Cu and Fe. Thus, this system has great potential of becoming the improved to a cost-effective as well as environment-friendly methane conversion technique. We will present our findings on this system in details in the following chapter.

5.3.1 Acetic Acid

Acetic acid (AcOH) is an excellent polar protic solvent and has been extensively used for chemical reactions, such as in the production of terephthalic acid (TPA) (a raw material for polyethylene terephthalate (PET)), and in Friedel-Crafts alkylation, to name a few. In the application of homogeneous catalysis for C-H bond activation, acetic acid and/or its aqueous solutions have also widely used as reaction media² With all the knowledge combined, we evaluated the possibility of applying ternary systems of Pt/ILs/AcOH to C-H activation and methane oxidation.

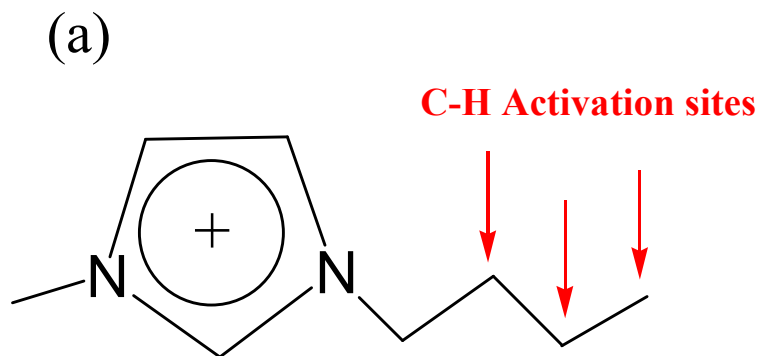
Similar to the sulfuric acid system, the compatibility between ionic liquids, Pt-based catalysts, and acetic acid was the first thing we need to study (Table 5.3).

Table 5.3: Compatibility studies of Pt/ILs/AcOH systems. The concentration of Pt species was 12.5 mM. AcOH was added as 1 mL.

Ionic Liquid	Pt Species	Molar Ratio	Treatment Temp. (°C)	Soluble in AcOH at R. T.?
[bmim][Cl] (PEER-1)	PtCl ₂	≥ 6:1	180-200	Yes
	K ₂ PtCl ₄	≥ 6:1	200	Yes
	PtCl ₄	≥ 6:1	200	Yes
	H ₂ PtCl ₆	≥ 6:1	200	Yes
[bmim][CH ₃ COO] (PEER-1)	PtCl ₂	10:1	200	Yes; also soluble in 10 wt% H ₂ O
	(bpym)PtCl ₂	10:1	200	Yes
	PtCl ₄	≥ 6:1	200	Yes
IL-003 (PEER-1)	PtCl ₂	6:1	≤ 200	No

	K_2PtCl_4	6:1	200	Very little
	$PtCl_4$	6:1	200	Very little
	$PtCl_2$	20:1	200	Yes
	K_2PtCl_4	20:1	200	Yes
IL-004 (PEER-1)	$PtCl_2$	6:1	≤ 200	No
	K_2PtCl_4	6:1	200	Very little
	$PtCl_4$	6:1	200	Very little
	$PtCl_2$	20:1	200	Yes
	$PtCl_4$	20:1	200	Most
IL-050 (PEER-6)	Any Pt	6:1	200	No
	$PtCl_2$	20:1	200	Very little

As shown in Table 5.3, the compatibility of pre-treated Pt/ILs in AcOH depends on a number of factors: (1) the treatment temperature. It seems that most Pt/ILs systems need to be heated above 180 °C to enable a complete dissolution in AcOH at room temperature. (2) the cation nature of ionic liquids. PEER-6 type ionic liquid systems seem more difficult in terms of solubility in AcOH than the PEER-1 type ionic liquid systems. (3) alkyl groups attached to an ionic liquid ring also make a remarkable difference on solubility. 1-butyl-3-methylimidazolium chloride readily dissolves most Pt species at the ratio of 6:1 at 200 °C, but ionic liquids with shorter chains such as IL-003/004 need a ratio of 20:1. On the contrary, the nature of Pt species, such as $PtCl_2$ vs. $PtCl_4$, has less impact on the solubility. Mechanistic understanding for these observations is currently under investigation.



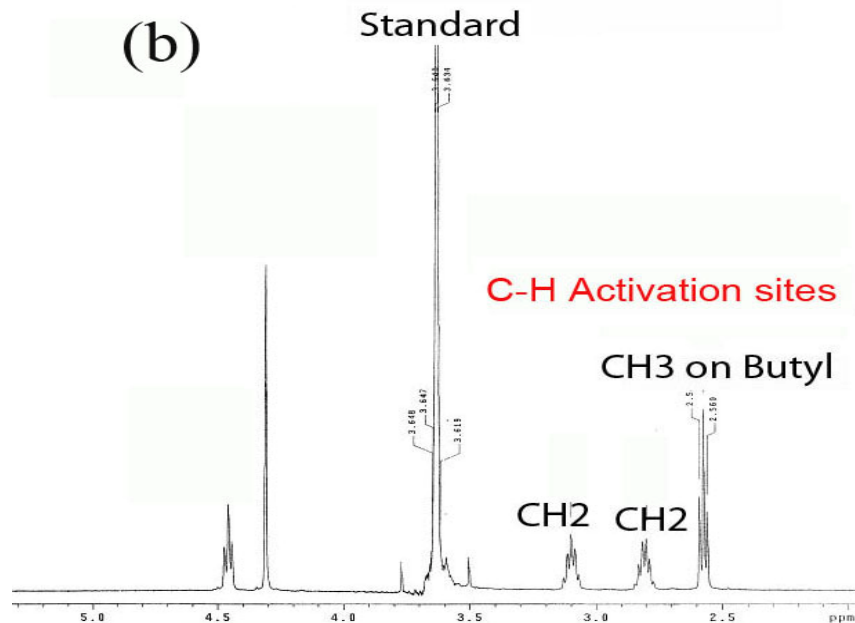


Figure 5.3: Possible sites in an ionic liquid containing [bmim] as the cation for C-H activation that are similar to methane C-H bonds. (a) Schematic structure; and (b) ^1H NMR spectrum.

Also demonstrated in Table 5.3 is that we have successfully identified a few compatible ternary systems of Pt/ILs/AcOH, such as $\text{PtCl}_2/[\text{bmim}][\text{CH}_3\text{COO}]/\text{AcOH}$. Next steps include the stability tests for these systems and eventually the catalytic reactivity tests for methane oxidation. Stability of ionic liquids themselves in a catalytic system is a major challenge considering that methane is one of the most inert hydrocarbons. In Pt/ILs/ H_2SO_4 systems, Sulfuric acid plays roles of reaction media and oxidant simultaneously, but in AcOH systems we expect no oxidation would occur due to the lack of oxidant. One convenient way to evaluate the stability is then to measure the H/D exchange between a regular ionic liquid and deuterated acetic acid. This strategy has actually been applied to the Pt reactivity studies in Pt/ILs/ H_2SO_4 systems where [bmim] ionic liquid was used as a model compound for oxidation. Here in AcOH systems, we use [bmim] ionic liquid as the model compound for C-H activation. Possible activation sites that are similar to methane C-H bonds are illustrated in Figure 5.3(a) and (b).

C-H bond activation of alkanes by Pt species in acetic acid might start from a temperature as low as $100\text{ }^\circ\text{C}$, but our experiments showed that significant H/D exchange only started at temperatures above $180\text{ }^\circ\text{C}$. Considering the boiling point of acetic acid is below $120\text{ }^\circ\text{C}$, an appropriate reactor is desired that can sustain high pressure vapor and keep part of acetic acid as liquid at higher temperatures. Characterization after H/D exchange was performed with ^1H NMR in D_2SO_4 . Decrease in peak integration indicates deuterium replacement for hydrogen (Figure 5.3 (b)).

Similarly, with [bmim] ionic liquid as the model compound, C-H activation in different Pt/ILs/AcOH systems was investigated as summarized in Table 5.4. Usually the Pt catalysts were used as 20 mM and first dissolved in 200 mM ionic liquid

([bmim][CH₃COO]). Then the prepared Pt/IL mixture was dissolved in 1 mL deuterated acetic acid (or its aqueous solution) at room temperature. H/D exchange rates can be determined from ¹H NMR peak integration.

Table 5.4: C-H bond activation of the butyl group in [bmim] ionic liquid via H/D exchange in Pt/IL/AcOH-d₄ systems at 250 °C.

Pt species + IL	Reaction Media	C-H Activation Site	H/D Exchange Rate (%)			
			0	4 hr	12 hr	20 hr
PtCl ₂ + [bmim][AcO]	CD ₃ CO ₂ D	-CH ₂ -CH ₂ -CH ₃	100	25	33	39
		-CH ₂ -CH ₂ -CH ₃	100	19	29	34
		-CH ₂ -CH ₂ -CH ₃	100	12	22	25
PtCl ₂ + [bmim][AcO]	CD ₃ CO ₂ D + D ₂ O (10 wt%)	-CH ₂ -CH ₂ -CH ₃	100	40		
		-CH ₂ -CH ₂ -CH ₃	100	31		
		-CH ₂ -CH ₂ -CH ₃	100	25		
PtCl ₄ + [bmim][AcO]	CD ₃ CO ₂ D	-CH ₂ -CH ₂ -CH ₃	100	21		
		-CH ₂ -CH ₂ -CH ₃	100	18		
		-CH ₂ -CH ₂ -CH ₃	100	13		

The most remarkable observation from Table 5.4 is the ternary system of PtCl₂/IL/AcOH-d₄ catalyzed much more H/D exchange in aqueous solution of CD₃CO₂D + D₂O than in pure CD₃CO₂D. In other words, Pt reactivity is actually promoted by the presence of water. This is in sharp contrast to the Pt/IL/H₂SO₄ systems where Pt catalysts would be poisoned by trace amount of water due to the ground state effect. Also worth noting is the comparison between PtCl₂ and PtCl₄. The preliminary data suggest that both Pt(II) and Pt(IV) can activate C-H bond activation at a similar rate. Therefore, we expect different C-H activation mechanisms for Pt/IL/AcOH aqueous systems.

5.3.2 Triflic Acid

Triflic acid (CF₃SO₃H) is known as a superacid and its acidity is about a thousand times stronger than 100% sulfuric acid, but it is of little oxidizing power comparing with a concentrated H₂SO₄. We dissolved the Periana catalyst, (bpym)PtCl₂, into a mixed acid solution (0.5 mL 96% H₂SO₄ and 0.5 mL CF₃SO₃H) which has higher acidity and half water concentration comparing with 1 mL 96% H₂SO₄. Methane oxidation experiments were conducted using the mini gold tube and the results of ¹H NMR for each liquid phase were presented in Figure 5.4.

The methanol yield of the mixed acid case (Figure 5.4 (b)) was about twice higher than the H₂SO₄ case (Figure 5.4 (a)). Considering the water concentration drops half and the acidity increases many times, we tend to confirm that water (either bonding with Pt or reducing the oxidizing power of SO₃) is the major cause for the catalyst deactivation.

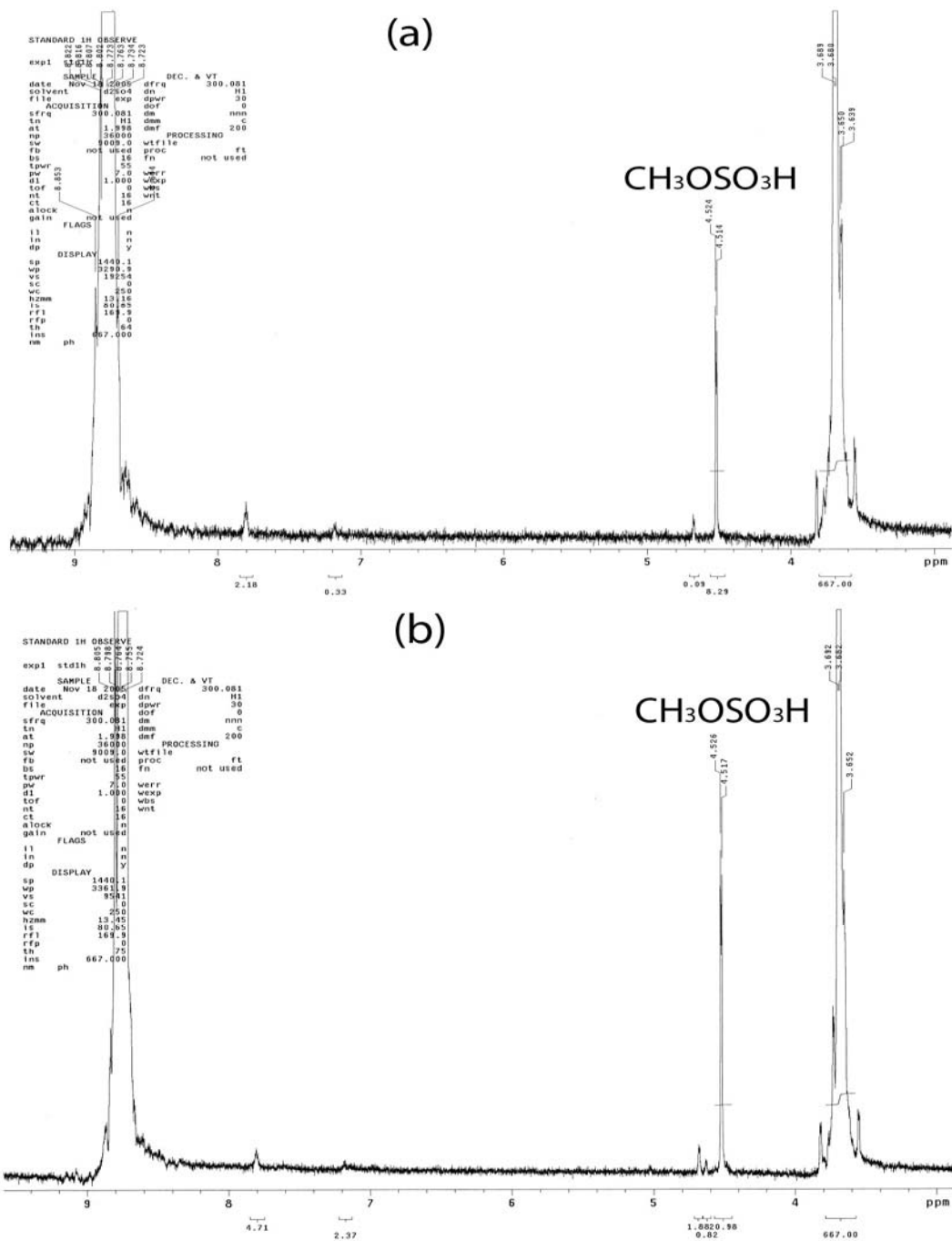


Figure 5.4: ¹H NMR spectra of the liquids from mini gold tube reactors at 200 °C for 4 hrs. (a) 50 mM (bpym)PtCl₂ in 1 mL 96% H₂SO₄; and (b) 50 mM (bpym)PtCl₂ in 0.5 mL 96% H₂SO₄ + 0.5 mL CF₃SO₃H. Acetic acid was used as the internal standard.

5.3.3 Melting Salts (eg. NH_4HSO_4)

For the stable ionic liquids we have identified so far (PEER-4: pyrazinium-based, PEER-5: triazolium-based, and PEER-6 pyrazolium-based), the instability mainly comes from the N-heterocyclic ring decomposition, which limits the operating temperature of the catalytic system. In this sense, another type of ionic liquid, melting salts can also have the super dissolution capability serving as dissolution media or solvent in the catalyst/oxidant/solvent ternary catalytic system for direct methane to methanol conversion. The major advantage of melting salts is that they can be stable at relatively high temperatures.

Table 5.5: Solubility tests on several potential transition metal catalysts with NH_4HSO_4 as dissolution media or solvent.

Catalysts	NH_4HSO_4	H_2SO_4 (96%)	Solubility
V_2O_5	as solvent	No	Completely dissolved
Re-01	No	Yes	Completely dissolved
Ru-01	10:1	Yes	Partially dissolved
	No	Yes	Not dissolved
Ru-02	10:1	Yes	Partially dissolved
Ir-01	10:1	Yes	Not dissolved
	50:1	Yes	Not dissolved

Note: to assist dissolution, 30 min of oil bath at 200 °C was applied to each test.

Table 5.5 lists the solubility tests on several potential catalysts with NH_4SO_4 as dissolution media or solvent. Based on the solubility test results, several experiments were conducted with the mini gold tube reactor to look for new potential methane to methanol conversion catalytic systems. As well known, V_2O_5 is a very cheap compound which can be used as both catalyst and/or oxidant in chemical reactions. A gold tube experiment was conducted with $\text{V}_2\text{O}_5+\text{NH}_4\text{HSO}_4+\text{CH}_4$ system at 200 °C for 4 h. Although, no methanol was detected, a small amount of CO_2 was generated indicating the occurrence of methane activation and oxidation. Therefore, suitable catalysts and oxidants need to be identified.

5.4 TRANSITION METAL CATALYSTS

In the Periana-Catalytica system, the specially designed (bpym) PtCl_2 catalyst can be easily dissolved in concentrated sulfuric acid while presenting excellent catalytic ability on selective methane oxidation by sulfuric acid. However, this catalyst is deactivated upon water or methanol formation and precipitation forms when the concentration of sulfuric acid is lower than certain value. We have found that most of Pt-

compounds can be dissolved in concentrated sulfuric acid if pre-treated with suitable ionic liquids. Instead of the complicate (bpym)PtCl₂ catalyst, we have utilized several commercially available Pt-compounds including PtCl₂, PtCl₄, PtO₂, H₂PtCl₆, K₂PtCl₄. All these Pt-compounds showed comparable reactivity in the catalytic systems with application of appropriate ionic liquids. This finding can significantly reduce the cost for catalyst production and thus greatly advances the realization of a cost-effective methane conversion process. As pointed previously, if PtO₂ is used as the catalyst, Cl⁻ needs to be provided from other sources.

With the assistance of the super solubility of ionic liquids, we have been able to achieve many other homogenous catalytic systems with other transition metal based catalysts. For example, we have tested the Pd(CH₃COO)₂, (NH₃CH₂CH₂NH₃)PdCl₂, AuCl₃, RuCl₃, ReCl₃, ReCl₅, IrCl₅ and some Os(III) and Os(IV)-compounds catalysts on the solubility, stability and reactivity on C-H bond activation. For the first time, it is found that high valent Osmium compound (III or IV) can also catalyze the C-H activation of methane in concentrated sulfuric acid. However, we have not yet found any effective systems for methane oxidation with catalysts other than Pt-compounds.

Table 5.6: Methane C-H activation catalyzed by selected Re- and Ru-based catalysts, in comparison with Os-based catalysts monitored by H/D exchange in gold tube reactors at 250 °C for 4 h.

Entry	Catalyst	Reaction Media	Exchange Ratio (%)	
			$\frac{CD_xH_{4-x}}{CH_4}$	$\frac{D}{H}$
1	Re-01	D ₂ SO ₄ (98%)	85	48
2	Ru-01	D ₂ SO ₄ (98%)+NH ₄ HSO ₄ (10:1)	44	26
3	Ru-02	D ₂ SO ₄ (98%)+NH ₄ HSO ₄ (10:1)	80	44
4	Os-01	D ₂ SO ₄ (98%)	72	43
5	Os-02	D ₂ SO ₄ (98%)	83	45

Note: All catalysts were added at 20 mM and totally 0.3 mL reaction liquid and 100 μmol of CH₄ were loaded into the gold tube reactors.

Table 5.6 shows the H/D exchange between CH₄ and D₂SO₄ catalyzed by selected transition metal catalysts. Quantification was realized by GC-MS analysis. The selected Re-based and Ru-based catalysts were found to have comparable reactivity to Os-based catalysts on C-H bond activation of CH₄. For the Ru-catalysts, which are insoluble in concentrated sulfuric acid, NH₄HSO₄ served as good dissolution media. The distribution of different CD_xH_{4-x} isotopomers of the H/D exchange experiments with Re-, Ru- and Os-based catalysts shares the same trend: single exchange is easier than multiple exchanges. Such a trend is different from that of the H/D exchange experiments involving Pt-catalysts investigated previously, in which the amount CD₄ is much larger than CDH₃. Thus, we can probably expect some different mechanisms for C-H activation of methane catalyzed by these different transition metal-based compounds.

Using various precious metal-complexes to catalyze methane activation has been investigated intensively. However, only one experimental study on methane activation catalyzed by Os(0) was reported by Flood et al.³ more than twenty years ago. For the first time, we reported in our project that C-H activation of methane can be catalyzed by relatively high valence Os-based compounds in concentrated sulfuric acid.

Table 5.7: Preliminary results of methane C-H activation in selected Os-based systems monitored by H/D exchange in gold tube reactors.

Entry	Catalyst	Reaction Media	T (°C)	Exchange Rate (%)	
				$\frac{CD_xH_{4-x}}{CH_4}$	$\frac{D}{H}$
1	Os-01	KOH(10 wt%)+D ₂ O	220	0	0
2	Os-02	D ₂ O	220	0	0
3	Os-03	KOH(2.5 wt%)+D ₂ O	250	0	0
4	Os-03	D ₂ SO ₄ (98%)	220	75	31
5	Os-03	D ₂ SO ₄ (98%)	250	61	37
6	Os-03	D ₂ SO ₄ (98%)	250	72	43
7	Os-03	D ₂ SO ₄ (85%)	250	13	4
8	Os-04	D ₂ SO ₄ (98%)+IL-007 (6:1)	250	53	28
9	Os-04	D ₂ SO ₄ (85%)+IL-007 (6:1)	250	34	12
10	Os-05	D ₂ SO ₄ (98%)	250	83	45
11	Os-05	D ₂ SO ₄ (85%)	250	29	10
12	Os-05	CF ₃ SO ₃ D	150	2.4	0.6
13	Os-05	CF ₃ SO ₃ D	200	20	5
14	Os-05	CF ₃ SO ₃ D	250	-----	-----

^a Reaction conditions: Os-based catalyst, 0.02 mmol; ionic liquid, 0.3 mmol; total liquid volume, 0.3 mL; CH₄, 64.7 psi, 100 μmol; external hydraulic pressure 3700 psi.; heating time 4 h. ^b IL-007 is PEER-1 type, imidazolium-based.

As listed in Table 5.7, we tested five types of Os-based catalysts with different ligands. Osmium in Os-01, 02 and 03 is at a higher valence state, while in Os-04 and 05 is at a lower valence state. The preliminary results show that Os-complexes don't have any reactivity in basic or neutral pure aqueous solution (entries 1-3). While, Os-complexes with either higher valence or lower valence show significant reactivity on methane C-H bond activation in sulfuric acid, even as diluted as 85% (entries 4-11). However, when sulfuric acid was further diluted, the H/D exchange rate (C-H activation) was decreased, the same trend as observed in those Pt/D₂SO₄ systems investigated before. More work needs be done on the fundamental understanding of the reaction mechanisms. We expect different mechanisms in Os/H₂SO₄ systems and Pt/H₂SO₄ systems due to their very different electronic structures and other intrinsic properties. Efforts have also been

put on characterizing the actual state of the Os-complexes in the reaction liquid under the experimental conditions.

Comparison between entry 4 and 5 shows the effect of the reaction temperature. The exchange rate based on methane molecule decreased from 75 to 61% when the temperature increased from 220 to 250 °C. However, the H/D exchange rate of H atom at 220 °C was lower than that at 250 °C.

Figure 5.5 depicts the difference between entry 4 and 5 in more details by showing the percentages of different isotopomers. As the reaction temperature increases, i.e. as H/D exchange is promoted, more exchange will occur on the same molecule.

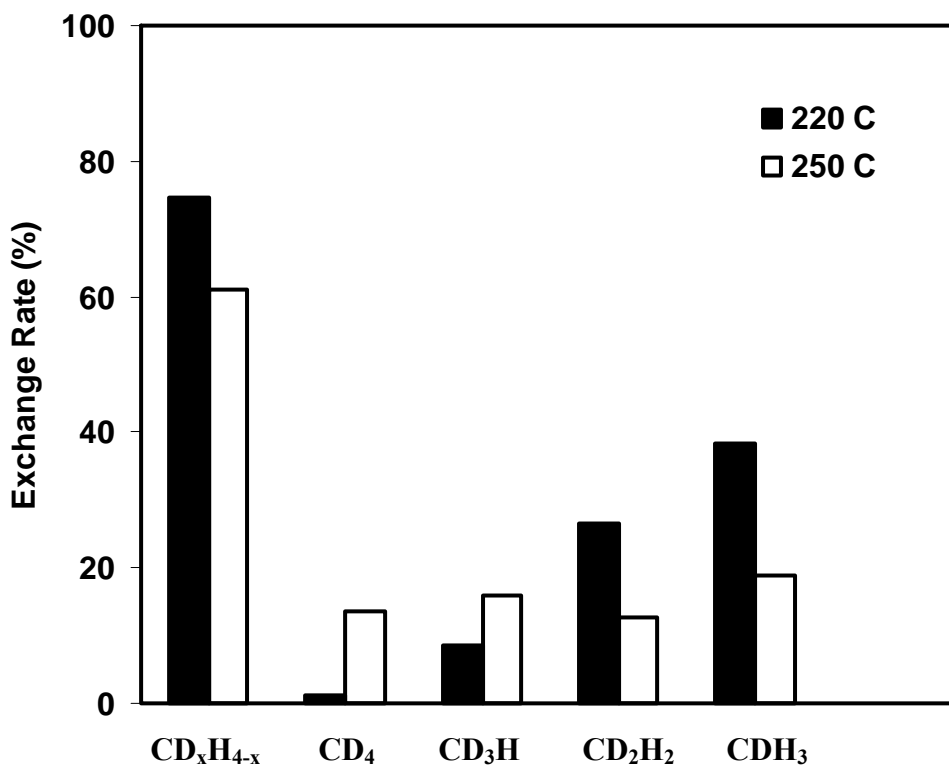


Figure 5.5: Ratios of different methane isotopomers to the original methane after H/D exchange experiments in Os-03/D₂SO₄ (98%) at 220 and 250 °C, respectively.

In order to replace H₂SO₄, we also tried CF₃SO₃H, a super acid with acidity as 1000 times as that of H₂SO₄. We first conducted the experiment with Os-05/CF₃SO₃D/CH₄ at 250 °C for 4 hour (entry 14) producing a large amount of CO₂ and SO₂ gases with very little CH₄ left. Therefore, at this temperature, not only C-H bond activation but also over-oxidization of CH₄ occurred in this system. In addition, CF₃SO₃D was proved to have not only acidity but also significant oxidizing ability at 250 °C. For the next step, we tried lower reaction temperatures to avoid over-oxidization while to keep reasonable reactivity on C-H activation. We found that, almost no H/D exchange

occurred at 150 °C (entry 12), while some H/D exchange occurred at 200 °C. Experiments using CF₃SO₃H instead of CF₃SO₃D need to be run for further identify the oxidized product. At the same, some oxidants can be introduced to this system wishing to get stable intermediate oxidized product of methane, for example CH₃CF₃SO₃, which can be further converted to CH₃OH.

In a short summary, Os-complexes have shown very good reactivity in C-H activation of methane, which makes them promising candidates for the catalysts of an efficient system in methane to methanol conversion. Both the components of the reaction system and the experimental conditions need to be further tuned for better results. Therefore, we further advanced our efforts to the effects of ionic liquids on Os/H₂SO₄ systems (Table 5.8).

Table 5.8: Effects of ionic liquids on C-H activation of methane catalyzed by Os-04 and Os-05 in sulfuric acid (98 and 85%) at 250 °C for 4 h.

Entry	Catalyst	D ₂ SO ₄	Ionic Liquid	H/D Exchange Ratio (%)	
				CH ₄ -based	H-based
1	Os-04	98%	IL-007 (6:1)	53	28
2	Os-04	98%	IL-048 (6:1)	88	50
3	Os-04	85%	IL-007 (6:1)	34	12
4	Os-04	85%	IL-048 (10:1)	12	4
5	Os-05	98%	-----	83	45
6	Os-05	98%	IL-048 (6:1)	101	79
7	Os-05	85%	-----	29	10
8	Os-05	85%	IL-007 (6:1)	15	5

We have tested two Os-complexes, one insoluble (Os-04) and one soluble in sulfuric acid (Os-05). For Os-04, ionic liquid is necessary for dissolving the catalyst (190 °C, 30 min). In 98% D₂SO₄, the H/D exchange ratio in the system with IL-048 (PEER 6 type) is around 40-50% higher than that in the system with IL-007 (PEER 1 type) (both at mole ratio of 6:1); While, in 85% D₂SO₄, IL-048 (10:1) was found to result in a lower H/D exchange ratio than IL-007 (6:1). In case of Os-05, IL-048 was found to increase the H/D exchange ratio compared to the system without IL in 98% D₂SO₄, but to decrease the H/D exchange ratio in 85% D₂SO₄. Therefore, more work need to be done to identify the most efficient compositions of the reaction media as well as to understand the mechanisms of the interactions between ionic liquid, sulfuric acid and Os-based catalysts.

As the initial effort to study the mechanisms in C-H activation of methane catalyzed by the Os/H₂SO₄ system we tested the selectivity of Os-based catalysts on C-H activation with [bmim]-ionic liquid as the model compound.

Table 5.9: H/D exchange at different C-H sites of [bmim]- ionic liquid in Os/[bmim]Cl/D₂SO₄ (98%) quantified by ¹H NMR with D₂SO₄ (98%) as solvent and CH₃COOH as internal standard.

Catalyst	Temperature	Activation Site	Exchange %		
			4 h	8 h	12 h
Os-01	200 °C	N- CH₃	2	-3	----
		N- CH₂ -CH ₂ -CH ₂ -CH ₃	-2	-6	----
		N-CH ₂ - CH₂ -CH ₂ -CH ₃	-1	-2	----
		N-CH ₂ -CH ₂ - CH₂ -CH ₃	-1	-3	----
		N-CH ₂ -CH ₂ -CH ₂ - CH₃	6	8	----
	220 °C	N- CH₃	11	15	----
		N- CH₂ -CH ₂ -CH ₂ -CH ₃	10	16	----
		N-CH ₂ - CH₂ -CH ₂ -CH ₃	12	11	----
		N-CH ₂ -CH ₂ - CH₂ -CH ₃	11	11	----
		N-CH ₂ -CH ₂ -CH ₂ - CH₃	27	39	----
Os-02	220 °C	N- CH₃	7	15	26
		N- CH₂ -CH ₂ -CH ₂ -CH ₃	6	18	29
		N-CH ₂ - CH₂ -CH ₂ -CH ₃	10	19	29
		N-CH ₂ -CH ₂ - CH₂ -CH ₃	9	18	30
		N-CH ₂ -CH ₂ -CH ₂ - CH₃	24	44	59

Note:

- (1) Reaction conditions: Catalyst: 20 mM; [bmim]Cl: 100 mM; D₂SO₄: 98%
Oil bath with magnetic stirring in glass vials
- (2) ¹H-NMR: Solvent: D₂SO₄ (98%); Internal Standard: CH₃COOH
- (3) Negative values for Os-01 at 200 °C reflect the scattering of the measurements.
Such results can be read as no significant exchange occurred at these sites.

As described in Table 5.9, experiments to identify H/D exchange between [bmim] and D₂SO₄ (98%) catalyzed by two different Os-compounds were conducted at 200 and 220 °C for 4, 8 and 12 h, respectively. Quantification was conducted by ¹H-NMR with D₂SO₄ as solvent and CH₃COOH as internal standard. The integrated peak area is proportional to the amount of -H with certain chemical shift. Most of the -H on the ring were exchanged in each experiment. At 200 °C, no significant exchange was observed; while, at 220 °C, H/D exchange occurred at all C-H sites on the [bmim] side chains with the terminal -CH₃ site as the preferred attacking site. H/D exchange at the other alkyl sites was similar and much smaller than that at the terminal site. Though, the H/D exchange at 220 °C increased with longer reaction time, the exchange rate obviously decreased for Os-01. In H/D exchange experiments between CH₄ and D₂SO₄ catalyzed by

Os-01 and Os-02, dark coating was observed on the walls of the gold tube reactors for Os-01, but not for Os-02. Such catalyst deactivation is consistent with the decreased H/D exchange rate in the selectivity experiments. On the other hand, no NH^{4+} peaks were observed on the NMR spectra of the Os-01 system (Because Os-02 is an amine-containing compound, small NH^{4+} peaks were detected in this system.) indicating that the [bmim]Cl ionic liquid is very stable in D_2SO_4 (98%) at 220 °C with the presence of Os-catalyst.

CHAPTER SIX: HIGH-TEMPERATURE SHILOV-LIKE SYSTEM

6.1 SUMMARY

Both experimental and theoretical work has shown that the PEER system, the Pt/IL/H₂SO₄ ternary system, is a combination of the Shilov system and the Catalytica system, while it is much closer to the Shilov one. As depicted in Figure 6.1, both the relative stability and the charge distribution of the C-H activation product of the PEER system are between those of the Shilov and Catalytica systems, but closer to the former one.

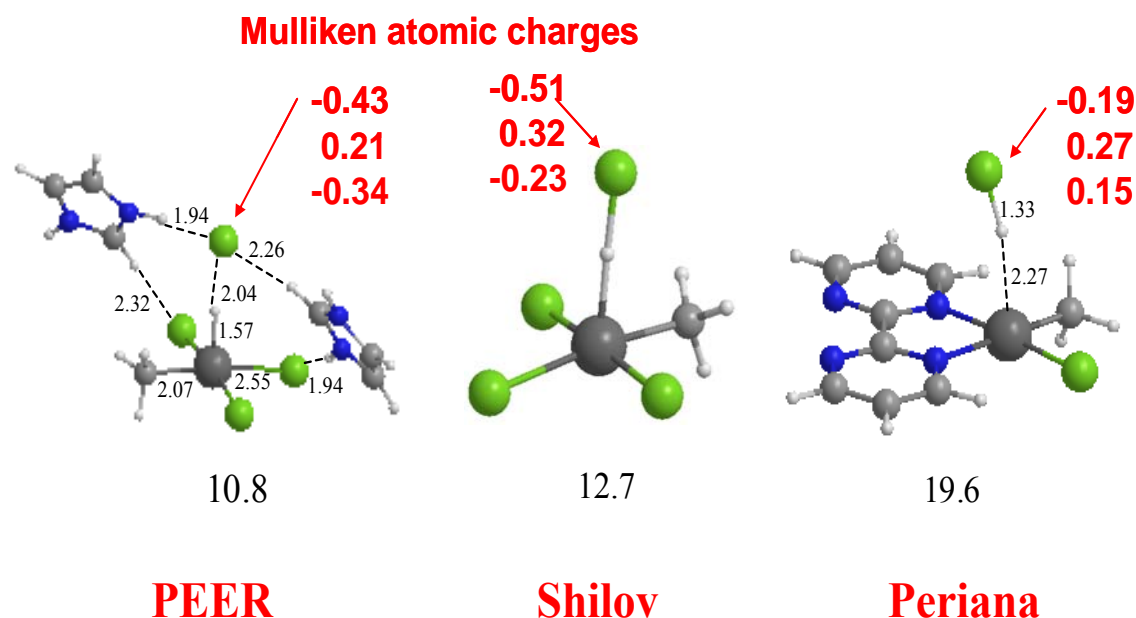


Figure 6.1: Comparison of the C-H activation products of the PEER, Shilov and Periana-Catalytica system.

As the first breakthrough in direct methane to methanol conversion, the Shilov system has three major drawbacks: catalyst deactivation through Pt(0) precipitation, expensive Pt(IV) oxidant and low conversion rate. However, compared to the Catalytica system, the Shilov system is operated under a mild condition (water or acetic acid solution v.s. concentrated sulfuric acid or even oleum) and the product separation is easier. As described above, our PEER system might be a Shilov-like system. Therefore, significant efforts were taken to investigate a high temperature Shilov-like system targeting at stabilizing the Pt-catalyst, replacing the Pt(IV) oxidant by some other cheap ones and increasing the reaction rate with the application of ionic liquids at relatively high temperatures. With our unique experimental apparatus, we have been able to carry out experiments with the Shilov-like system at 250~300 °C and successfully stabilize the Pt-catalysts. In addition, FeCl₃ and CuCl₂ have been found to present comparable, if not superior, oxidization performance for direct methane oxidation.

6.2 C-H ACTIVATION IN THE SHILOV SYSTEM

One of the most promising advantages of the Shilov's system compared to the Catalytica system is that the C-H activation is much faster at the same temperature. Therefore, the first priority in the study of the Shilov system is to increase the reaction temperature to achieve desirable C-H activation rate while preventing catalyst precipitation. Table 6.1 through Table 6.3 present several series of H/D exchange experiments to explore the effects of acids, ionic liquids, and catalyst valance on C-H activation in the Shilov's system with some preliminary conclusions followed.

Table 6.1: H/D Exchange Experiments at 140 °C in Shilov's System

Entry	Catalyst	Reaction Media	Ionic Liquid (6:1)	Time (h)	H/D Exchange Ratio (%)		TON C-H
					CD _x H _{4-x}	CDH ₃	
1			-----	4	7.2	3.3	0.5
2		D ₂ O	[pyrz][HSO ₄] ^H	4	1.9	1.8	0.1
3			[pyrz][HSO ₄] ^R	4	2.0	1.7	0.1
4			-----	4	13.0	5.1	2.1
5		D ₂ O +	-----	12	13.1	5.0	2.1
6	K ₂ PtCl ₄	CD ₃ COOD	[1mim]Cl ^H	4	2.2	1.7	0.4
7		(30%)	[1mim][HSO ₄] ^H	4	2.2	1.8	0.4
8			[1mim]Cl ^R	4	3.1	2.2	0.5
10		CD ₃ COOD (30%)+DCl (8.4M)		4	2.8	2.0	0.47
11		CD ₃ COOD (30%)+ D ₂ SO ₄ (1M)		4	2.9	1.0	0.48
12		D ₂ O +	-----	12	19.4	7.3	3.2
13	H ₂ PtCl ₆	CD ₃ COOD (30%)	[1mim]Cl ^R	12	6.2	3.5	1.0
14	K ₂ PtCl ₄ + H ₂ PtCl ₆	D ₂ O + CD ₃ COOD (30%)	-----	12	31.4	8.3	0.8
15	K ₂ PtCl ₄	D ₂ O + F ₃ COOD (20%)	-----	5	18.0	9.9	2.6

Note:

- (1) Systematic Error: ~+2%
- (2) Shaded: Coating
- (3) Experimental conditions: Gold tube experiments were conducted at 140 °C with 3700 Psi external hydraulic pressure.

- (4) For Entries 1-3 and 15: K_2PtCl_4 (50 mM); for Entry 14: K_2PtCl_4 (20 mM) + H_2PtCl_6 (100 mM); for other entries: K_2PtCl_4 was at 20 mM.
- (5) CH_4 loaded at 50 Psi (about 100 μ mol)
- (6) $[pyrz][HSO_4]^{H^+}$: the ionic liquid and the catalyst were heated at 150 °C for 30 min, and added into the CD_3COOD solution after cooling down.
 $[pyrz][HSO_4]^R$: the ionic liquid, the catalyst and the CD_3COOD solution were mixed together at room temperature.

Table 6.2; H/D Exchange Experiments at 185 °C in Shilov's System

Entry	Catalyst	Reaction Media	Ionic Liquid (6:1)	Time (h)	H/D Exchange Ratio (%)		TON C-H
					CD_xH_{4-x}	CDH_3	
16	K_2PtCl_4	$D_2O(30\%)+DCl(8.4M)$		24	54.1	11.8	30.6
17		$CD_3COOD(30\%)+DCl(8.4M)$		4	22.6	11.2	3.8
18				24	66.5	22.5	37.7
19		$D_2O + CD_3COOD(30\%)$	$[1mim]Cl$	4	9.5	5.0	1.6
21	H_2PtCl_6	$CD_3COOD(30\%)+D_2SO_4(4.2M)$		4	35.5	18.0	5.9
22		$D_2O + CD_3COOD(30\%)$	$[1mim]Cl$	4	15.9	8.8	2.7
23		$CD_3COOD(30\%)+DCl(8.4M)$		4	7.8	4.7	1.3
24	$Pt(0)(30mM)$	$D_2O + CD_3COOD(30\%)$		4	2.0	1.7	0.2
25	$Pt(0)(24mM)$	$CD_3COOD(30\%)+DCl(8.4M)$		4	17.5	9.0	2.4
26	$Pt(0)(20mM)$	$D_2SO_4(98\%)$		4	2.8	2.6	SO_2 and CO_2

Note:

- (1) Experimental conditions: Gold tube experiments were conducted at 185 °C with 3700 Psi external hydraulic pressure.
- (2) For Entries 16 and 18: K_2PtCl_4 (5mM); for other Entries 17, 19-23: K_2PtCl_4 (20 mM).
- (3) CH_4 loaded at 50 Psi Entries 1, 3: about 85 μ mol; the other entries: about 100 μ mol

Table 6.3: H/D Exchange Experiments at 185 °C with Varied Cl⁻ Concentration (K₂PtCl₄ (20mM) + 30% CD₃COOD)

Entry	Stabilizer	[Cl ⁻] (M)	H/D Exchange Ratio (%)		Coating
			CD _x H _{4-x}	CDH ₃	
27	DCI	0.7	61.0	29.0	Silver
28		2.8	60.7	33.7	Silver
29		4.2	61.1	22.5	Silver
30		4.9	65.5	22.6	Very Slight Silver
31		5.6	58.8	22.0	No
32		6.3	43.3	18.8	No
33		8.4	22.6	11.2	No
34	KCl	4*	8.6	5.2	Silver
35	KCl with 10% CF ₃ SO ₃ D	4*	20.7	10.6	Silver

Note:

- (4) Experiments were conducted in gold reactors with 3700 Psi external hydraulic pressure.
- (1) ~100 umol of CH₄ and 0.3 mL of reaction liquid with 20 mM K₂PtCl₄ were loaded.
- (2) Except an 8 hour reaction for Entry 28, the reaction time of the other reactions was 4 hour.
- (3) For Entries 34 and 35, 4M KCl solutions were prepared, however only part of KCl was dissolved.

Preliminary Conclusions:

1) Effects of CH₃COOH

As claimed by Shilov,^{2(a)} at least 30 times acceleration should be caused by the addition of CH₃COOH as the combined results of enhanced solubility of CH₄ and chelate formation. However, Shilov only published data from experiments with the addition of 50% or 30% acetic acid, and the choice of concentration was claimed as for convenience.^{2(a), 4, 5} We took these claims as assumptions and conducted experiments mainly with 30% CH₃COOH working on the stabilization of the catalyst and the improvement of the H/D exchange rate.

We do observe enhanced H/D exchange conversion from entries 1 v.s. 4. However, since Pt(0) coating was also observed, precise quantification of the enhancement is not achievable. One possibility is that the addition of acetic acid could slow down the Pt precipitation resulting in higher exchange ratio. For Entries 2, 3 and 6, 7, 8, the addition of ionic liquids stabilized the Pt(II), while slowing down the H/D exchange. Considering our experimental scatter, the differences caused by CH₃COOH addition still can not be quantified. The experiments at higher temperature with higher conversion (Entries 16 v.s 18) indicate that the effect of acetic acid probably is not as significant as claimed by Shilov.

2) Deactivation of catalysts

For those entries with shades on the TONs (Turn Over Number), coatings were observed on the inside wall of the gold tube reactors. Upon the formation of coating, the catalyst is deactivated as indicated by entries 4 v.s.5, further heating did not produce more exchange.

3) The effects of ionic liquids

Entries 1-8, 12-13 showed that the addition of ionic liquids can prevent Pt(II) from precipitation at the price of slowing down the H/D exchange rate. However, one concern is that, when ionic liquid was present, H/D exchange also occurred on them, which could also inhibit the H/D exchange on methane.

When the experimental temperature was increased to around 185 °C, coatings were also formed even with addition of ionic liquids. Limited by the stability of ILs, the experimental temperature can not exceed 220 °C.

4) Effects of HCl

The addition of 8.4 M HCl effectively prevents the coating formation while slowing down the exchange rate. However, at relatively high temperatures the exchange is fast enough compared to the following oxidation and/or functionalization steps. Therefore, application of HCl is an effective way for getting significant exchange rate at high temperatures without coating formation.

The stabilization effect of HCl can mainly be attributed to the addition of large amount of Cl⁻ ions, which can inhibit the Pt(0) formation reaction ($2PtCl_4^{2-} \rightarrow Pt(0) + PtCl_6^{2-} + 2Cl^-$) as well as the H/D exchange reaction. Therefore, the higher the reaction temperature is, the higher the Cl⁻ concentration is required for acceptable catalyst lifetime. As presented in Table 4.3, about 5.6 M Cl⁻ is necessary for prevent observable Pt(0) formation for a 4 hour experiment at 185 °C, which gives higher H/D exchange rate than the other entries with higher HCl concentrations. Limited by the solubility, chloride salts are not as effective as HCl (Entries 34 and 35). In addition, the acidity of the solution also has some influences on the H/D exchange process.

5) Other acids

Entry 11 showed that D₂SO₄ could neither stabilize the catalyst nor accelerate the H/D exchange (compared to Entry 4).

Entry 15 showed that H/D exchange also occurred in 20% F₃COOD with Pt(0) coating observed on the gold tube reactor. In addition, the resulting TON is comparable to Entry 4 with 30% CD₃COOD. Is it an indication of similar function due to COO⁻.

6) Pt(0), Pt(II) and Pt(IV)

Entries 13 v.s. 8 and 12 v.s. 4 suggested that at 140 °C more H/D exchange occurred when Pt(IV) was added as catalyst instead of Pt(II). However, entries 17 and 23 showed an opposite trend. Anyway, all results are comparable at the same magnitude. Thus, we can conclude that Pt(IV) can also catalyze H/D exchange in methane or it is first reduced to Pt(II) to be effective. Coatings were observed without addition of stabilizer. However, it might be a slower precipitating process with Pt(IV).

Pt(0) was observed active at high temperatures. And the addition of HCl actually enhanced the reaction according to Entries 24 and 25.

6.3 KINETICS STUDY ON THE H/D EXCHANGE REACTION IN HIGH-TEMPERATURE SHILOV SYSTEM [K₂PTCL (5 MM) + CD₃COOD (30%) + DCL (9M WITH D₂O) + CH₄]

The previous investigations reported on H/D exchange in Shilov system were mostly limited at reaction temperature not higher than 120 °C due to the poor stability of the Pt-catalyst. The low reaction rate and the reactor design lead to very low conversion ratio in those low temperature H/D exchange experiments. In our mini gold tube reactor, the application of 3700 psi hydraulic external pressure provides excellent contact between the CH₄ molecules and the reaction liquid and assures 100% mass balance. In our study, the conversion ratio can reach 100% so that data of the whole range of exchange ratio can be achieved for kinetics study. A set of experiments with the same reaction conditions but varied reaction time were conducted to discover the kinetics of H/D exchange in the High-Temperature-Shilov system (Table 6.4 and Figure 6.2).

Multiple H-D exchange on methane has been observed and reported in low temperature Shilov system. A proposed mechanism for the occurrence of multiple H-D exchange involves the formation of methylene-platinum complex. While, another possibility is that the activation energy for the CH₄ uptake step is comparable to that for the C-H bond cleavage step. In this case, each CH₄ uptake may result in more than one C-H bond cleavage and thus H-D exchange. Kinetics fitting may provide information on the activation energy for the generation of each isotopomers and thus provide clues on the activation mechanism. In order to get rid of the scatter caused by the actual amount of CH₄ sealed in each gold tube reactor, the distribution of different exchange products, CD_xH_{4-x} isotopomers relative to the total amount of exchange methane molecules is plotted in Figure 6.2(b), which can more accurately reflect the ratio of multiple exchange. Work on kinetics fitting has already kicked out and will be one of the tasks for next quarter.

Table 6.4: H/D Exchange in High-Temperature-Shilov system [K₂PtCl (5 mM) + CD₃COOD (30%) + DCl (9M with D₂O) + CH₄] at 200 °C for varied reaction time

Entry	Time(h)	H/D Exchange Ratio (%)					
		$\frac{CD_xH_{4-x}}{CH_4}$	$\frac{D}{H}$	CD ₄	CD ₃ H	CD ₂ H ₂	CDH ₃
1	4	4.90	1.58	0.00	0.00	1.43	3.47
2	8	13.09	5.50	0.00	1.96	4.99	6.14
3	8	22.72	9.81	0.00	3.86	8.78	10.07
4	20	59.32	32.67	8.69	14.41	16.45	19.77
5	24	90.99	62.56	26.48	30.23	19.34	14.93
6	32	87.51	58.23	24.81	26.31	18.38	18.01
7	120	100	100	86.93	13.07	0	0

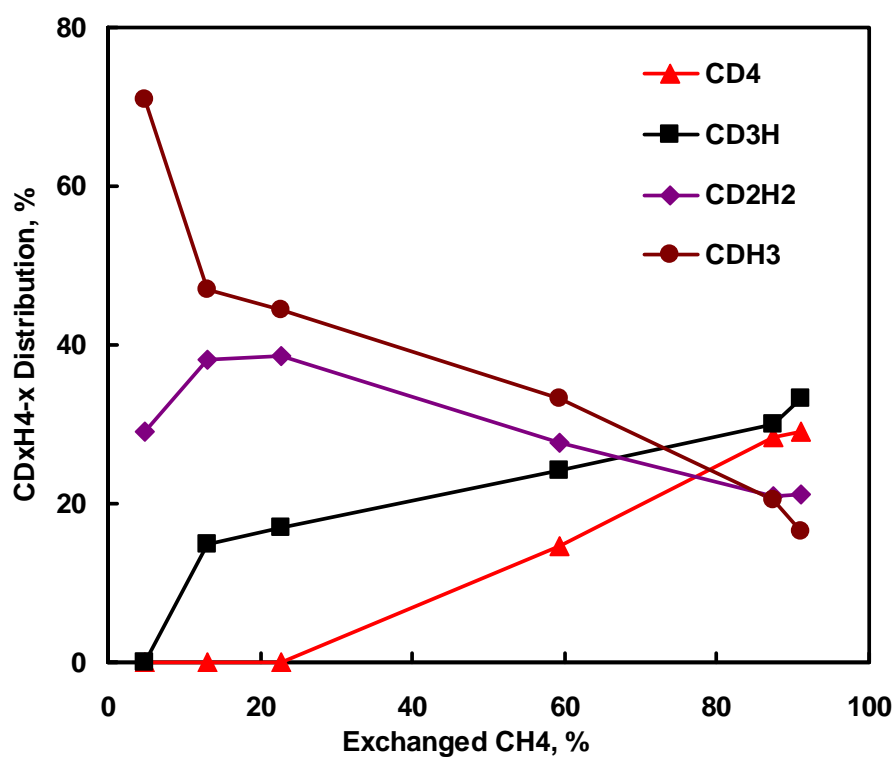
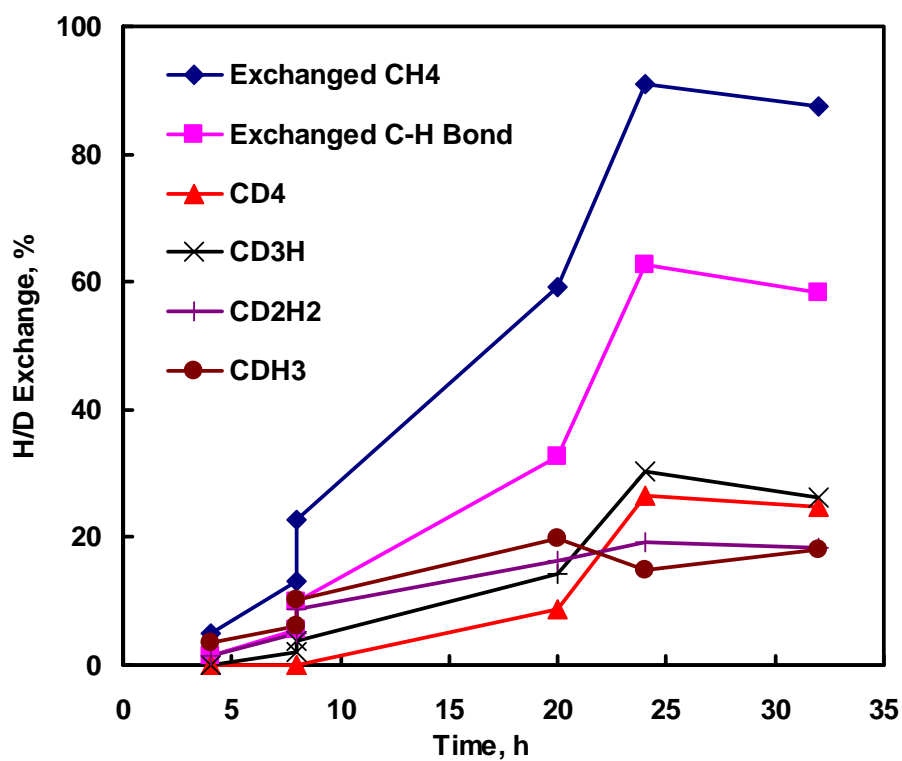


Figure 6.2: CD_xH_{4-x} isotopomer distribution of methane H/D exchange experiments in $[K_2PtCl_6] (5 \text{ mM}) + CD_3COOD (30\%) + DCl (9M \text{ with } D_2O) + CH_4]$ at $200^\circ C$ (a) exchange ratio v.s. time and (b) relative isotopomer distribution.

Besides the thermodynamic study through molecular modeling computations, we have also conducted empirical kinetic study on methane H/D exchange in our HT-Shilov system. The quantum mechanical computation, the empirical kinetic fitting and the experimental observation can crosscheck each other as well as give integrated understanding of the underneath mechanisms. Such fundamental mechanistic understandings will be greatly helpful in optimizing the catalytic system and the experimental conditions.

As defined in

Table 6.5, there are totally 13 possible reactions during the H/D exchange experiments in Shilov system among which Reactions 1, 6 and 10 depict the generation of the precursors for the final deuterated methane isotopomer products. For each reaction, the rate constant k is determined by three factors (temperature T , frequency A_f , and activation energy E_a) as in $k = A_f e^{-E_a/RT}$. Because 100% mass balance is guaranteed for experiments conducted in our mini gold tube reactors, distribution of the 5 different methane isotopomers is only decided by the rate constant of each reaction and the reaction time. Employing the data listed in

Table 6.4, kinetic fitting has been preceded with a program named PMOD. Several simplifications are made for the fitting in order to achieve some preliminary results based on the limited experimental data. Because the frequency factor and the activation energy interact with each other and all experiments were conducted at the same temperature, we set the frequency factor for each reaction as a constant of 10^9 . In addition, the reactions producing those precursors are expected to be similar with each other but relatively fast compared to the following reactions producing the methane isotopomers, so that the activation energies for Reactions 1, 6 and 10 are all set as 20 kCal/mol.

Table 6.5 also lists one set of the fitting results of the activation energies and the coefficients. As presented in Figure 6.3, the calculated methane isotopomer distribution agrees pretty well with the experimental data. Though, this empirical kinetics study is still very inconclusive, it suggests that, for each exchange event single or double H/D exchange is the majority, while exchange with three or four H/D pairs is unlikely to happen under our experimental conditions.

Rudakov et al. proposed the formation of platinum-carbene (Pt=C) to explain the methane isotopomer distribution of the H/D exchange experiments in Shilov system. However, our molecular modeling computations show that the formation of platinum-carbene presents unrealistically high energy barriers. With more experimental data, we

will be able to conduct more precise fitting to give more conclusive description of the H/D exchange kinetics in Shilov system and thus providing information for the reaction mechanism.

Table 6.5: Definition of reactions occurred in methane H/D exchange experiments for kinetics fitting and the preliminary fitting results

I.D.	Reaction	Ea, kCal/mol
1	$\text{CH}_4 \rightarrow a_{11}\text{CH}_3\text{D-p1} + a_{12}\text{CH}_2\text{D}_2\text{-p1} + a_{13}\text{CHD}_3\text{-p1} + a_{14}\text{CD}_4\text{-p1}$ <i>$a_{11}=0.506, a_{12}=0.492, a_{13}=0.00198, a_{14}=0.0000129$</i>	20
2	$\text{CH}_3\text{D-p1} \rightarrow \text{CH}_3\text{D}$	29.9
3	$\text{CH}_2\text{D}_2\text{-p1} \rightarrow \text{CH}_2\text{D}_2$	30.0
4	$\text{CHD}_3\text{-p1} \rightarrow \text{CHD}_3$	30.1
5	$\text{CD}_4\text{-p1} \rightarrow \text{CD}_4$	37.2
6	$\text{CH}_3\text{D} \rightarrow a_{21}\text{CH}_2\text{D}_2\text{-p2} + a_{22}\text{CHD}_3\text{-p2} + a_{23}\text{CD}_4\text{-p2}$ <i>$a_{21}=0.414, a_{22}=0.567, a_{23}=0.019$</i>	20
7	$\text{CH}_2\text{D}_2\text{-p2} \rightarrow \text{CH}_2\text{D}_2$	31.9
8	$\text{CHD}_3\text{-p2} \rightarrow \text{CHD}_3$	28.2
9	$\text{CD}_4\text{-p2} \rightarrow \text{CD}_4$	30.3
10	$\text{CH}_2\text{D}_2 \rightarrow a_{31}\text{CHD}_3\text{-p3} + a_{32}\text{CD}_4\text{-p3}$ <i>$a_{31}=0.735, a_{32}=0.265$</i>	20
11	$\text{CHD}_3\text{-p3} \rightarrow \text{CHD}_3$	26.5
12	$\text{CD}_4\text{-p3} \rightarrow \text{CD}_4$	30.4
13	$\text{CHD}_3 \rightarrow \text{CD}_4$	25.7

Notation:

- 1) a_{11} : coefficient of the corresponding product with a sum of 1 for all the products of each reaction.
- 2) $\text{CH}_3\text{D-p}$: the precursor of CH_3D product
- 3) number in bold: set value; number in bold and italic: fitted value

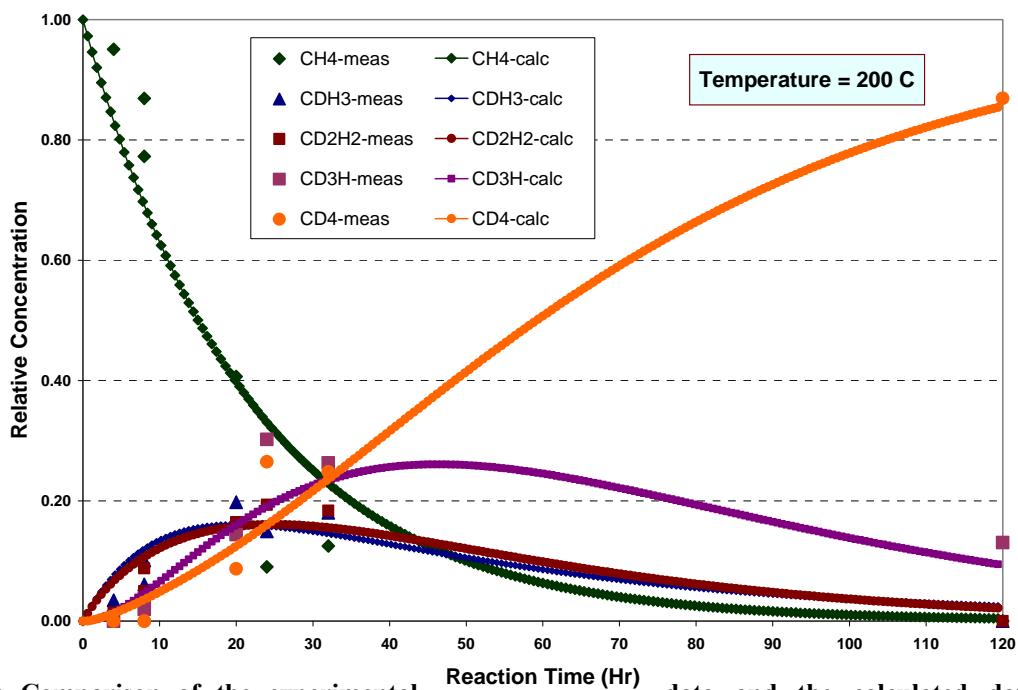


Figure 6.3: Comparison of the experimental data and the calculated data from empirical fitting for H/D exchange experiments in the HT-Shilov-like system.

6.4 STABILITIES OF VARIOUS PARTIAL OXIDATION PRODUCTS OF METHANE

As described in our previous quarterly reports, the C-H activation step of the methane partial oxidation processes we are currently developing is relatively successful. Mechanistic calculations indicate that the activation step is the most energetically difficult step during the activation-oxidation-functionalization three-step homogeneously catalyzed methane oxidation process. However, the current experimental results show that the oxidation step is indeed the rate limiting step. While putting efforts on the theoretical investigation of the possible oxidation approaches during our Pt-catalyzed methane oxidation process, we are also trying to accelerate the oxidation step by using

stronger oxidants or increasing the reaction temperature. However, such approaches will raise the concerns of over-oxidation, i.e. poor selectivity of the catalytic system.

The strength of C-H bond in CH₄ is stronger than any of those in its partially oxidized derivatives, such as CH₃OH, HCHO, HCOOH and CH₃Cl. Therefore, the selectivity issue is a common obstacle for most methane conversion processes. If a system is strong enough to break the C-H bond in CH₄, it is most likely very efficient in breaking the C-H bond or other functional group in the partial oxidized products of CH₄ resulting in production of the undesirable over-oxidized CO₂. The poor selectivity is the main reason why radical reactions for CH₄ conversion processes are not favorable. With the application of appropriate catalyst, reaction media and experimental conditions, it is possible to achieve good selectivity in methane conversion processes. Because a heterogeneously catalyzed process usually requires higher reaction temperature than a homogeneously catalyzed process, the latter is usually intrinsically superior to the former on achieving better selectivity. Two classic homogeneously catalyzed methane-methanol processes, the Shilov system and the Periana system both demonstrate excellent selectivity. In the Shilov system, the methane oxidation products were characterized as almost 50% CH₃OH and 50% CH₃Cl. The lack of over-oxidized product, CO₂, might be attributed to the low reaction temperature (~120 °C). In the Periana system, over-oxidation is avoided by the formation of methylbisulfate (CH₃OSO₃H), which is more stable than methane in highly concentrated sulfuric acid under the Pt-based catalysts at temperatures lower than 220 °C.

As a very important part of optimizing our developed catalytic systems, systematic experiments have been conducted on the studies of stability of various methane partial oxidation products to provide insightful guidance on improving process selectivity.

First, experiments were designed to investigate the protecting effect of forming methylbisulfate over methanol under different reaction conditions. At room temperature, the hydrolysis reaction $CH_3OSO_3H + H_2O \rightarrow CH_3OH + H_2SO_4$ occurs when the reaction media contains significant amount of water, i.e. the concentration of sulfuric acid is not high enough. However, preliminary quantum mechanical calculations indicate that the equilibrium should move to the left as temperature increases. Though, without accurate data from the theoretical calculations, experiments were conducted to discover whether stable methylbisulfate can be formed in relatively dilute sulfuric acid. Table 6.6 lists several typical experiments testing the stability of methanol under various reaction conditions.

Table 6.6: Gold-tube experiments on methanol stability tests under various reaction conditions.

Entry	Reaction Media	Temperature (°C)	Time (h)	CO ₂ (μmol)
1	H ₂ SO ₄ (64 w.t.%)	280	3	14

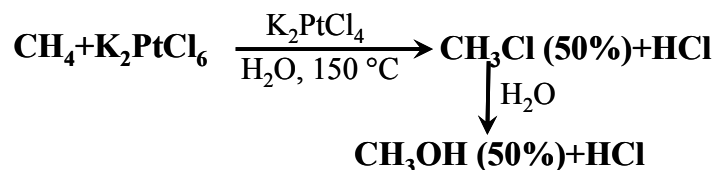
2	H ₂ SO ₄ (85 w.t. %)	250	3	18
3	H ₂ SO ₄ (96 w.t.%)	250	3	19
4	CuCl ₂ (300 mM)+HCl(8.4M)	250	3	2
5	CuCl ₂ (300 mM)+HCl(8.4M)	300	3	14
6	CuCl ₂ (300 mM)+K ₂ PtCl ₄ (5 mM)+HCl(8.4M)	300	2	16

All these experiments were conducted in our custom-made mini-gold-tube reactors. 10 μ L of methanol was added into 1mL of reaction liquid with designed compositions and about 0.3 mL of the final reaction liquid was loaded into the gold tube reactor. The addition of methanol into the sulfuric acid solution was operated with the vial dipped in ice-water mixture to avoid methanol vaporization due to heat releasing. After loading the reaction liquid, the gold tube reactor was flushed and filled with N₂ gas and sealed with a welder gun. An external hydraulic pressure about 3400 PSi was applied through a steel autoclave during the reaction. After heating, the autoclave was taken out of the air-circulating oven and quenched in cold water. Gas analysis was conducted through a HP5890 GC equipped with an FID detector as well as two TCD detectors. The CO₂ quantification was realized through a calibration curve of the TCD signal peak area v.s partial pressure of the injected CO₂ amount.

Entries 1 to 3 suggest that protecting methanol through formation of methylbisulfate does not work at temperatures higher than 250 °C even at concentration as high as 96%. Methanol is so active that dilute sulfuric acid is strong enough to oxidize it to carbon dioxide. However, in our newly developed high temperature Shilov-like system the chemistry could be different with the presence of highly concentrated HCl acid. Entries 5 and 6 show that methanol has been oxidized by CuCl₂ to carbon dioxide with/without Pt(II) catalyst at 300 °C. While, at lower temperature (250 °C), no significant amount of carbon dioxide was observed without Pt(II) catalyst (Entry 4). However, for entries 4 to 6, significant amount of CH₃Cl was observed. In summary, these experiments suggest the instability of methanol at high temperatures (above 250 °C) under our typical catalytic methane conversion conditions. On the other hand, the coexistence of CH₃OH and HCl might result in the formation of CH₃Cl which can possibly survive under certain experimental conditions. Therefore, new chemistry or experimental protocols need to be developed for the methane conversion processes to avoid complete over-oxidation, i.e formation of CO₂.

In our high temperature Shilov-like system, we have detected the formation of three major oxidation products of methane: methylchloride (CH₃Cl), formic acid (HCOOH) and CO₂ as previously reported. Such product distribution is quite different from that claimed by the conventional Shilov system (about 50% CH₃OH and 50%

CH₃Cl). In fact the proposed mechanism of the conventional Shilov system can be described as below



in which the formation of CH₃OH through hydrolysis of CH₃Cl mostly likely occurs due to the low reaction temperature and the long reaction time. In fact, the equilibrium of hydrolysis reaction of CH₃Cl under high concentration of HCl is highly favorable to the CH₃Cl side. Obviously, CH₃Cl is more stable than CH₃OH and stands more chances surviving under the catalytic methane oxidation conditions since the catalyst may selectively activate the C-H bond in methane but stay relatively inert to CH₃Cl. Therefore, our next set of experiments was conducted to test the stability of CH₃Cl under various conditions. Because we don't have pure CH₃Cl gas in stock, the reactant gas is a mixture of 90% CH₄ and 10% CH₃Cl. The preliminary results are listed in Table 6.7

Table 6.7: Gold-tube experiments on methylchloride stability tests under various reaction conditions.

Entry	Reaction Media	Temp. (°C)	Time (h)	CH ₄ (%)	CH ₃ Cl (%)	CO ₂ (%)
1	CuCl ₂ (300 mM)+HCl(8.4M)	250	3	84	16	0
2	CuCl ₂ (300 mM)+HCl(8.4M)	300	3	56	31	13
3	CuCl ₂ (300 mM)+K ₂ PtCl ₄ (5 mM)+HCl(8.4M)	250	3	57	30	13
4	CuCl ₂ (300 mM)+K ₂ PtCl ₄ (5 mM)+HCl(8.4M)	250	6	59	22	19
5	CuCl ₂ (300 mM)+K ₂ PtCl ₄ (5 mM)+HCl(8.4M)	230	12	57	28	15

In these experiments, 0.3 mL of reaction liquid was loaded into each gold tube followed by the loading of about 60 μmol [CH₄(90%)+CH₃Cl(10%)] gas mixture. After sealing, the gold tube reactor was placed into a high pressure autoclave with application of about 3400 PSi external hydraulic pressure and heated in an air-circulating oven at the desired temperatures for certain time periods. It needs to be pointed out that the gas loading procedure can not be precisely controlled so that the total amount of gas loaded may vary as much as 10 μmol for each experiment. In addition, the currently employed gas transfer protocol uses a cold trap of about ~-80 °C mixture of liquid nitrogen and ethanol. Recently, it was discovered that the variation of the cold trap temperature can also affect the amount of CH₃Cl transferred into the gas analysis system due to the

relatively high boiling point of CH₃Cl (-24.2 °C). In addition, the percentage of each gas component was calculated assuming a 100% of all gas-phase products (CH₄, CH₃Cl and CO₂). Therefore, the current gas analysis results presented by percentage of each gas product are only qualitative data.

Entries 1 to 3 indicate that the Pt-catalyst promotes the oxidations both of CH₄ and CH₃Cl. Without the Pt-catalyst, no significant amount of CO₂ was observed at 250 °C. When the temperature was increased to 300 °C, some of the CH₃Cl was oxidized to CO₂ even without the Pt-catalyst. Entries 3 to 5 show that a longer reaction time did not proportionally/significantly increase the CH₄ conversion, but resulted in a worse selectivity (increased CO₂ percentage). Lowering the reaction temperature as increasing the reaction time did not improve the selectivity either. The preliminary conclusions from these experiments are: (1) the high-temperature Shilov-like system can have significant methane conversion at ~250 °C; (2) significant amount of CO₂ will also be produced as the further oxidation product of CH₃Cl; (3) longer reaction time can result in worse selectivity.

In fact, most industrial production of CH₃Cl is prepared through the reaction of CH₃OH + HCl → CH₃Cl + H₂O, either by bubbling HCl gas through boiling methanol with or without a ZnCl₂ catalyst, or by passing combined CH₃OH and HCl vapors over an Al₂O₃ catalyst at 350 °C. It is suggested that CH₃Cl is stable at temperature as high as over 350 °C and the reaction moves quickly (in seconds) towards the CH₃Cl side, while the reverse reaction is much slower. Therefore, it might be possible to achieve good selectivity in our high temperature Shilov-like system through quick contact (short reaction time), high temperature reactions as long as the Pt-catalyst can survive at that temperature and acceptable methane conversion can be achieved during the quick contact. In order to realize the desirable short contact high temperature reactions, a fast heating system has been developed as described in the following section.

6.5 OPTIMIZATION OF THE HT-SHILOV-LIKE SYSTEM

According to literatures and our preliminary quantum mechanistic calculations, the rate limiting step in the Shilov system should be the C-H activation step. i.e. the oxidation and functionalization steps should proceed much faster than the C-H activation due to relatively lower energy barriers. However, our experimental observations indicate the presence of some high energy-barrier step since the final oxidized methane is much less than the activated one. Entry 26 in Table 6.2 shows a case of over oxidation, where lot of SO₂ and CO₂ were observed, but the remaining methane did not contain much exchanged isotopomers as the result of slower C-H activation than oxidation. In many of our high temperature (above 200 °C) experiments (exchange experiments and oxidation experiments), we detected a large percentage of methane which has been activated but not oxidized. Thus, the next critical step to achieve optimized catalytic performance should be the optimization of the oxidation and functionalization steps.

With FeCl₃ and CuCl₂ as oxidants to replace the expensive Pt(IV)-oxidant, we have developed systematic protocols to identify and quantify the oxidation products as

the foundation of further optimization of the catalytic system and mechanistic understanding.

An HP 6890 GC system equipped with a Gas Pro column, an FID detector as well as a TCD detector and coupled with a Wasson ECE TCD detector is utilized to quantify the gas phase products. The customized gas transfer system attached to the GC system is able to provide the total amount of gas in the reaction gas mixtures. Standard CH₄ with 15% He as internal standard is used to quantify the methane conversion. In order to obtain a significant change on CH₄/He ratio to reduce the influence of the scatter of the GC results, we decided to decrease the amount of CH₄ loaded from ~100 μmole to ~25 μmole. Both the over-oxidized product, CO₂ and the partial-oxidized product CH₃Cl were detected by this GC system.

The liquid products have been characterized by GC-MS revealing that the major liquid oxidation product is formic acid (HCOOH). However, the quantification of formic acid formation is difficult with GC-MS. The reaction liquid is strongly acidic (PH~-1), which is not tolerable for the GC-MS system. Thus, the reaction liquid has to be neutralized to about PH3 before measurements. However, due to the small amounts of reaction liquid and gas, the neutralization means at least 5-10 times dilution and thus a very low concentration of formic acid. In addition, the formic acid contained sample always has some remaining at the injection port of the GC-MS. Therefore, GC-MS is not effective for formic acid quantification for our current experiments.

To precisely quantify the formic acid, we have developed a protocol based on HPLC-UV technique. Good repeatability has been achieved with selection of appropriate sample treatment, column and other parameters. The major uncertainty comes from the pretreatment of the sample. More calibrations need to be done to estimate to formic acid concentration change after the sample passes two cartridges for Cl⁻ and Fe³⁺/Cu²⁺ ions removal. The quantification can be greatly improved if applying the modified Parr reactor with larger volume of reaction liquid and possible higher formic acid concentration in the reaction liquids.

Figure 6.4 shows the GC-MS chromatograph (a) and spectrum (b) of an experiment conducted in 8.4 M DCl and D₂O solution with K₂PtCl₄ (5mM) and FeCl₃ (300mM). As compared with the standard spectrum of HCOOH (c), the oxidation product was identified as HCOOD. This is strong evidence for that the formic acid is formed during the experiment instead of from contamination. GC-MS analysis was also conducted on the gas phase products with exploration of almost 100% exchanged CD_xH_{4-x} and CD_xH_{3-x}Cl for this experiment.

Though, only semi-quantified results have been achieved, we have found that significant oxidation occurred at temperature of 280 °C or even lower. Further increasing the temperature can increase the conversion but at the same time will probably result in high ratio of over oxidation and short catalyst lifetime. Therefore, one of the major targets of optimization is to improve the product selectivity while keeping, if not enhancing the methane conversion.

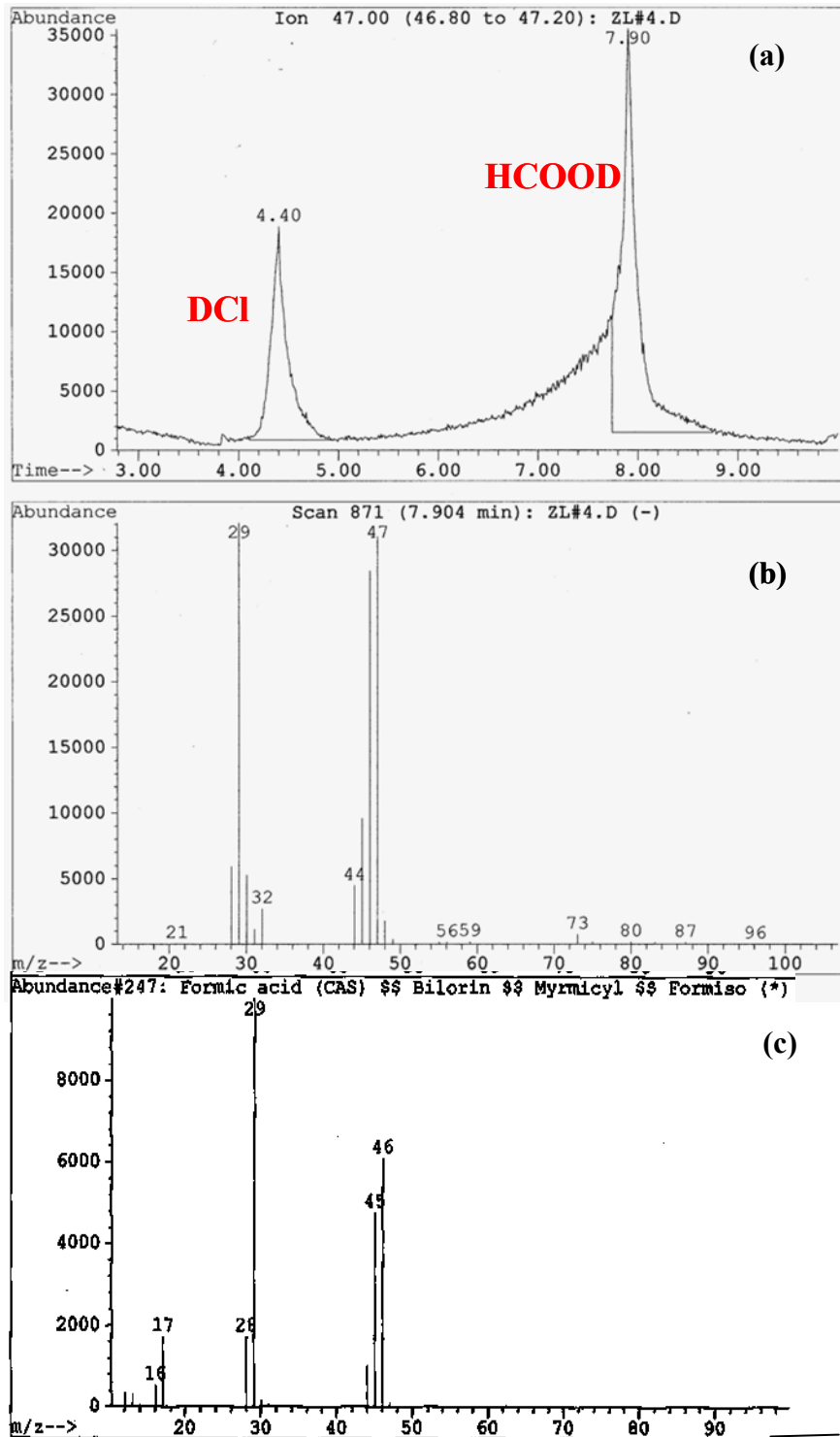


Figure 6.4: GC-MS chromatogram and spectrum for liquid products of reaction [0.3 mL D₂O (with 8.4 M DCl, 5mM K₂PtCl₄ and 300mM FeCl₃) + 100 μmole CH₄] in gold tube reactor with ~3700 PSI hydraulic external pressure at ~320 °C for 4 h. (a) Chromatogram, (b) Spectrum of the HCOOD peak, and (c) standard spectrum of HCOOH.

Stability tests have shown that CH₃OH will be converted to CO₂ in sulfuric acid (concentrated or diluted) and partially converted to CH₃Cl in about 26 w.t.% hydrochloric acid. The over oxidation to CO₂ seems like inevitable considering the C-H bond strength of CH₄ is stronger than any of its partially oxidized products if without any catalytic mechanism or protecting intermediates. In nature, the C-H bond in CH₃Cl is relatively strong among these partially oxidized products of methane. Experiments have found that CH₃Cl can survive at certain percentage if the temperature is not as high as 300 °C and the oxidant (like Cu(II) is not too strong. Such information suggests that if we can remove the CH₃Cl product in time, we might be able to greatly reduce the production of CO₂. As stated before, experiments conducted on our experimental apparatus are mostly at equilibrium state not allowing the instant removal of the product. However, quick reactions might give us some hints how the product equilibrium changes upon reaction temperature and time. Table 6.8 shows the results of several experiments conducted at set-temperatures of 280 and 310 °C with different reaction time. All experiments were conducted on the new fast heating system. Gas products were measured by an HP GC-6890 with one FID and two TCD detectors. Methane conversion was calculated through the internal standard He mixed in the original methane gas at 15 vol. %. Though, a significant CH₃Cl peak was identified on the FID chromatogram, accurate quantification has not been achieved yet, possibly due to the poor repeatability of the cold-trapping gas transfer process. Therefore, the amount of CH₃Cl was the calculated value assuming all reacted CH₄ was oxidized to CH₃Cl and CO₂. The selectivity is defined as the amount of CH₃Cl produced over the CH₄ reacted. As shown by Entries 1-3 and 4-6, the product selectivity decreases when the reaction time increases as well as when the reaction temperature increases. This is encouraging information indicating potential high product selectivity realized by instant removal of the CH₃Cl produced during the reaction when utilizing some appropriately designed flow reactor in the future larger scale demonstration or even industrial applications.

Table 6.8: Fast heating gold-tube experiments investigating the effect of reaction temperature and time on product selectivity of high-temperature Shilov-like system. (Experimental conditions: K₂PtCl₄ (5mM) + CuCl₂ (300 mM) + HCl (8.4 M) + CH₄ (~50 PSI) + Hydraulic Pressure (~ 3400 PSI))

Entry	Temp. (°C)	Time (min)	CH ₄ (%)	CO ₂ (%)	CH ₃ Cl* (%)	Selectivity* (%)
1	310	5	10	2	8	80
2	310	10	20	15	5	25
3	310	20	37	29	8	22
4	280	20	11	4	7	64
5	280	30	17	6	11	65
6	280	65	38	20	18	47

CHAPTER SEVEN: REAXFF METHOD AND VRP METHOD

7.1 A BRIEF SUMMARY ON CALIBRATING THE REAXFF METHOD WITH DFT CALCULATIONS

Favorable properties of ionic liquids (IL), such as a wide liquid temperature range, high density, high heat capacity, low volatility, and nonflammability, make these compounds an excellent replacement for volatile organic solvents, especially in the case of the Periana catalyst system where concentrated H_2SO_4 is used. To gain insight into the physics and chemistry of imidazole-based ionic liquids in the presence of sulfur-based acids we developed a ReaxFF potential for fluorinated and non-fluorinated neutral imidazoles, imidazole cations and sulfoxide-based acids. The ReaxFF reactive force field methodology combines a bond-order/bond distance approach with a geometry-dependent polarizable charge calculation, making it highly suitable for this application. In order to develop ReaxFF potentials for imidazolium/anion ionic liquids and their interaction for Pt-complexes we have performed quantummechanical (QM) calculations on a range of small compounds. By distorting bonds and valence angles in these compounds we obtained a QM-derived training set against which we could test and optimize the ReaxFF parameters. All QM-calculations were performed using the Jaguar-package. For the IL-related compounds (imidazolium/ PF_6/BF_4) we performed calculations using the hybrid DFT/B3LYP functional with a 6-311G**⁺⁺-basis set. For the Pt-complexes the QM-simulations were performed using the DFT/B3LYP functional, describing the metal atom with an LACVP**⁺⁺-basis set and all other elements with a 6-31G** basis set. The QM-data obtained from these simulations were used by the ReaxFF-program to optimize ReaxFF-parameters for the imidazolium cation, the BF_4 and PF_6 anions and for PtCl_2 -complexes.

This ReaxFF potential was tested against a wide range of QM-data, including hydrogen transfer reactions between imidazoles and imidazole cations, pKa-data for imidazoles and sulfoxide cations and imidazole dimer energies. We have performed molecular dynamics simulations with this ReaxFF potential and analyzed the proton diffusion behaviour as a function of imidazole cation/imidazole ratio.

Our ReaxFF method has been proved being able to reproduce quantum calculation results, which are accurate but expensive, in terms of charges distributions and energetics quite well (see Figure 7.1 and Figure 7.2). Furthermore, using ReaxFF MD-simulations, we have studied hydrogen transfer reactions between imidazole and imidazole cations at atomistic level, and calculated vehicular diffusion, that is measurable chemical/physical property. Figure 7.3 is a snapshot from a ReaxFF MD/NVT simulation on a trifluorimidazole cation/HTFS anion/trifluorimidazole mixture, showing a concerted hydrogen transfer event. Figure 7.4 shows the total and vehicular diffusion obtained from ReaxFF MD/NVT simulations at 400 K on 8% and 30% trifluorimidazole cation/trifluorimidazole/ HTFS anion mixtures. The excellent qualitative agreement with experimental results indicates that ReaxFF can successfully describe imidazole-based liquids.

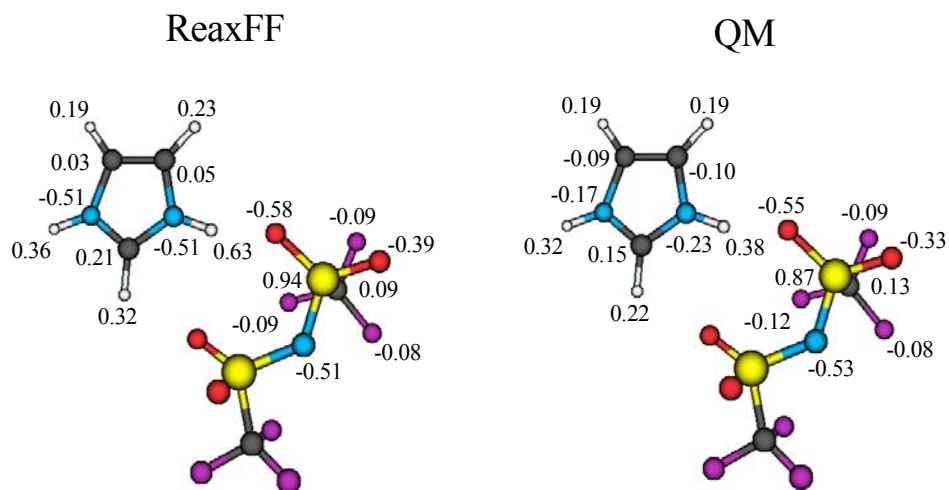


Figure 7.1: ReaxFF and QM (Mulliken) charge distributions for an imidazole cation/HTFS anion dimer.

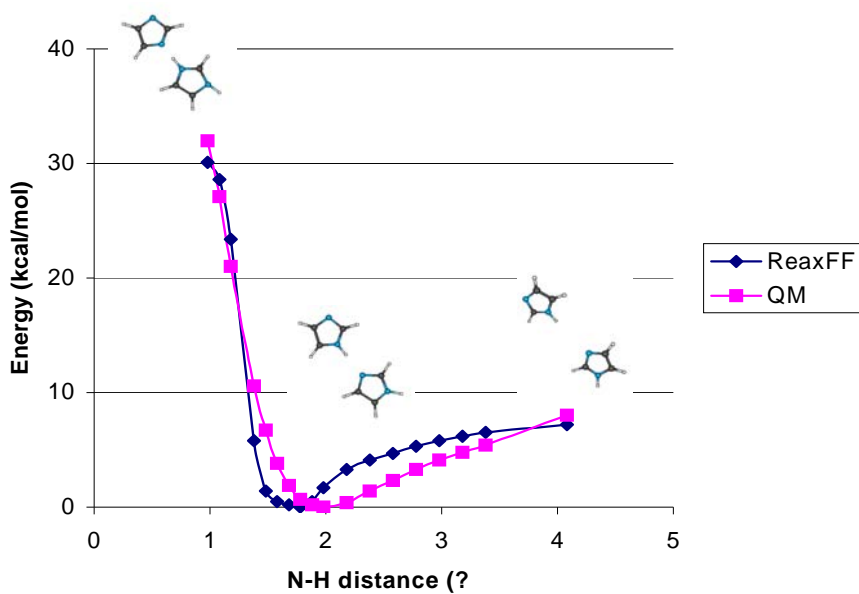


Figure 7.2: ReaxFF and QM-energies for an imidazole dimer as a function of intermolecular N-H distance.

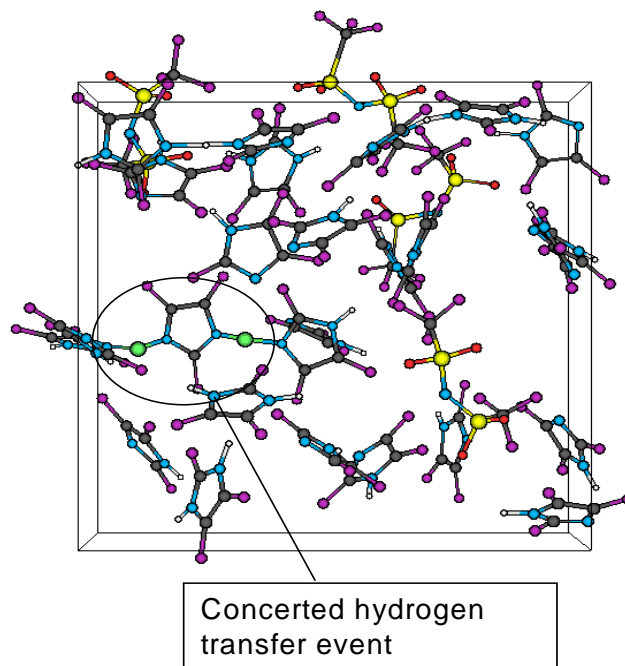


Figure 7.3: Snapshot from a ReaxFF MD/NVT simulation on a trifluorimidazole cation/HTFS anion/trifluorimidazole mixture, showing a concerted hydrogen transfer event. Hydrogens involved in the transfer event are bright green (for clarity), other hydrogens are white. Note that in the simulations ReaxFF uses the same atom type for all hydrogens.

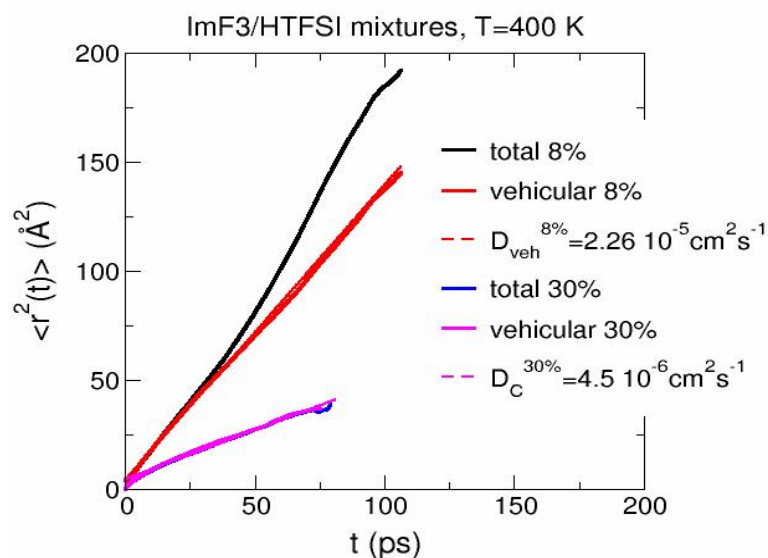


Figure 7.4 Total and vehicular diffusion obtained from ReaxFF MD/NVT (400K) simulations on 8% and 30% trifluorimidazole cation/trifluorimidazole/HTFS anion mixtures.

In summary, after achieving the ReaxFF potential parameters which can describe the intrinsic physical and chemical properties of ionic liquids, we are able to pursue the much more comprehensive mechanisms involved in the methane-methanol conversion catalyzed by our novel ternary catalyst/IL/acid systems and thus to provide efficient theoretical guidance in pursuing an optimized system.

7.2 THE REAXFF POTENTIAL FOR IONIC LIQUIDS AND QM STUDIES OF CATALYST STABILITY

7.2.1 Development of a ReaxFF potential for imidazolium/anion ionic liquids

To develop ReaxFF parameters for BF_4^- and PF_6^- anions we performed bond dissociation and angle distortion calculations using the QM-methodology described in the previous section. These data were used to derive ReaxFF parameters. To ensure that ReaxFF is capable of describing the solvent properties of imidazolium-based ionic liquids we compared the ReaxFF-derived atomic charges with Mulliken charges derived from the QM-calculations. Furthermore, we also compared the ReaxFF and QM dimerization energies for various imidazolium/anion pairs. To test the ReaxFF description for these liquid phases we performed a series of molecular dynamics (MD) simulations on a butylmethyl-imidazolium(BMIM)/ BF_4^- ionic liquid a simulated temperature of 300K. In this way we obtained a relation between energy and system density. ReaxFF finds an optimal density between 1.1 and 1.3 kg/dm^3 , which is in good agreement with the experimentally observed density for this IL (1.16 g/cm^3)

7.2.2 Development of a ReaxFF potential for Pt-complexes

To development of a ReaxFF description for Pt-complexes was initiated by fitting ReaxFF parameters to QM-data for Pt-X bond dissociation in a $\text{PtCl}(\text{NH}_3)_2$ complex, where $\text{X}=\text{H}$, OH , NH_2 , NH_3 , CH_3 or Cl . Figure 7.5 demonstrates that ReaxFF can be parameterized to reproduce the QM-dissociation profiles for these bonds. Importantly, ReaxFF can capture the difference in NH_2 and NH_3 -binding to the Pt-complex; the QM-data shows that the Pt- NH_2 bond is significantly stronger than the Pt- NH_3 bond and ReaxFF successfully reproduces this. As such, ReaxFF can describe the binding of both radical (NH_2 , OH , CH_3 , H) and non-radical (NH_3) to Pt-complexes, indicating that ReaxFF might be capable of reproducing QM-data for the catalytic conversion of methane by Pt-complexes.

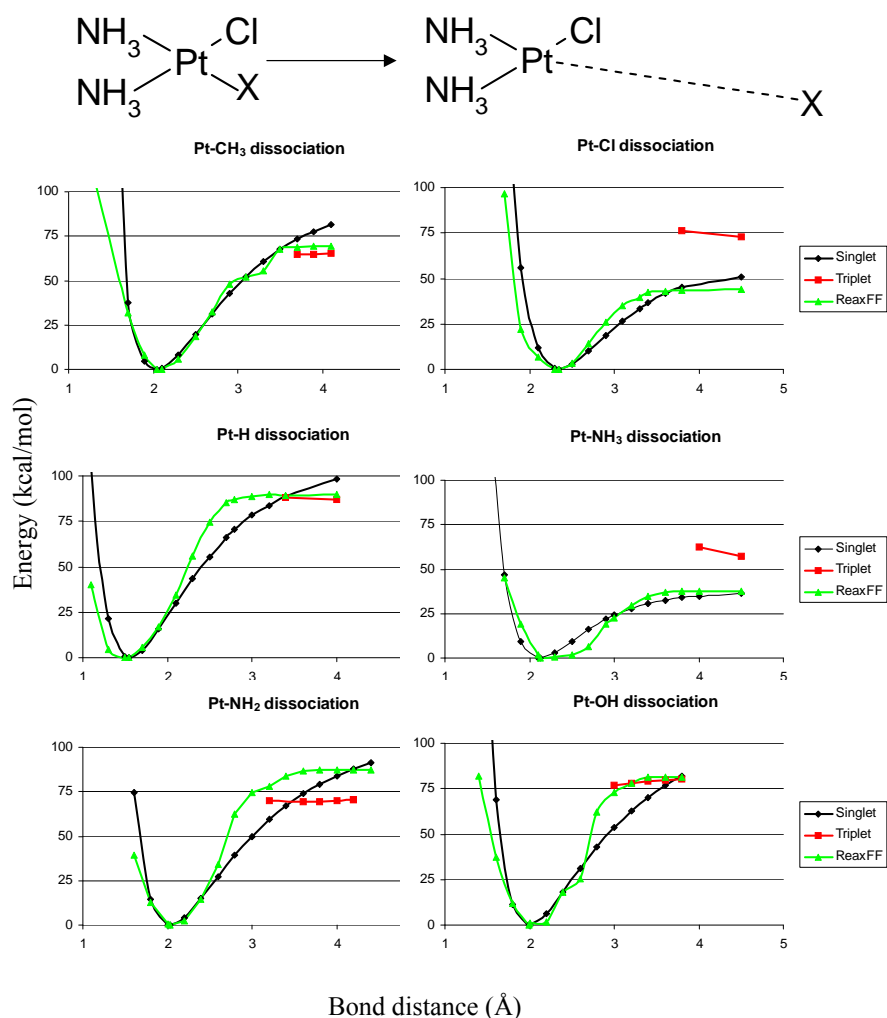


Figure 7.5: DFT singlet (black) /triplet (red) and ReaxFF (green) energies for Pt-X bond dissociation in PtClX(NH₃)₂-clusters.

Thus, by fitting parameters against QM-data describing bond dissociation, angle bending, charge distributions and cation/anion dimer energies we developed a ReaxFF description for imidazolium/anion ionic liquids. We also initiated the development of a ReaxFF description of Pt-catalyzed methane conversion by determining ReaxFF parameters for Pt-X bond dissociation, where X=H, Cl, OH, NH₂, CH₃ and NH₃. For all cases considered we have found good agreement between ReaxFF and QM, indicating that ReaxFF can provide a reliable, computationally inexpensive tool for studying the solubility and catalytic activity of Pt-complexes in ionic liquids.

7.2.3 Molecular modeling and calibration of the ReaxFF method on methane activation in ionic liquids

To understand why PtCl₂ dissolves in ionic liquids and what the possible structures of PtCl₂-ionic liquid complex are, we examined PtCl₂ in (substituted) imidazolium-chloride using QM-methods.

1) QM-studies on the structure of Pt complexes in ionic liquids – PtCl₂+[mmIm][Cl], PtCl₂+[mIm][Cl], PtCl₂+[Im][Cl]

We have studied the possible structures of complex resulting from PtCl₂ and several imidazolium-based ionic liquid salts. Geometry optimizations of PtCl₂+[mmIm][Cl], PtCl₂+[mIm][Cl], and PtCl₂+[Im][Cl] were carried out in vacuum and solvent. Here we report minima and other stationary states for all three types of complexes located on the singlet surface. In case of [mmIm][Cl] one minimum was found, for [mIm][Cl] three minima, and for [Im][Cl] two minima were found in gas phase. All these structures have similar symmetry and Cl-H distances. We found that solvation leads to longer Cl-H distances

2) Development of ReaxFF_{Pt/IL} potential for ionic liquid/Pt systems

We continued the development of a ReaxFF reactive force field for the simulation of Pt-complexes in an ionic liquid environment. The motivation for the development of a ReaxFF_{Pt/IL} potential stemmed from the desire to facilitate the fast and economical screening of solubility and catalytic activity of Pt-complexes in ionic liquids. To calibrate the ReaxFF potentials for imidazole(pyrazinium)/anion ionic liquids and their interactions for Pt-complexes, we performed quantum mechanical (QM) calculations on a range of anions, imidazolium cations, pyrazinium cations, and Pt-complexes (Figure 7.6).

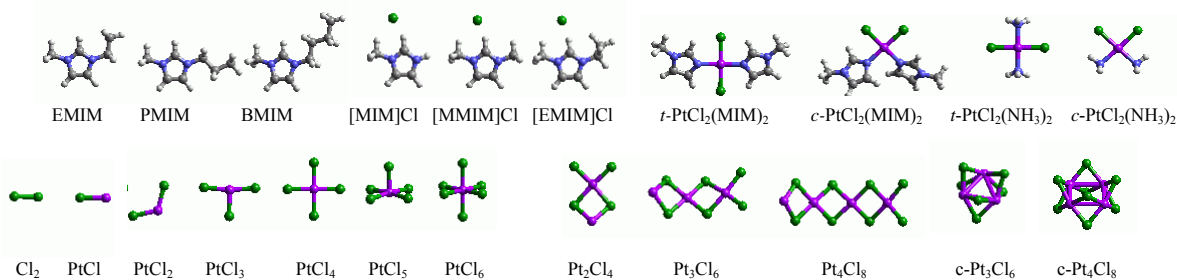


Figure 7.6: Imidazole/pyrazine cations, anions, and Pt-complexes obtained from DFT simulations and included in the ReaxFF training set. (White, gray, blue, green and purple balls represent H, C, N, Cl, and Pt atoms respectively.)

Extension of a ReaxFF_{IL} potential for ionic liquids to chlorine and pyrazines

ReaxFF parameters for anions were fitted to data obtained by performing bond dissociation and valence angle distortion calculation using QM-methods. We extended the ReaxFF_{IL} potential to include Cl-Cl, and Cl-H interactions and pyrazine ILs.

Proper description of solvent properties (charge polarization, dimerization energy, liquid density) for various IL prototypes are key to the development of a reactive force field that is suitable for screening/identifying the best ionic liquid for the optimal Pt-catalyst/IL system. ReaxFF atomic charges for IL systems were calibrated from

Mulliken charges derived from QM-calculations and ReaxFF charges are in good agreement with QM charges.

Extension of the ReaxFF description for Pt-complexes

Precipitation of PtCl_2 and Pt-phases, as observed during the application of the Periana amine catalyst ($\text{PtCl}_2(\text{NH}_3)_2$) in hot concentrated sulfuric acid, is an important obstacle in the development of a successful methane conversion catalyst. To enable simulations on the precipitation chemistry of Pt-complexes in the presence of ionic liquid, we combined both the ReaxFF ionic liquid and platinum descriptions into one potential and added the QM-data for platinum chloride compounds to the training set.

Application of the ReaxFF potential to platinum precipitation from an IL-medium

To test the reactive force field description for Pt/ PtCl_2 precipitation, we performed NVT-simulations at 300K on the precipitation of $(\text{PtCl}_2)_n$ -particles inside a $20\text{\AA} \times 20\text{\AA} \times 20\text{\AA}$ simulation box in the presence and absence of $[\text{MMIM}]\text{Cl}$. Cell compression-expansion runs were performed to obtain the optimal volume to particle density in the simulation box. ReaxFF found an optimal density of 1.19 g/cm^3 for the 1:1 ratio $[\text{MMIM}]\text{Cl}$ - PtCl_2 system. The simulation box was then subjected to NVT simulation at 300-600K for 10,000 iterations. We observed that $(\text{PtCl}_2)_n$ precipitation was significantly repressed in the PtCl_2 - $[\text{MMIM}]\text{Cl}$ case. In the absence of $[\text{MMIM}]\text{Cl}$, precipitation of PtCl_2 occurred at higher frequency and at lower temperature (300K).

To gain insight into the solubility and activity of Pt-complexes in IL-solvents, and the possible PtCl_2 -IL complexes that will be formed, we used DFT methods to examine a range of structures and relative energies of Pt-chloride complexes with substituted imidazolium. One possible concern was the precipitation of the catalyst out of solution; to address this issue we included condensed state phases of PtCl_2 and PtCl_4 and the relative energy of dimerization for various Pt_nCl_m clusters. We used these QM-data to develop a ReaxFF force field capable of efficient and fast screening of a Pt-catalyst/IL system. In our study, we used imidazolium-based salts as our model ionic liquid system. However, our methods are easily applicable and transferable to other ionic liquid systems

1) QM study of the $\text{PtCl}_2(\text{NH}_3)\text{X}$ complex: X = imidazole

To understand what species are being formed as PtCl_2 dissolves in imidazolium chloride, we analyzed the energetics of $\text{PtCl}_2(\text{NH}_3)\text{imidazole}$ for the various bondings of the Pt atom to the imidazole ring (Figure 7.7) using DFT methods. We found that structure *e* was the only complex where the imidazole ring was oriented planar to the rest of the $\text{PtCl}_2(\text{NH}_3)$ complex, probably due to steric forces.

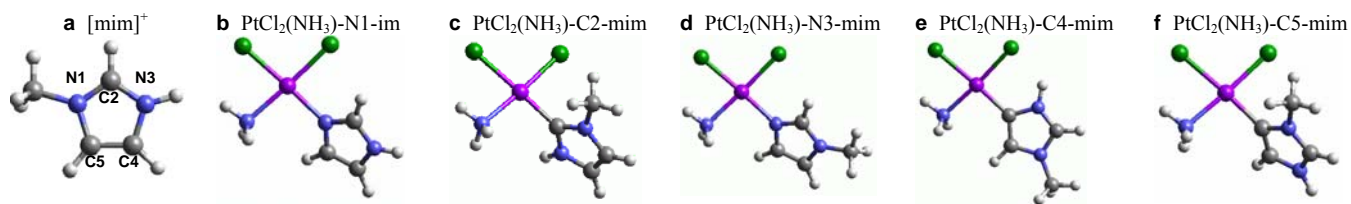


Figure 7.7: Various bonding configurations of a $\text{PtCl}_2(\text{NH}_3)$ complex to a) 1-methylimidazole cation $[\text{mim}]^+$ through the b) N1 atom, c) C2 atom, d) N3 atom, e) C4 atom, and the f) C5 atom. Blue, gray and white balls represent N, C and H atoms, respectively.

We compared the energies for the various $\text{PtCl}_2(\text{NH}_3)$ -imidazole complexes (Table 7.1). We found that the most favorable coordination site on the imidazole ring was at the C2 atom. This is not surprising since the C2 atom is the most electrophilic position on the ring. Charges obtained from Mulliken analysis for the N1, C2, N3, C4, and C5 atoms are -0.30 , 0.30 , -0.31 , 0.07 , and 0.04 respectively. Gas phase energies were corrected for solvation to obtain $\Delta E_{\text{soln}, 0\text{K}}$. From these results, we observed that the energy differences for the various coordination sites to the imidazoles are small except for the empty site. Pt(II) prefers to be four coordinated, square planar complex, thus the unsaturated $\text{PtCl}_2(\text{NH}_3)$ will coordinate to the 1-methyl imidazole.

We have also conducted preliminary investigations of competition between water and imidazole. The Periana (bpim) PtCl_2 system is severely inhibited by water, which is one of the main obstacles to commercial development. Experimental investigations indicated that the initial activity of the $\text{PtCl}_2/\text{imidazole}$ is not inhibited by water. Our calculations support this observation, as we find that replacing chloride with water is largely thermoneutral.

Table 7.1: Coordination energies for imidazole- $\text{PtCl}_2(\text{NH}_3)$ complexes at various position on the imidazole ring. All complexes with Pt were calculated using B3LYP/LACV3P**++ otherwise B3LYP/6311G**++. Diffuse functions were excluded in solvation-phase calculation.

$\text{PtCl}_2(\text{NH}_3)(\text{site-imidazole})$	$\Delta E_{\text{gas}, 0\text{K}}$ (kcal/mol)	$\Delta E_{\text{soln}, 0\text{K}}$ (kcal/mol)
$\text{PtCl}_2\text{NH}_3 + [\text{mimCl}]$	43.49	17.62
$\text{PtCl}_2\text{NH}_3(\text{N1-im}) + \text{HCl}$	1.01	2.77
$\text{PtCl}_2\text{NH}_3(\text{C2-mim}) + \text{HCl}$	0.00	0.00
$\text{PtCl}_2\text{NH}_3(\text{N3-mim}) + \text{CH}_3\text{Cl}$	2.96	1.47
$\text{PtCl}_2\text{NH}_3(\text{C4-mim}) + \text{HCl}$	7.60	2.87
$\text{PtCl}_2\text{NH}_3(\text{C5-mim}) + \text{HCl}$	12.15	3.87

However, replacing one of the Cl ligands with imidazole is very exothermic, with a calculated ΔH of -18 kcal/mol. Consequently, it is likely that the resting state of the catalyst is the cationic $\text{PtCl}(\text{mim})_3^+$ species. This is also most likely the cause of the initially lower activation, as this can be considered an inhibited ground state. Nevertheless, as the experimental activity is not so much lower as to account for 18

kcal/mol, it is also likely that the spectator imidazole ligands play an electronic role in facilitating the activation of CH₄.

Table 7.2: Relative energies of amidazole (mim), Cl⁻ and H₂O for PtCl₂ in imidazole. All complexes with Pt were calculated using B3LYP/LACV3P^{*} otherwise B3LYP/6311G^{***}. Diffuse functions were excluded in solvation-phase calculation.**

Complex	$\Delta E_{\text{gas}, 0\text{K}}$ (kcal/mol)	$\Delta E_{\text{solv}, 0\text{K}}$ (kcal/mol)
PtCl ₂ (mim) ₂ + H ₂ O + mim	-68.3	18.57
[PtCl(mim) ₃] ⁺ + Cl ⁻ + H ₂ O	0	0
[PtCl(mim) ₂ (H ₂ O)] ⁺ + Cl ⁻ + mim	25.4	18.28

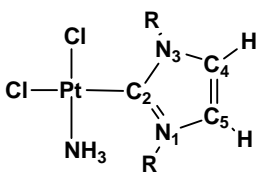
PtCl₂ condensed states

An obstacle to the development of commercial methane conversion catalysis has been precipitation of PtCl₂ and Pt-phases, as observed during the application of the Periana amine catalyst (PtCl₂(NH₃)₂) in hot concentrated sulfuric acid. DFT unilateral cell compression/expansion runs for α -PtCl₂ were performed and incorporated into the ReaxFF training sets.

We extended the ReaxFF_{IL} potential to include PtCl₂(NH₃)OH, PtCl₂(NH₃)H, PtCl₂(NH₃)CH₃, and PtCl₂(NH₃)OSO₃H complexes along with their associated bond distortion (Pt-O) and angle bending (N-Pt-H, Cl-Pt-H, N-Pt-O, Cl-Pt-O, N-Pt-C, Cl-Pt-C) profiles. ReaxFF provides good agreements to DFT derived values for each angle bending energy profile.

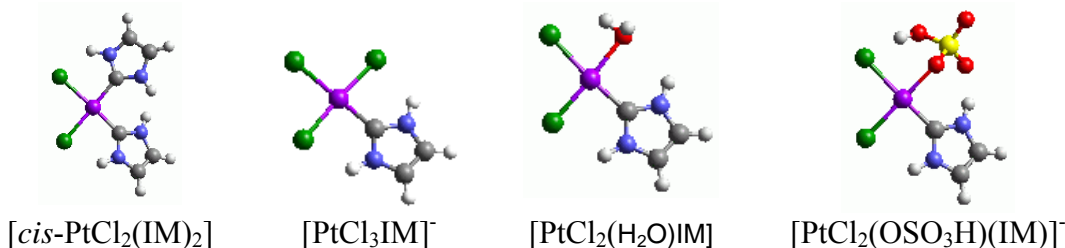
To establish potential catalyst structures, we specifically studied the binding imidazole binding modes to PtCl₂. Table 7.3 shows the results when comparing the most favorable Pt(NH₃)Cl₂(η^2 -IM) (abbreviated C4=C5) plus free Cl⁻ with the Pt-carbenoid at the N1, C2 and C4 positions. These simulations indicate that the carbon-sites are preferred over the nitrogen-sites for Pt/IM-binding. Furthermore, we find that for non-methylated IM (R=H) the carbene-form of the Pt-complex is quite stable, approximately thermoneutral with the η^2 ligand. These carbene-Pt complexes are in many ways similar to the nitrogen-linked bipyridine-complexes associated with the Periana-catalyst, but are anticipated to have significantly different catalytic properties due to their vastly increased electron donating properties.

Table 7.3: Coordination energies for imidazole-PtCl₂(NH₃) complexes at various position on the imidazole ring. All complexes with Pt were calculated using B3LYP/LACV3P^{*} otherwise B3LYP/6311G^{***}. Diffuse functions were excluded in solvation-phase calculations.**

	Coordination site	R = H	R = CH ₃
		$\Delta E_{\text{solv}, 0\text{K}}$ (kcal/mol)	$\Delta E_{\text{solv}, 0\text{K}}$ (kcal/mol)
	N1 + RCl	4.96	6.72
	C2 + HCl	0.56	5.69
	C4 + HCl	5.37	9.29
	C4=C5 + Cl ⁻	0.00	0.00

Having established that the carbene complex is feasible with respect to the Pt-imidazole complex, we also investigated the stability with respect to water, HSO_4^- and Cl^- . The results of our preliminary calculations are summarized in Table 7.4. These results indicate that it is favorable to replace the carbene-bound IM with either water, HSO_4^- or Cl^- , with the PtCl_3 -complex being the most stable of these four options, although more possible conformations must be sampled before a definite conclusion can be made. Nevertheless, it seems that the carbene complex should be thermodynamically unstable under the high acid concentrations of the reaction conditions. This does not necessarily preclude the possibility of an active carbene complex, as it might be kinetically stable. Indeed, this is the case for the Periana (bpym) PtCl_2 complex, as the reaction $(\text{bpym})\text{PtCl}_2 + 2\text{HCl} \rightarrow \text{PtCl}_4^{2-}$ is exothermic, but the chelating nature of bpym prevents easy ligand dissociation and consequent protonation.

Table 7.4: Relative energies of L-PtCl(IM) complexes and ligands. All complexes with Pt were calculated using B3LYP/LACV3P^{**++} otherwise B3LYP/6311G^{**++}. Diffuse functions were excluded in solvation-phase calculations.



Reaction	X= IM $\Delta E_{\text{sol}, 0\text{K}}$ (kcal/mol)
<i>cis</i> -PtCl ₂ (IM) ₂ + H ₂ SO ₄ + HCl + H ₂ O	13.87
[PtCl ₃ (IM)] ⁻ + H ₂ O + H ₂ SO ₄ + [IM] ⁺	0.00
[PtCl ₂ (H ₂ O)IM] + [HSO ₄] ⁻ + [IM] ⁺ + HCl	9.19
[PtCl ₂ (OSO ₃ H)(IM)] ⁻ + [IM] ⁺ + H ₂ O + HCl	10.50

By optimizing ReaxFF parameters against a QM-based training set, containing a wide range of molecular and multimolecular data including charge distributions, bond dissociation energies, angle distortion energies, hydrogen transfer barriers and intermolecular potential energy curves, we have managed to obtain a ReaxFF description for imidazoles, fluorinated imidazoles, imidazole cations and sulfoxide anions. This ReaxFF potential was tested against a wide range of QM-data, including hydrogen transfer reactions between imidazoles and imidazole cations, pKa-data for imidazoles and sulfoxide cations and imidazole dimer energies. We performed a range of MD-simulations on fluorinated imidazole/imidazole cation/HTFS anion mixtures at different cation/neutral imidazole concentrations. We found the imidazole and sulfoxide anions to be stable throughout the entire simulation and observed frequent hydrogen transfer events. Furthermore, we found that at increased cation concentration the influence of hydrogen transfer reactions on the overall diffusion disappears. This is in good qualitative agreement with experimental results, indicating that ReaxFF can successfully describe imidazole-based liquids.

7.2.4 ReaxFF simulation for the Pt complexes in H₂SO₄ with ionic liquids

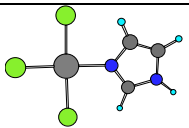
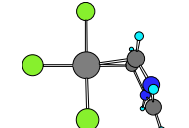
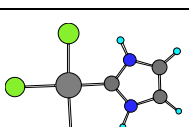
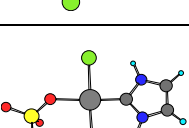
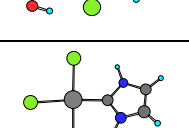
As very little is known about the behavior of Pt complexes in the sulfuric acid solution with ionic liquids, identifying the stable and active species in the solutions is a daunting but also a ‘must’ task.

We first tested ReaxFF for proton binding energies in H₂SO₄ and imidazole and performed ReaxFF simulations at elevated temperatures to check the behavior of this method under realistic conditions.

As experiments have shown that PtCl₂ is soluble in the imidazolium-based ionic liquid with concentrated sulfuric acid, we investigated the possible Pt complexes in the solutions by looking at a series of chemical reactions and calculating the relative reaction energies. The relative energies of each reaction are compared to the reaction energy (29.4kcal/mol in H₂SO₄ solution) of the model reaction (PtCl₂)₆ → 6PtCl₂. The purpose of this part was to screen possible Pt complexes and identify the species which may serve as the starting reagent in the catalytic cycle of the methane oxidation.

Since the imidazolium has been found to be the favored state in the acidic solution, we considered this cationic species as a possible ligand for the Pt(II) complex. Other possible ligands include Cl⁻, HSO₄⁻, H₂O, un-protonated imidazole (IM) and imidazole in carbene coordination mode.

Table 7.5: Relative stabilities of selected Pt(II) complexes in H₂SO₄ solutions.

	Structure of Complex	Related Chemical Reaction	Energy (kcal/mol)
1		$\text{PtCl}_2 + [\text{HIM}]^+ + 2\text{Cl}^- \rightarrow \text{HCl} + [\text{PtCl}_3(\text{N}^1\text{-IM})]^-$	-23.5
2		$\text{PtCl}_2 + [\text{HIM}]^+ + \text{Cl}^- \rightarrow \text{PtCl}_3(\eta^2\text{-HIM})$	-30.8
3		$\text{PtCl}_2 + [\text{HIM}]^+ + 2\text{Cl}^- \rightarrow \text{HCl} + [\text{PtCl}_3(\text{C}^2\text{-IM})]^-$	-32.2
4		$\text{PtCl}_2 + [\text{HIM}]^+ + 2\text{HSO}_4^- \rightarrow [\text{trans-PtCl}_2(\text{C}^2\text{-IM})(\text{HSO}_4)]^- + \text{H}_2\text{SO}_4$	-34.5
5		$\text{PtCl}_2 + [\text{HIM}]^+ + 2\text{HSO}_4^- \rightarrow [\text{cis-PtCl}_2(\text{C}^2\text{-IM})(\text{HSO}_4)]^- + \text{H}_2\text{SO}_4$	-32.1


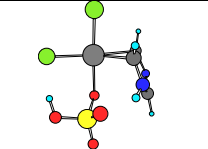
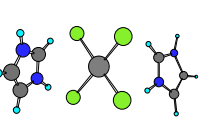
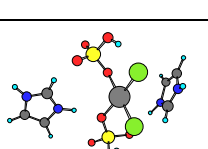
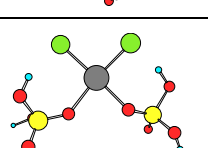
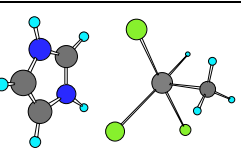
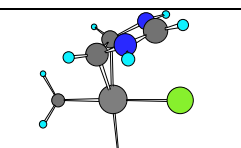
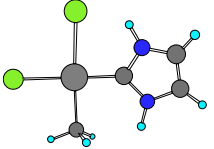
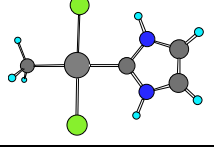
6		$\text{PtCl}_2 + [\text{HIM}]^+ + \text{HSO}_4^- \rightarrow \text{trans-PtCl}_2(\eta^2\text{-HIM})(\text{HSO}_4)$	-23.0
7		$\text{PtCl}_2 + [\text{HIM}]^+ + \text{HSO}_4^- \rightarrow \text{cis-PtCl}_2(\eta^2\text{-HIM})(\text{HSO}_4)$	-22.7
8		$\text{PtCl}_2 + 2[\text{HIM}]^+ + 2\text{Cl}^- \rightarrow [\text{PtCl}_4][\text{HIM}]_2$	-26.4
9		$\text{PtCl}_2 + 2[\text{HIM}]^+ + 2[\text{HSO}_4]^- \rightarrow [\text{PtCl}_2(\text{HSO}_4)_2][\text{HIM}]_2$	-20.0
10		$\text{PtCl}_2 + 2\text{H}_2\text{SO}_4 \rightarrow \text{PtCl}_2(\text{H}_2\text{SO}_4)_2$	-14.0

Table 7.5 shows the selected Pt(II) complexes and their relative stabilities in terms of the reaction energies of the related chemical reactions in the ionic liquid solutions of H_2SO_4 . We can see that, Structures **2-5** could be the stable species in the ionic liquid solutions because the related reactions are exothermic and can release more energy than that required by the endothermic model reaction of $(\text{PtCl}_2)_6 \rightarrow 6\text{PtCl}_2$. On the other hand, the formation energy of complex **10** (-14.0 kcal/mol) from PtCl_2 and H_2SO_4 is much less than the decomposition energy for the model reaction, in agreement with the experimental observation that PtCl_2 does not dissolve in neat H_2SO_4 .

Table 7.6: QM results for selected Pt(II) complexes react with methane.

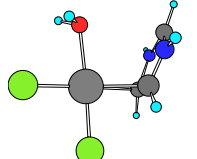
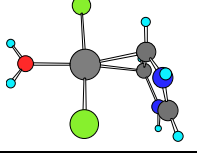
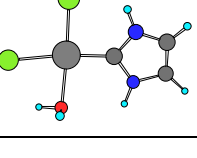
	Structure of Product	Reaction	Energy
11		$\text{PtCl}_3(\eta^2\text{-HIM}) + \text{CH}_4 \rightarrow [\text{PtCl}_3(\text{H})(\text{CH}_3)][\text{HIM}]$	6.9
12		$\text{PtCl}_3(\eta^2\text{-HIM}) + \text{CH}_4 \rightarrow \text{PtCl}_2(\text{HIM})(\text{CH}_3) + \text{HCl}$	18.9

13		$[\text{PtCl}_3(\text{C}^2\text{-IM})]^- + \text{CH}_4 \rightarrow \text{cis-PtCl}_2(\text{C}^2\text{-IM})(\text{CH}_3) + \text{HCl}$	29.0
14		$[\text{PtCl}_3(\text{C}^2\text{-IM})]^- + \text{CH}_4 \rightarrow \text{trans-PtCl}_2(\text{C}^2\text{-IM})(\text{CH}_3) + \text{HCl}$	45.5

We further considered Complexes **2-5** as candidates for methane oxidation reagents and calculated the reaction energies for CH₄ reacts with these Pt(II) complexes. Interestingly, our primary QM results (shown in Table 7.6) suggest that the PtCl₃(η²-HIM) complex can cleavage the H-C bond of methane with a modest energy cost of 6.9 kcal/mol and therefore may serve as the starting reagent for the catalytic reaction. Reactions of methane with complexes **2** and **3** producing Pt-CH₃ complexes and HCl are much more endothermic and therefore are not believed to be involved in the catalytic cycles.

Experimental results indicate that the initial activity of the PtCl₂/imidazole is not inhibited by water although the Periana (bpym)PtCl₂ system is severely inhibited by water, which is one of the main obstacles to commercial development. Our calculations (see Table 7.7) seem to support this observation, as we found that replacing a chloride with a water molecule in complexes **2** and **3** are indeed endothermic or less exothermic (-1.8kcal/mol) when compared to the similar reaction of the Periana system (-6.8 kcal/mol).

Table 7.7: QM results for replacing a chloride ligand in complexes 2 and 3 with a water molecule.

	Structure	Reaction	Energy
15		$\text{PtCl}_3(\eta^2\text{-HIM}) + \text{H}_2\text{O} \rightarrow [\text{cis- PtCl}_2(\eta^2\text{-HIM})(\text{H}_2\text{O})]^+ + \text{Cl}^-$	2.2
16		$\text{PtCl}_3(\eta^2\text{-HIM}) + \text{H}_2\text{O} \rightarrow [\text{trans- PtCl}_2(\eta^2\text{-HIM})(\text{H}_2\text{O})]^+ + \text{Cl}^-$	1.4
17		$[\text{PtCl}_3(\text{C}^2\text{-IM})]^- + \text{H}_2\text{O} \rightarrow \text{cis-PtCl}_2(\text{C}^2\text{-IM})(\text{H}_2\text{O}) + \text{Cl}^-$	-1.8

In a short summary, it is proposed for the first time that $[\text{im}]_2[\text{PtCl}_4]$ is likely the starting effective complex for methane activation in our ternary Pt/IL/ H_2SO_4 systems. Furthermore, we found the energy barrier to activate C-H bond of methane is ternary systems are much lower than the Catalytica reaction, which is in general agreement with our experimental finding of higher deuterium exchange rate for CH_4 catalyzed by PtCl_2 in sulfuric acid solution with ionic liquids.

7.3 A VIRTUAL RAPID PROTOTYPING (VRP) METHOD FOR FAST-SCREENINGS OF APPROPRIATE IONIC LIQUIDS

To select the right ionic liquids for the methane to methanol conversion process, on one hand we have done extensive experimental work to test their solubility and stability in reaction media; and on the other hand, theoretical tools such as quantum chemistry calculation can also provide useful insights about their stability. The thermal stability of the ionic liquid is one of the most critical properties for a commercial system. Based on the extensive experimental and theoretical work, we successfully developed a Virtual Rapid Prototyping (VRP) methodology for fast screenings of stable ionic liquids. VRP is a Quantum Mechanics-based theoretical protocol developed by our group to screen a large number of potential synthetic targets and quickly weed out targets that do not pass established criteria. If the number of calculations required can be reduced to two or three for each species, we can achieve a substantial advantage in speed compared to experimental testing.

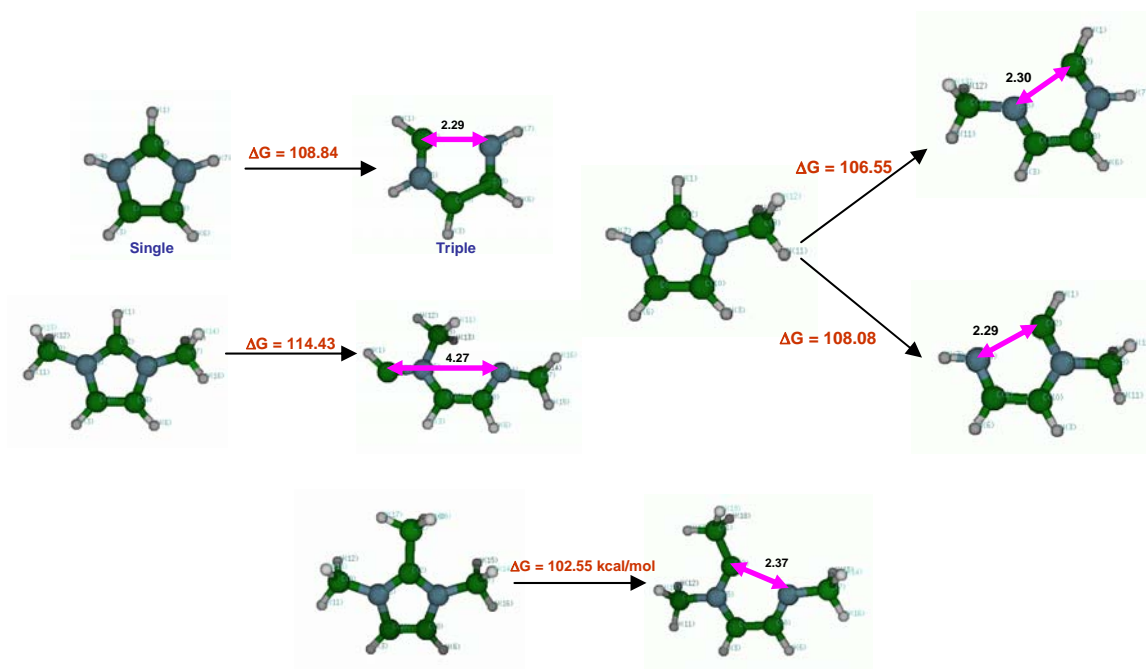


Figure 7.8: Optimized molecular geometry of the stable and ring-opened imidazole and their derivatives for different C-N bond ruptures.

Table 7.8: Calculated C-N Bond Rupture Energies of Imidazolium and their Derivatives.

Anion	Bond	Gibbs' Free Energy (Hartree)		Solvation Energy (kcal/mol)		ΔG (kcal/mol)
		Stable	di-Radical	Stable	di-Radical	
		Singlet	Triplet	Singlet	Triplet	
IM	C-N	-226.500256	-226.328255	-67.0550	-66.1516	108.84
MIM	C-NH	-265.789322	-265.620979	-60.5199	-59.6038	106.55
MIM	C-NCH ₃	-265.789322	-265.616799	-60.5199	-60.6966	108.08
MMIM	C-N	-305.077693	-304.894162	-55.4641	-56.2017	114.43
Me-MMIM	C-N	-344.377054	-344.214318	-52.5452	-52.1153	102.55

Notes: All calculations are at the DFT/B3LYP/6-31G** Level.
 ΔG is the Gibbs' Free energy difference at T = 200 °C.
 Sulfuric Acid (H₂SO₄) as Solvent ($\epsilon = 100$, $r_0=4.33$).
 1 Hartree = 627.5095 kcal/mol

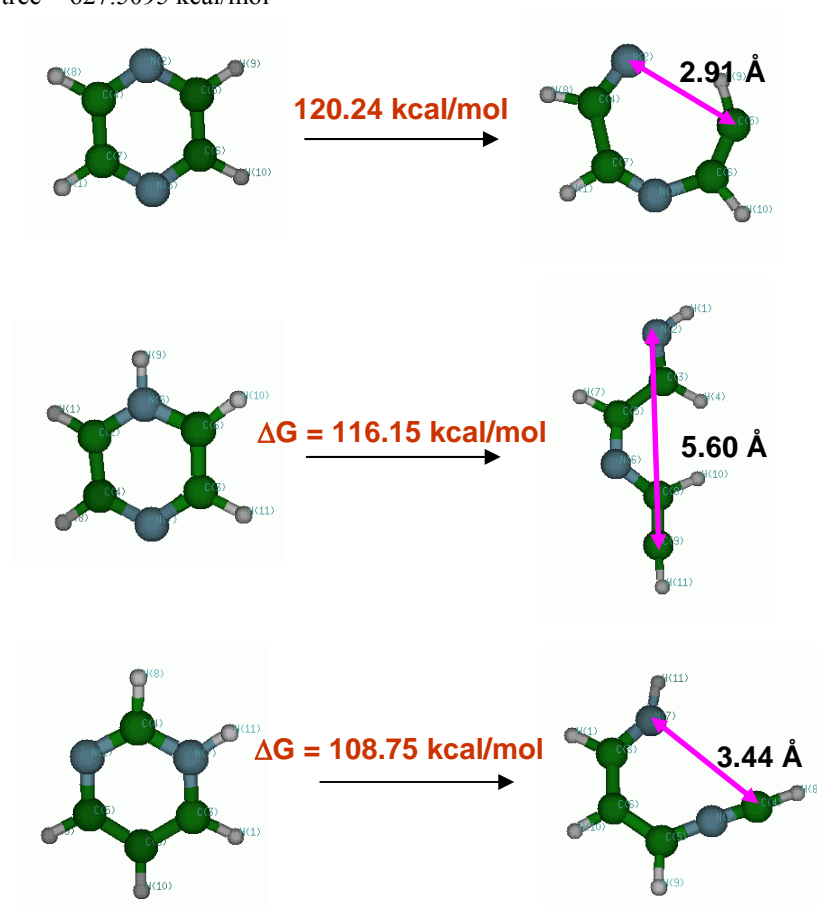


Figure 7.9: Optimized molecular geometry of the stable and ring-opened diazine and their derivatives for different C-N bond ruptures.

Table 7.9: Calculated C-N Bond Rupture Energies of Diazine and their Derivatives.

Molecule	Spin State	E ₀	ZPE	ΔG	E _{sol}	ΔG	ΔΔG
		(Hartree)	(kcal/mol)	(kcal/mol)	(kcal/mol)	(kcal/mol)	(kcal/mol)
1,4-N2-Diazine	singlet	-264.323102	51.813	-28.456	-5.7231	-165819.17	120.24
	triplet	-264.122825	46.298	-33.539	-5.6471	-165698.93	
1,4-N2H-Diazine	singlet	-264.676489	61.561	-29.180	-68.9261	-166094.38	116.15
	triplet	-264.485752	56.382	-33.913	-67.2829	-165978.22	
1,3-N2-Diazine	singlet	-264.329594	51.898	-29.103	-8.3677	-165825.80	105.57
	triplet	-264.171421	53.660	-31.512	-3.8188	-165720.24	
1,3-N2H-Diazine	singlet	-264.687104	61.720	-29.795	-68.4498	-166100.40	108.73
	triplet	-264.505843	56.682	-33.264	-68.4289	-165991.68	

We report on molecular stabilities, represented with the calculated C-N bond rupture energies at different ring positions. The molecular structures of both the stable configuration (singlet) and the bond-opening configuration (triplet) have been fully optimized and their Gibbs' free energy differences are calculated. From Figure 7.8, we can be seen that all configurations are relatively stable with the C-N bond energy ~ 100 kcal/mol. This indicates that most of imidazoles and their derivatives are thermally stable without the presence of the special catalysts such as Pt. Similar results are also found for the diazine and their derivatives (Figure 7.9).

Calculated C-N bond rupture energies of imidazole family and diazine family are compiled in Table 7.8 and

Table 7.9, respectively. In the case of imidazole and its derivatives, 1,3-dimethylimidazole has the strongest C-N bond; and in the case of diazine and their derivatives, pyrazine has the strongest C-N bond. All these results are in excellent agreement with our experimental work, e.g., 1,3-dimethylimidazolium ionic liquids experienced the least decomposition in the presence of Pt and H₂SO₄, and pyrazinium ionic liquids are stable up to 200 °C.

We calculated the molecular stabilities and the Mulliken charge distributions of various diazine family members (pyrazine, pyrimidine, pyridazine) with two nitrogen atoms at different substituted positions and their protonated and methyl-substituted derivatives. In addition, we calculated the pK_a values (acidity) of selected molecules.

For the stability of the ionic liquids, we have established that destruction of the cation occurs through oxidation of the C-H bond, most likely via a mechanism similar to the one leading to methyl bisulfate. Once the cationic ring is oxidized, complete oxidation to CO₂ and NH₃ is believed to be rapid, and if we assume that the rate of oxidation of the Pt-R intermediate is proportional only to the relative concentration of the Pt-R intermediate, we can predict the thermal stability of any individual ionic liquid

based on the feasibility of the first C-H activation event. Furthermore, if we assume that the *rate* of C-H activation is proportional to the relative exothermicity of the C-H activation step according to the Hammond postulate, we can reduce the number of data points required for the prediction of any ionic liquid to exactly one, i.e. the relative energy of the Pt-R intermediate.

The energy of this intermediate can easily be calculated through the reaction sequence $[\text{PtCl}_4][\text{HR}]_2 \rightarrow [\text{PtCl}_3\text{-R}][\text{HR}] + \text{HCl}$, where $[\text{PtCl}_4][\text{HR}]_2$ is the anionic PtCl_4^{2-} species stabilized by two ionic liquid cations (HR^+) and $[\text{PtCl}_3\text{-R}][\text{HR}]$ is the CH activated intermediate. Thus, calculations on the ionic liquid [H-Imidazole][Cl] ([Him][Cl]) show that the reaction $[\text{PtCl}_4][\text{Him}]_2 \rightarrow [\text{PtCl}_3\text{-Im}][\text{Him}] + \text{HCl}$ is exothermic by -0.1 kcal/mol, while calculations on the ionic liquid [H-Pyrazolium][Cl] ([HPz][Cl]) show that the reaction $[\text{PtCl}_4][\text{HPz}]_2 \rightarrow [\text{PtCl}_3\text{-Pz}][\text{HPz}] + \text{HCl}$ is endothermic by 8.9 or 12.1 kcal/mol, depending on what carbon coordinates to the Pt. Consequently, our calculations predict that [Him][Cl] should be thermally *unstable* during the reaction conditions, while [HPz][Cl] should be thermally *stable*, which is consistent with experimental observations.

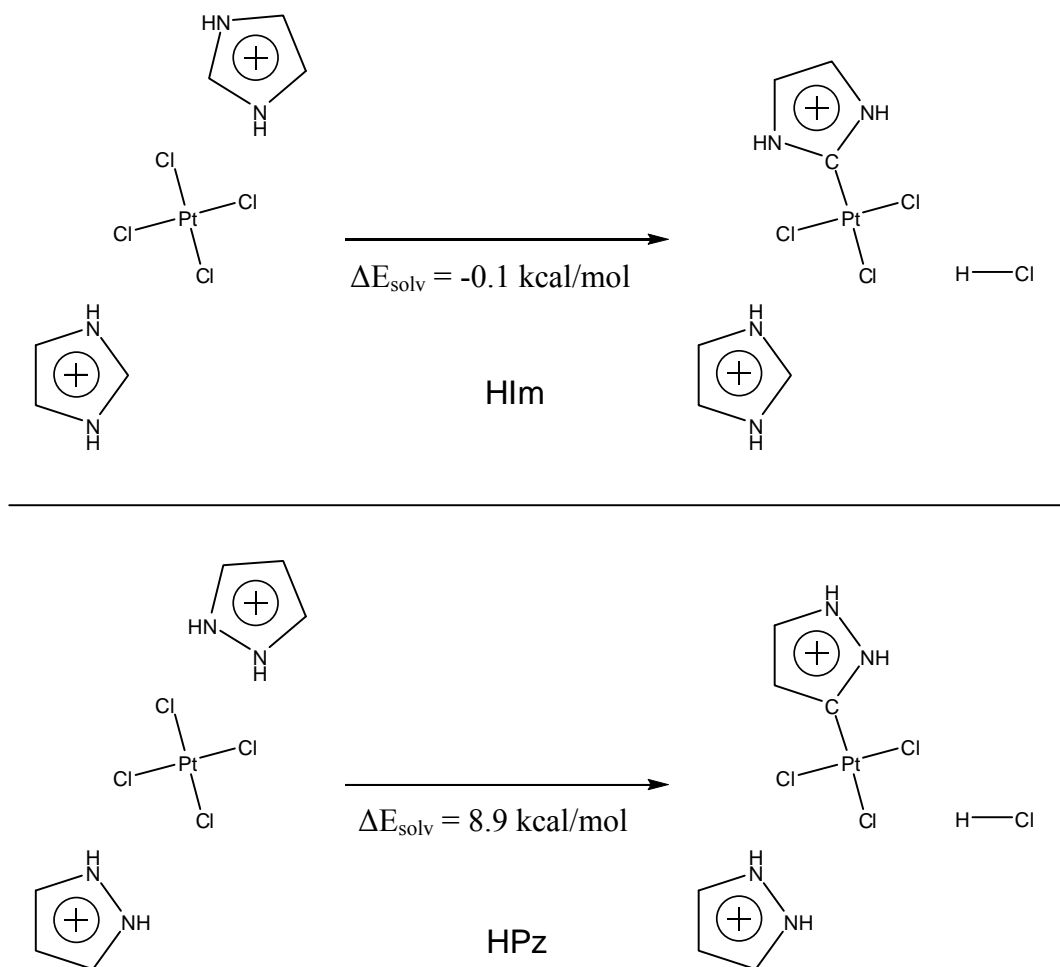


Figure 7.10: Development and applications of the Virtual Rapid Prototyping (VRP) to identify stable ionic liquids in the presence of the Pt catalyst. that the reaction $[\text{PtCl}_4][\text{Him}]_2 \rightarrow [\text{PtCl}_3\text{-Im}][\text{Him}] +$

HCl is exothermic by -0.1 kcal/mol, while calculations on the ionic liquid [H-Pyrazolium][Cl] ([HPz][Cl]) show that the reaction $[\text{PtCl}_4][\text{HPz}]_2 \rightarrow [\text{PtCl}_3\text{-Pz}][\text{HPz}] + \text{HCl}$ is endothermic by 8.9 or 12.1 kcal/mol.

CHAPTER EIGHT: MECHANISTIC INVESTIGATION

8.1 TYPICAL QUANTUM MECHANICAL METHODS UTILIZED

Quantum mechanical computations on methane oxidation mechanisms have been performed using the B3LYP density functional. Detail information related to the computation method can be found in the literatures. This functional is a combination of the hybrid three-parameter Becke exchange functional⁶ (B3) and the Lee-Yang-Parr correlation functional⁷ (LYP). Past basis sets used with B3LYP were constructed as follows. For platinum we used the core-valence effective core potential of Hay and Wadt⁸ with a triple-zeta contraction of valence orbitals, while the Pople-style 6-311G**++⁹ basis set was utilized for hydrogen, carbon and oxygen atoms. Recently the newer M06¹⁰ functional has been increasingly employed for a more accurate description of non covalent interactions.

All calculations correct for the effect of solvent interactions by using the polarizable continuum model (PCM) of solvation¹¹. We solvate with water, with a dielectric constant of 80.37 and a probe radius of 1.4 Å. Geometries are optimized withing the solvent model. Calculations were made with the Jaguar 6¹² or 7.0207 computational package.

The reported total free energies are computed at each stationary point and used for relative free energy calculations (at 298.15 K). The final free energy expression for species A is:

$$G_A = E_{\text{SCF}}^{\text{SP}} + E_{\text{ZPVE}} + H_{\text{Tot}} - TS_{\text{vib}} + \Delta G^{0 \rightarrow *}$$

in which G_A is the net free energy of species A, $E_{\text{SCF}}^{\text{SP}}$ is the solution-phase (continuum) electronic energy, E_{ZPVE} is the zero-point vibrational energy, H_{Tot} is the thermal contribution to the free energy (the vibrational thermal energy along with a PV term), and $-TS_{\text{vib}}$ is the vibrational contribution to the entropic free energy. For the absolute free energy of the proton a pH= 0, we use the value of -270.29 kcal mol⁻¹, which is obtained using the experimental solvation energy of a proton of -264.0 kcal mol⁻¹ (obtained from Tissandier et al¹³), and the relation $G_{\text{SP}}(\text{H}^+) = \Delta G_{\text{solv}}(\text{H}^+) + G_{\text{GP}}(\text{H}^+)$, and ideal gas approximations were made to evaluate $G_{\text{GP}}(\text{H}^+)$.

8.2 REACTION MECHANISM OF C-H ACTIVATION CATALYZED BY PtCl_4^{2-} IN IONIC LIQUID SOLUTIONS

We first compared the influences between hydronium (H_3O^+) and pyrazolium. Figure 8.1 shows the energy profile based on quantum chemical calculations for the C-H activation of CH_4 catalyzed by PtCl_4^{2-} in acidic condition (a system neutralized by H_3O^+). We can see that the CH_4 uptake step has a lower barrier (H-TS1 of 19.5 kcal/mol) than that of the C-H activation step (H-TS2 of 21.2 kcal/mol), indicating that the C-H activation step is the control step for the C-H activation process. The immediate product (H-MD2) of the C-H activation step is a ‘hydride-like’ complex with a short Pt-H distance of 1.58Å. Interestingly, the interaction between the leaving Cl^- and the ‘hydride-

like' ligand (H) remains rather strong, indicating by the short Cl-H distance (1.99Å) which is similar to that of a strong hydrogen bond. Also, the two hydroniums (H_3O^+) interact with the leaving Cl^- and the other three Cl ligands with strong hydrogen bonds (indicated by the short Cl-H distances of about 2.0 Å). All these interactions make H-MD2 a quite accessible complex during the action procedure, with a relative stability of only 7.2 kcal/mol higher than the reactant H-RT.

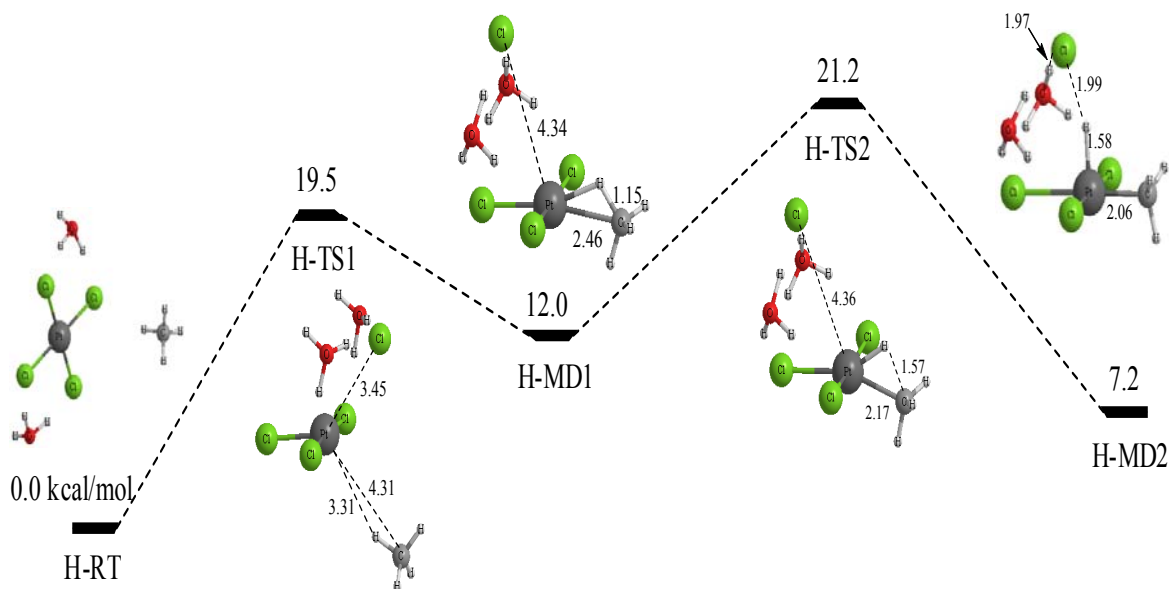


Figure 8.1: Reaction energy profile of C-H activation catalyzed by PtCl_4^{2-} in acidic condition (relative energies are in kcal/mol)

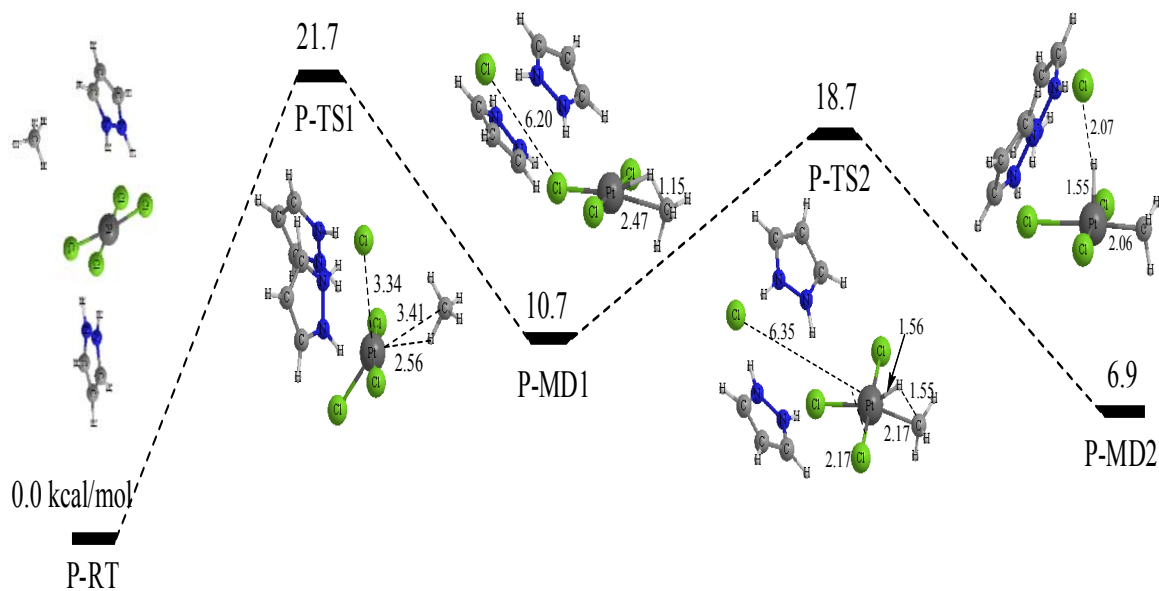


Figure 8.2: Reaction energy profile of C-H activation catalyzed by PtCl_4^{2-} in pyrazolium based ionic liquid solution (relative energies are in kcal/mol)

kcal/mol, which is higher than that of the Shilov system but significantly lower than that of the Periana system. Such findings stimulated our enhanced efforts (both theoretical and experimental) on the Shilov chemistry.

We present results on several different portions of Shilov Chemistry, focusing first on the equilibria the reference catalyst, PtCl_4^{2-} has with water, then the conventional Shilov uptake and oxidative addition pathways, and finally the various mechanisms possible when acetic acid is present.

A. Equilibria in water

The PtCl_4^{2-} catalyst can undergo substitution reactions with water to form the mono-, di-, tri- and tetra-aquo species. The relative free energies of these species are shown in Table 8.1.

Table 8.1: Free energies, relative to PtCl_4^{2-} in kcal mol⁻¹, for substituted Pt^{II} species.

	ΔG^0 Comp	ΔG^0 Expt. ¹¹
PtCl_4^{2-}	0.0	
$\text{PtCl}_3\text{OH}_2^-$	3.7	2.1
$\text{PtCl}_2(\text{OH}_2)_2$	5.9	6.1
$\text{PtCl}(\text{OH}_2)_3^+$	6.4	
$\text{Pt}(\text{OH}_2)_4^{2+}$	8.2	

Taking into account a high water concentration would lower each of these ΔG s by 1-2 kcal mol⁻¹. We should emphasize the large error bars on the computed values for the two cationic species. Formation of these species results in the formation of a very high number of charged species, consider $\text{PtCl}_4^{2-} + 4\text{H}_2\text{O} \rightleftharpoons \text{Pt}(\text{OH}_2)_4^{2+} + 4\text{Cl}^-$, in which the products have 5 charged moieties. Current continuum methods have difficulty dealing with this type of situation. What we can say with confidence is that the mono- and di-aquo species are the dominant forms and are all that we will consider.

B. Conventional Shilov Chemistry: Methane uptake

The first step of the Shilov mechanism is methane uptake, namely the substitution of a chloride or water with a methane, for example $\text{PtCl}_4^{2-} + \text{CH}_4 \rightleftharpoons \text{PtCl}_3\text{CH}_4^+ + \text{Cl}^-$. This can happen via a stepwise dissociative path, or a concerted associative way. We consider the dissociative pathway first.

The dissociative pathway would entail the formation of trivalent T-shaped species like PtCl_3^- , and the free energies of these species are shown in Table 8.2. Note that the lowest energy species is PtCl_3^- at 25.6 kcal mol⁻¹.

Table 8.2: Free energies, relative to PtCl_4^{2-} in kcal mol^{-1} , for dissociative methane uptake intermediates.

	ΔG^0
PtCl_3^-	25.6
PtCl_2OH_2 <i>cis</i>	31.2
PtCl_2OH_2 <i>trans</i>	33.5
$\text{PtCl}(\text{OH}_2)_2^+$ <i>cis</i>	32.5
$\text{PtCl}(\text{OH}_2)_2^+$ <i>trans</i>	29.0

Before we consider the associative methane uptake transition states, we first consider the water uptake transition state, shown in Figure 8.4. The barrier for water uptake is $13.0 \text{ kcal mol}^{-1}$. Figure 8.4 also includes three other possible associative methane uptake transition states. The lowest energy methane uptake is $\mathbf{1c}^\ddagger$ in which methane displaces a water molecule from the platinum catalyst with a barrier of $14.6 \text{ kcal mol}^{-1}$. The two other methane uptake transition states are significantly higher in energy, consistent with the prior work of Ziegler et al. Several other uptake transition states are possible, but we were unable to find them on our potential energy surface, however they are almost positively higher in energy than the 14.6 barrier of $\mathbf{1c}^\ddagger$ (as seen in the very high barrier for $\mathbf{1d}^\ddagger$).

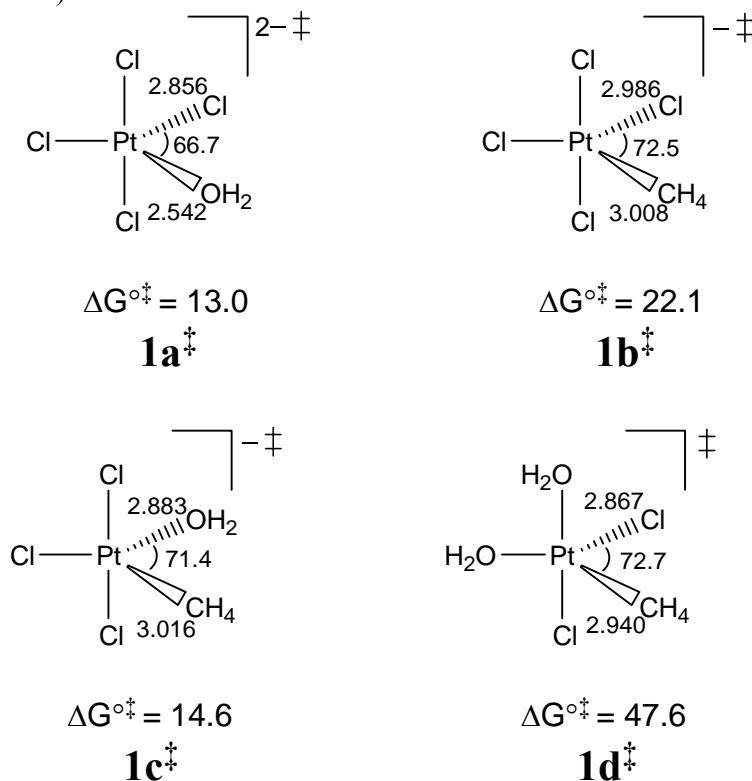


Figure 8.4: Schematics and free energies, relative to PtCl_4^{2-} in kcal mol^{-1} , for four methane uptake transition states.

The methane uptake products are the complexes methane make with the T-Shaped dissociative intermediates. 5 different orientations of chlorides, water and methane are possible and the relative free energies are listed in Table 8.3. Any substitution of water leads to higher energy methane complexes

Table 8.3: Free energies, relative to PtCl_4^{2-} in kcal mol⁻¹, for the methane uptake products.

	ΔG^0
$[\text{PtCl}_3\cdot\text{CH}_4]^-$	18.0
$[\text{PtCl}_2\text{OH}_2\cdot\text{CH}_4]$ <i>cis</i> ^a	22.7
$[\text{PtCl}_2\text{OH}_2\cdot\text{CH}_4]$ <i>trans</i>	23.3
$[\text{PtCl}(\text{OH}_2)_2\cdot\text{CH}_4]^+$ <i>cis</i>	24.7
$[\text{PtCl}(\text{OH}_2)_2\cdot\text{CH}_4]^+$ <i>trans</i>	24.4

^a. *cis/trans* refers to the orientation of the two identical ligands on the metal. e.g. in *cis* $[\text{PtCl}_2\text{OH}_2\cdot\text{CH}_4]$ the Cl atoms are *cis*.

C. Conventional Shilov Chemistry: Oxidative Addition

The second step in the activation process is the oxidative addition of the methane to the platinum center. Figure 8.5 highlights the 5 distinct oxidative addition transition states and concomitant products in which the Pt center is formally a Pt(IV). The activation barrier is directly proportional to the stretch in the C-H bond of methane. The lowest energy barriers are $2\mathbf{a}^\ddagger$ and $2\mathbf{d}^\ddagger$ which both have the smallest stretch of the C-H bond. Species $2\mathbf{d}^\ddagger$ actually has the lowest absolute activation barrier for oxidative addition, that is when we compare the transition state to the methane complex (consistent with $2\mathbf{d}^\ddagger$ having the shortest C-H distance), however the relatively high energy of the *trans* $[\text{PtCl}_2\text{OH}_2\cdot\text{CH}_4]$ complex leads to $2\mathbf{d}^\ddagger$ having a higher *net* barrier than $2\mathbf{d}^\ddagger$. However when the high concentration of water is taken into account, $2\mathbf{d}^\ddagger$ has a very similar net barrier to $2\mathbf{a}^\ddagger$. In addition to oxidative addition we looked for a metathesis barrier in which a proton would get transferred to a chloride (from the $[\text{PtCl}_3\cdot\text{CH}_4]^-$ complex). This process has a barrier of 28.6 kcal mol⁻¹. We were unable to find an electrophilic substitution in which a methane would donate a proton to a chloride in PtCl_4^{2-} in a concerted fashion.

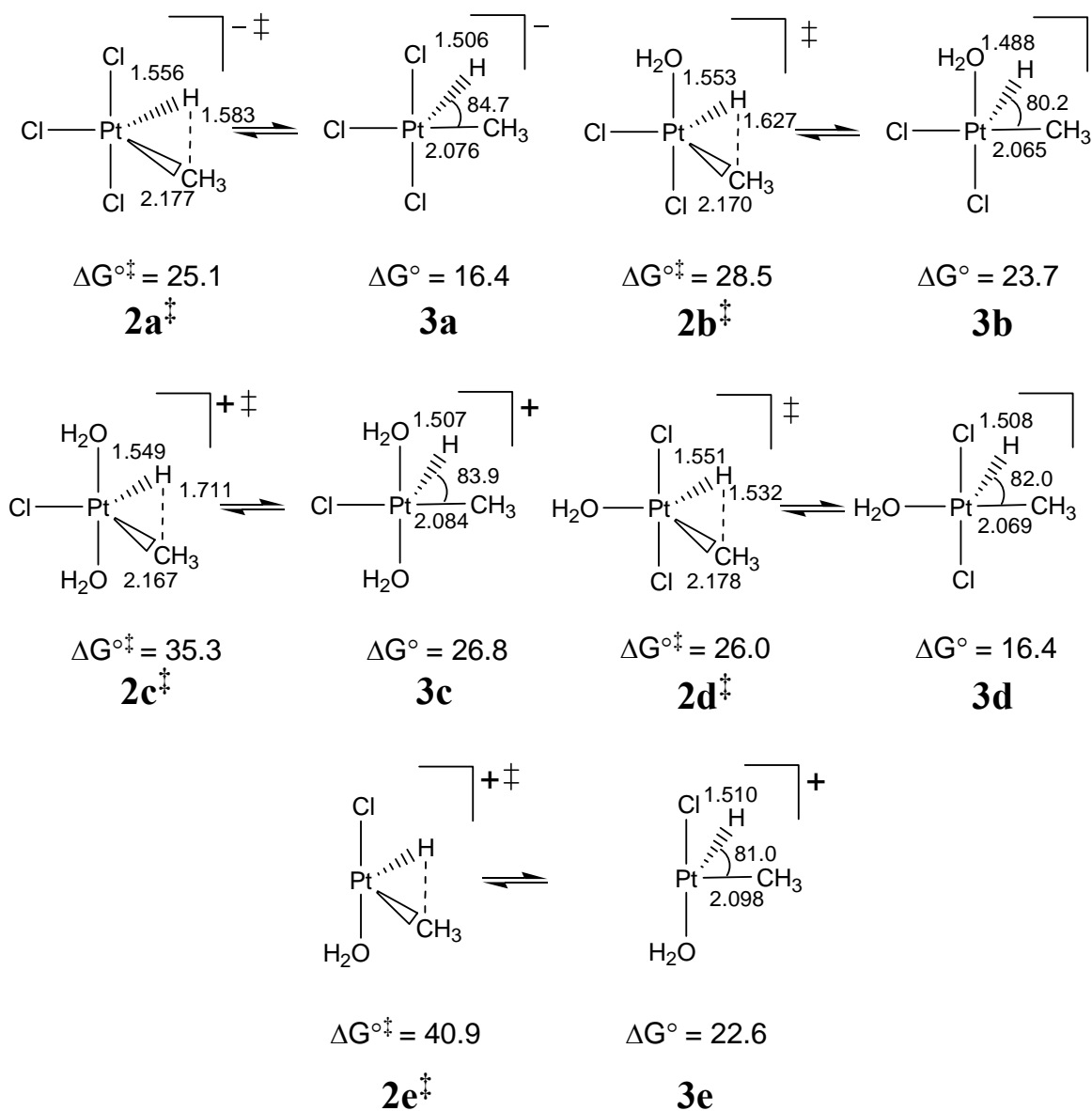


Figure 8.5: Reaction schematic for oxidative addition transition state and pyramidal product for the 5 possible cases. Free energies are in kcal mol⁻¹, bond distances in Angstroms and angles in degrees.

The final step in the activation process would be for a solvent water molecule to abstract the proton, converting the Pt center back to Pt(II). The free energies for these deprotonated species are shown in Table 8.4.

Table 8.4: Free energies, relative to PtCl_4^{2-} in kcal mol^{-1} , for the deprotonated oxidative addition products.

	ΔG^0
$\text{PtCl}_3\text{CH}_3^{2-}$	0.8
$\text{PtCl}_2\text{OH}_2\text{CH}_3^-$ <i>cis</i> ^a	6.7
$\text{PtCl}_2\text{OH}_2\text{CH}_3^-$ <i>trans</i>	1.3
$\text{PtCl}(\text{OH}_2)_2\text{CH}_3$ <i>trans</i>	8.3
$\text{PtClOH}_2\text{CH}_3^b$	11.5

^a. *cis/trans* refers to the orientation of the two identical ligands on the metal. e.g. in *cis* $[\text{PtCl}_2\text{OH}_2\cdot\text{CH}_4]$ the Cl atoms are *cis*. ^b This molecule has an empty site *trans* to the methyl, following from product **2e** in Figure 8.5.

After considering all of the data presented thus far we highlight the lowest energy pathway to methane activation and formation of the final $\text{Pt}^{\text{II}}\text{-CH}_3$ species in Figure 8.6. The final net barrier for activation is $25.1 \text{ kcal mol}^{-1}$.

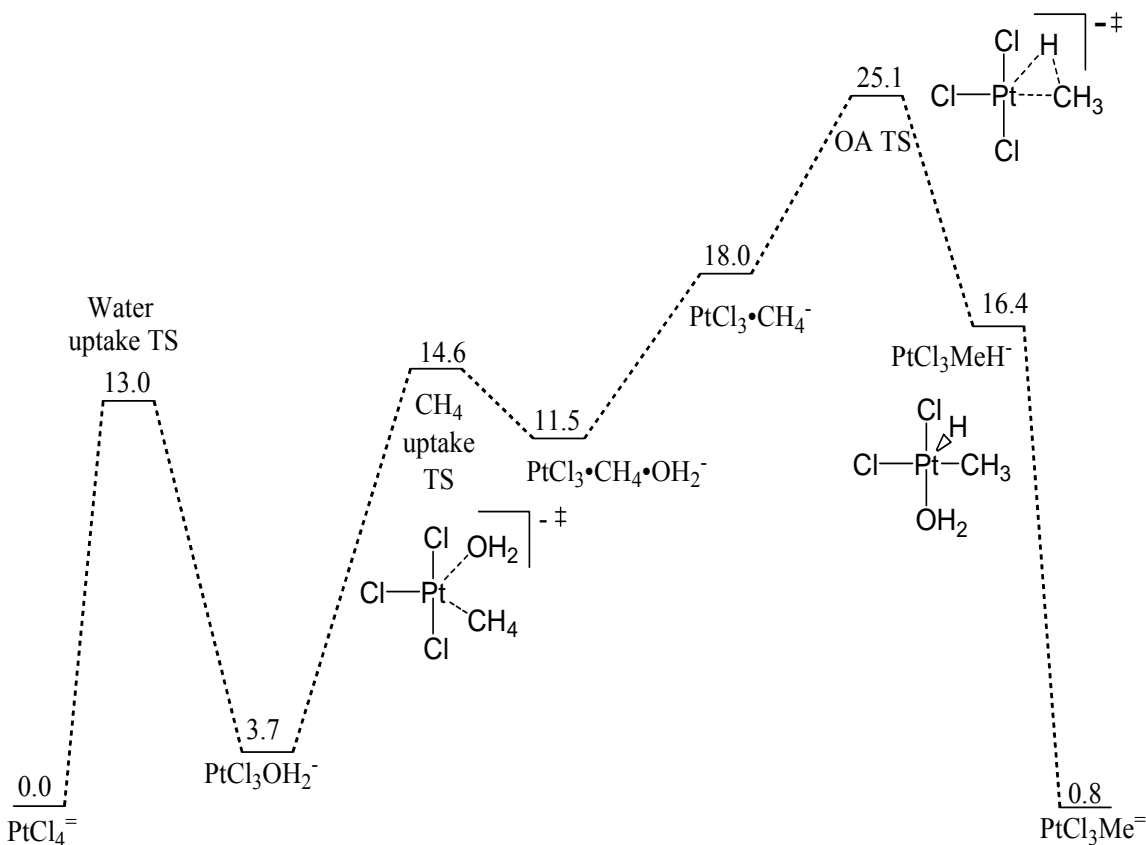


Figure 8.6: Free energy schematic for lowest energy mechanism to form activated $\text{Pt}^{\text{II}}\text{-CH}_3$. All free energies are in kcal mol^{-1} .

D. Catalyst Equilibria when Acetic Acid is Present

Experimental observations indicate that rate of H-D exchange between methane and the solvent is increased upon the presence of a high concentration of acetic acid. This is indicative of a lowering of the overall net barrier for methane activation. As such we will explore the same series of reactions as shown in sections B and C, but with acetic acid. We first consider the equilibria between various substituted reference Pt^{II} species, as shown in Table 8.5. When only a single acetate is bound to the platinum center, water in all cases destabilizes the catalyst. Placement of two acetate moieties also destabilizes the the platinum species relative to the ground state PtCl₃OAc²⁻.

Table 8.5; Free energies, relative to PtCl₄²⁻ in kcal mol⁻¹, for the deprotonated oxidative addition products.

	ΔG^0
Single Acetate	
PtCl ₃ OAc ²⁻	-7.9
PtCl ₂ (OH ₂)OAc ⁻ <i>cis</i> ^a	0.5
PtCl ₂ (OH ₂)OAc ⁻ <i>trans</i>	-0.9
Two Acetates	
PtCl ₂ (OAc) ₂ ²⁻ <i>cis</i>	-1.6
PtCl ₂ (OAc) ₂ ²⁻ <i>trans</i>	-1.7

E. Shilov Activation Chemistry with a Single Acetate Attached to Platinum

We explored the activation of methane with respect to the ground state single acetate molecule, PtCl₃OAc²⁻, and show this schematic in Figure 8.7. We have not explored the uptake mechanisms as they will be lower in energy. Both the *cis* and *trans* methane complexes lead to oxidative addition barriers larger than the conventional Shilov mechanism. We also explored a number of additional mechanisms, including metathesis mechanism in which the hydrogen was passed to the alpha oxygen (barrier of 36.6 kcal mol⁻¹, not shown in Figure 8.7) and one in which the proton was transferred to the gamma oxygen (barrier of 30.7 kcal mol⁻¹, shown in Figure 8.7). Based on our work it does not seem likely that any of the shown mechanisms involving the platinum catalyst with a single acetate are responsible for the increased rate of methane activation.

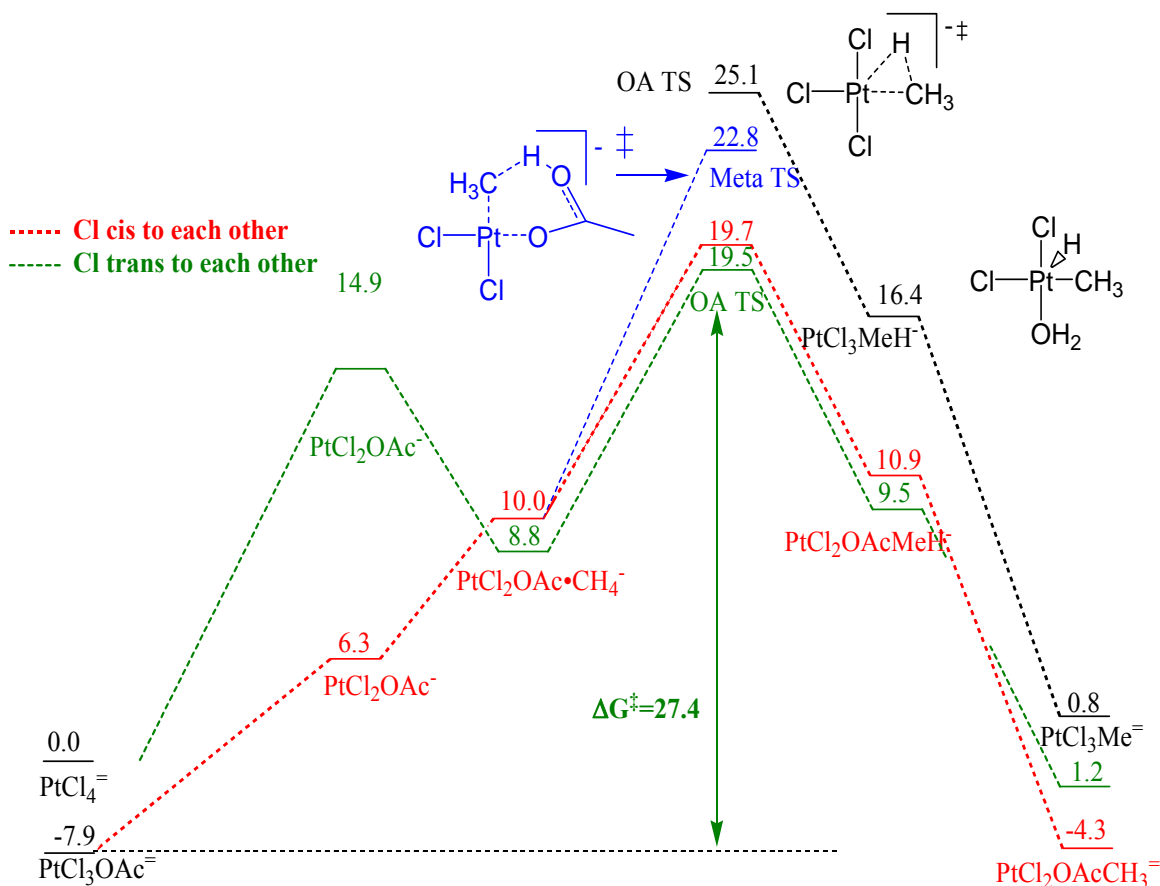


Figure 8.7: Free energy diagram, relative to PtCl₄²⁻ in kcal mol⁻¹, for methane activation using the lowest energy single acetate species, PtCl₃OAc²⁻.

F. Shilov Activation Chemistry with Two Acetate Moieties Attached to Platinum

As per our previous discussion of the equilibrium with acetic acid, PtCl₃OAc²⁻ is the ground state from which all barriers must be referenced. In

Figure 8.8, we highlight the relative oxidative addition barriers when two acetate moieties are bonded to the central platinum. We again have not listed uptake barriers which should be lower than the oxidative addition. The most salient point is the net barrier of 24.7 kcal mol⁻¹ for oxidative addition starting from the *trans* PtCl₂OAc₂²⁻ species. This is 0.4 kcal mol⁻¹ smaller than the conventional Shilov system. The *cis* pathway has a larger barrier of 30.7 kcal mol⁻¹.

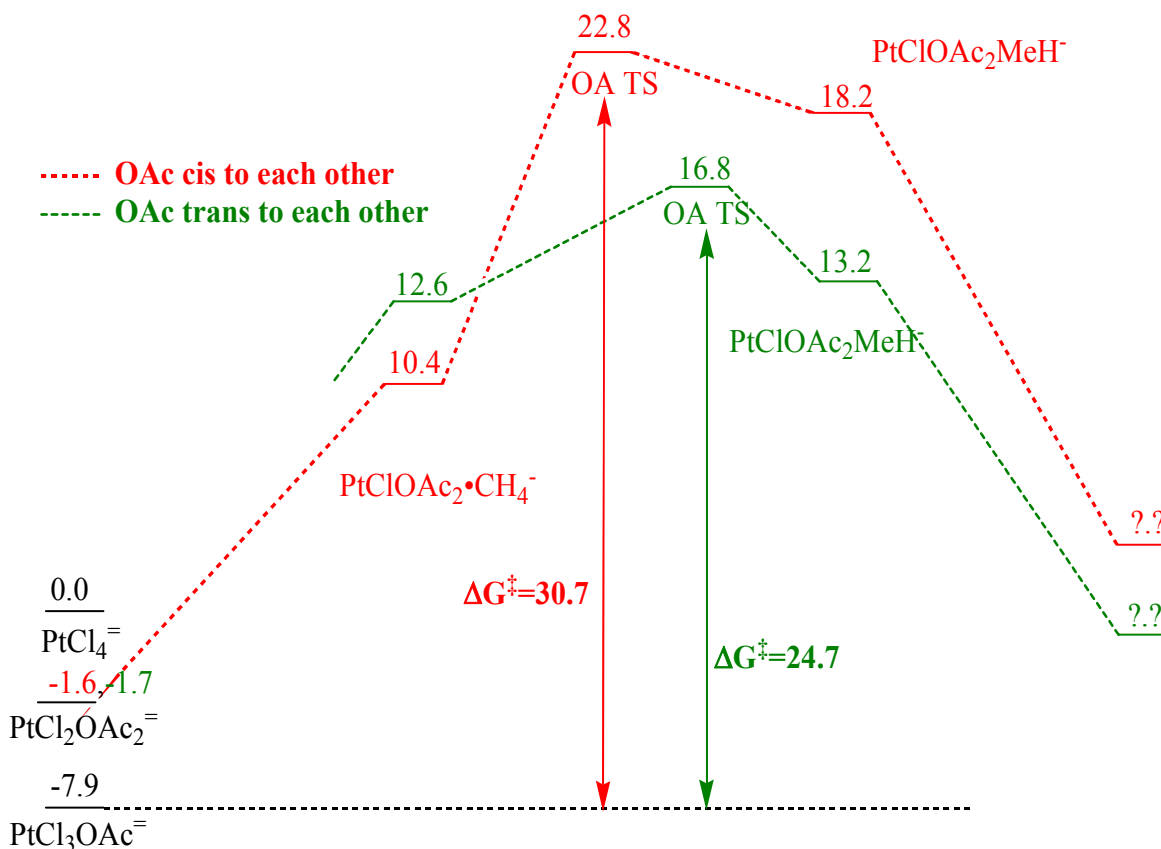


Figure 8.8: Free energy diagram, relative to PtCl_4^{2-} in kcal mol^{-1} , for methane activation using the *cis* and *trans* bis-acetate species, $\text{PtCl}_2\text{OAc}_2^{2-}$.

This result is pretty encouraging. However, the experimental data indicate that the addition of acetic acid increases the rate 10-100 times, consistent with a decreased barrier of 2-3 kcal mol^{-1} . During our earlier analysis we made the observation that explicit waters are very important in the description of the equilibrium between PtCl_4^{2-} and $\text{Pt}(\text{OH}_2)_2(\text{OAc})_2$, but they can also play an important role in the description of the $\text{PtCl}_3\text{OAc}^-$. $\text{PtCl}_3\text{OAc}^-$ is not as nucleophilic as PtCl_4^{2-} and should be stabilized less with explicit waters. Preliminary work with 2 explicit waters on the platinum species show some interesting results. The conventional Shilov barriers changes little, from 25.1 kcal mol^{-1} to 25.5 kcal mol^{-1} . The mono-acetate barriers actually get larger from 27.4 to 30.3 kcal mol^{-1} (for the *cis* case), this is despite the fact that the $\text{PtCl}_3\text{OAc}^-$ complex is destabilized to a relative energy of -5.8 kcal mol^{-1} (from -7.9) when 2 explicit waters are included. However the *trans* bis-acetate net barrier is reduced to 22.5 kcal mol^{-1} . This is 3.0 kcal mol^{-1} less than the conventional Shilov system, in line with experimental results.

G. Methodological Improvements for Describing Shilov Chemistry

We are concerned with the accurate calculation of redox potentials for platinum and other metals which may be useful as oxidants. Tabulated reference data for three chemical oxidations was used to determine the basis functions which are required by our metals for accurate thermochemistry. Table 8.6 compares the performance of the “off-the-shelf” pseudopotential and basis set of Hay and Wadt with the performance of a valence basis we have created by adding additional p- and f-angular momentum functions. The p-functions allow expansion or contraction of the 6p electrons of platinum as charge is donated or withdrawn from the atom. F-functions allow angular optimization of the bonding orbitals in environments far from spherical. These additional functions are very effective in correcting deficiencies in the standard bases.

Table 8.6: Comparison of the performance of the standard Los Alamos pseudopotentials and valence basis functions with a valence basis augmented with additional p- and f-functions.

Reaction	ΔG_{rxn} (kcal/mol)			
	Experiment	B3LYP Los Alamos standard valence	Los Alamos augmented valence	Explicit solvent
$\text{Pt}^{\text{II}}\text{Cl}_4^{2-} (1\text{M}) + \text{Cl}_2 (1\text{atm}) \rightarrow \text{Pt}^{\text{IV}}\text{Cl}_6^{2-} (1\text{M})$	-29.0	-20.1	-30.9	-32.2
$\text{Pt}^{\text{II}}(\text{NH}_3)\text{Cl}_3^{1-} + \text{Cl}_2 \rightarrow \text{Pt}^{\text{IV}}(\text{NH}_3)\text{Cl}_5^{1-}$	-30.9	-18.9	-29.9	–
$\text{Pd}^{\text{II}}\text{Cl}_4^{2-} + \text{Cl}_2 \rightarrow \text{Pd}^{\text{IV}}\text{Cl}_6^{2-}$	-3.1	2.8	-3.1	–

We repeated the platinum tetrachloride oxidation, including six explicit water molecules around the platinum chloride complexes which could accept fractional charge from the anions. The continuum dielectric is still used outside of the entire metal-water cluster. Table 8.7 also shows that this role of explicit solvent is unnecessary and has little effect on the calculated free energy change.

Table 8.7: Comparison of two pseudopotentials (by Los Alamos and Ermler, et al.)

Reaction	ΔG_{rxn} (kcal/mol)		
	Exp.	B3LYP Los Alamos augmented	Ermler(2f)
$\text{Pt}^{\text{II}}\text{Cl}_4^{2-} + \text{Cl}_2 \rightarrow \text{Pt}^{\text{IV}}\text{Cl}_6^{2-}$	-29.0	-30.9	-30.5
$\text{Pt}^{\text{II}}(\text{NH}_3)\text{Cl}_3^{1-} + \text{Cl}_2 \rightarrow \text{Pt}^{\text{IV}}(\text{NH}_3)\text{Cl}_5^{1-}$	-30.9	-29.9	-28.7
$\text{Pd}^{\text{II}}\text{Cl}_4^{2-} + \text{Cl}_2 \rightarrow \text{Pd}^{\text{IV}}\text{Cl}_6^{2-}$	-3.1	-3.1	–

For the same three testing reactions we compared two pseudopotentials and two density functionals (Table 8.7). The more recent pseudopotential of Ermler, et al¹⁴, (again with f-functions added) offered similar performance to the Los Alamos pseudopotential.

Table 8.8: Evaluation chlorine thermodynamics with and without d- and f-angular momentum polarization functions

Reaction	ΔH_{rxn} (kcal/mol)		
	Exp.	B3LYP 6-311G**++	6-311G++-3df
$\frac{1}{2}\text{Cl}_2 + \text{e}^- \rightarrow \text{Cl}^-$	-57.2	-63.6	-58.8
$\frac{1}{2}\text{Cl}_2 \rightarrow \text{Cl}\cdot$	29.1	24.7	29.4
$\frac{1}{2}\text{Cl}_2 \rightarrow \text{e}^- + \text{Cl}^+$	331.1	327.8	332.5

Capturing the thermochemistry of chlorine is equally important in our investigations. Table 8.8 compares the performance of the moderately sized 6-311G**++ basis to the same basis augmented with d- and f-angular momentum polarization functions. Without the polarization functions, chlorine in a nonspherical environment (e.g. Cl_2 or M-Cl) is consistently destabilized relative to chlorine in a spherical potential (e.g., free Cl^-). The addition of polarization functions corrects this behavior.

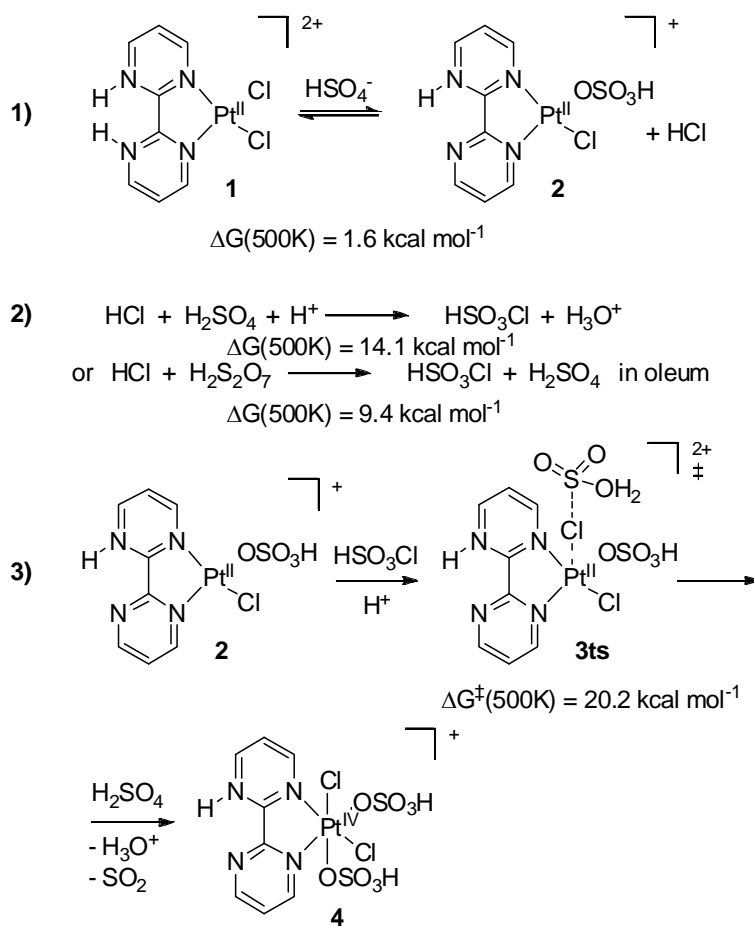
These expanded basis sets, along with the density functional and solvation model validated here and in other calculations, give us great confidence in predicting the thermochemistry of new and interesting oxidation reactions.

8.4 EFFECTIVE OXIDATION STATE OF PT-CATALYST IN HOT CONCENTRATED SULFURIC ACID FOR CATALYTIC METHANE CONVERSION

This multi-year project started from the Catalytica system reported by Periana et.al in 1998 in which (bpym)Pt^{II}Cl₂ efficiently catalyzes the partial oxidation of CH₄ to CH₃OSO₃H in hot concentrated H₂SO₄. The high selectivity, relatively high reaction rate and system stability make this low temperature methane conversion approach highly attractive for economically utilization of abundant yet untapped natural gas resources. However, critical hurdles need to be overcome for this approach including the system deactivation upon water/methanol production, high product separation cost and utilization of highly corrosive concentrated sulfuric acid. In-depth understanding on the reaction mechanisms has critical significance on improving the Catalytica system. Our latest work has revealed that the concentrated sulfuric acid not only serves as the oxidant but also functions as a co-catalyst. In addition, we have explored the possible pathway for the stabilization of the effective oxidation state of the Pt-catalyst.

Experimental observations on the Catalytica system showed that 1) Pt(IV) is the inactive species for C-H activation in CH₄; 2) Pt(IV) is the highest thermodynamically accessible (i.e. the stable oxidation state instead of Pt(II)) under the reaction conditions for the Catalytica methane to methanol conversion system; 3) the over-oxidation of Pt(II) to Pt(IV) through hot concentrated H₂SO₄ with generation of SO₂ gas is irreversible

Firstly, we investigated how the oxidation of the non-methylated (bpym)Pt^{II} complex could occur. The previously proposed mechanism by Ziegler et al.¹⁵ was found, in our hands, to have an inaccessible barrier of 44 kcal mol⁻¹ (for oxidant = H₂SO₄, 39 when oxidant = H₂S₂O₇). Another path was located which starts with replacement of one of the chlorides on **1** to yield the bisulphate complex **2** and HCl. HCl and H₂SO₄ is known to react to give chlorosulfonic acid. We calculate that reaction to be endergonic by 14.1 kcal mol⁻¹ (9.4 kcal mol⁻¹ for reaction between HCl and H₂S₂O₇). The chlorosulfonic acid can then react with the non-methylated Pt^{II} complex **2** via an inner-sphere electron transfer (**3ts**) similar to that proposed for Pt^{II} and Pt^{IV} interchange to give the Pt^{IV} complex **4** and water and SO₂. The overall barrier for the electron transfer relative to **1** and H₂SO₄ was found to be 35.9 kcal mol⁻¹ (31.2 kcal mol⁻¹ for H₂S₂O₇) and the overall reaction was found to be exergonic by 1.0 kcal mol⁻¹ (6.x kcal mol⁻¹ for H₂S₂O₇). The value we calculate for the barrier is very close to the value reported for the overall catalytic conversion of methane to methanol. This shows that the complete oxidation of the non-methylated form of the (bpym)Pt^{II} catalyst under the optimal reaction conditions (102% H₂SO₄) will be complete within a few turnovers. As can be seen from the transition state for the inner-sphere reaction, the reaction is facilitated by the high proton availability that leads to protonation of the OH group of the chlorosulfuric acid. This protonation facilitates both the kinetics and thermodynamics of the inner-sphere transfer. Thus, protonation activates the chlorosulfonic acid by reducing the energy of the Cl-S anti-bonding orbital, the LUMO, to attach of the Pt(II) d_z² HOMO at the Cl-group with water instead of OH⁻ as the leaving group. This contrasts to the classic self-exchange studies by Basolo where the [PtCl₄]²⁻ d_z² HOMO energy is increased by coordination of Cl⁻ generate a five coordinate [PtCl₅]³⁻ intermediate that attacks the Cl-Pt anti-bonding orbital, the LUMO, of [PtCl₆]²⁻.



Overall barrier from **1** to **3ts** = $35.9 \text{ kcal mol}^{-1}$
 ($31.2 \text{ kcal mol}^{-1}$ in oleum)

Figure 8.9.: Oxidation of the Pt^{II} complex **1** to the Pt^{IV} complex

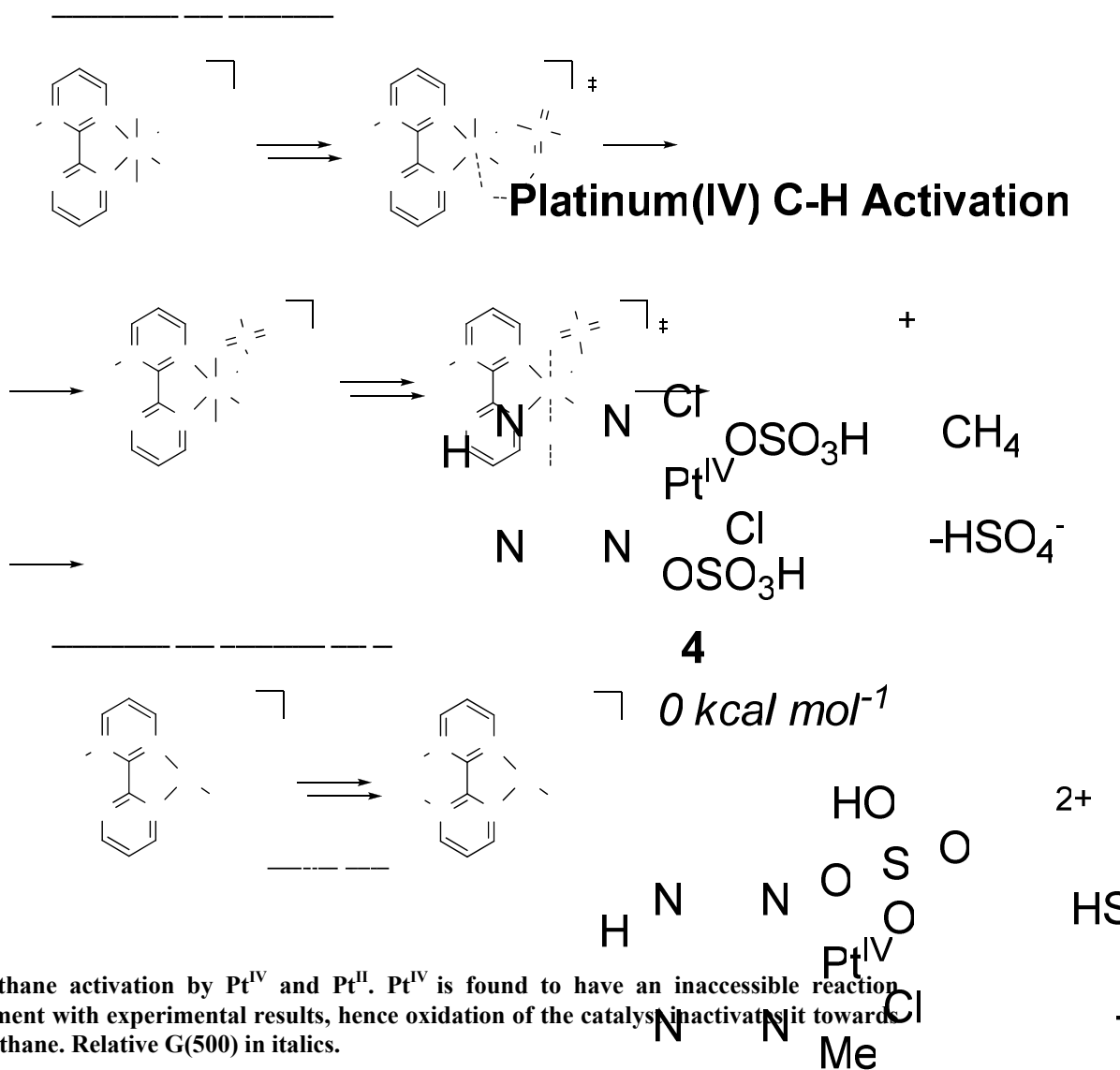
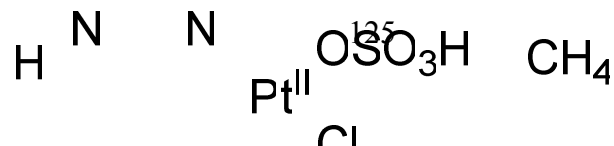


Figure 8.10: Methane activation by Pt^{IV} and Pt^{II}. Pt^{IV} is found to have an inaccessible reaction barrier in agreement with experimental results, hence oxidation of the catalyst inactivates it towards reaction with methane. Relative G(500) in italics.

Theoretical calculations also support the view that it is (bpy)Pt(II) **6** not (bpy)Pt(IV) acting as the active catalyst for the C-H activation. The lowest energy calculated barriers corresponding to the (bpy)Pt(IV) catalyst are substantially higher than the observed barriers for catalyzed oxidation reaction of methane to methanol. The highest point on the path for reaction between (bpy)Pt^{IV} and methane is the C-H cleavage which is calculated to have a barrier of 41.2 kcal mol⁻¹. This can be compared to the barrier of **2** which we recently published, of 27.7 kcal mol⁻¹. Moreover we find that functionalization of the Pt^{IV} methyl has a barrier of 23.3 kcal mol⁻¹, while the protonation of the same Pt^{IV} methyl bond, which is the microscopic reverse of the reaction of **4** and methane, has a barrier of 43.9 kcal mol⁻¹. These results are not compatible with the experimental observation that the methyl group of the methyl bisulfate product is deuterated when the reaction is performed in D₂SO₄. Pt^{II} however has been shown to incorporate multiple deuterium atoms in the reversible C-H activation of methane in D₂SO₄, and we believe that this further proves that Pt^{II} is the active state of the catalyst.



If CH Activation by Pt^{IV} is eliminated, then the basis for the stability of the Catalytic system remains to be elucidated. Another possibility is the known reaction between Pt^{IV} and Pt^{II}-CH₃ as has been shown for the Shilov system. However, to be the basis for the high stability of the system, this reaction would have to be competitive with the over-oxidation of resulting from the reactions of Pt^{II} with solvent H₂SO₄. Since the steady state concentrations of Pt^{II} and Pt^{IV} would be in the ppt and ppm respectively, this reaction would certainly have to operate at diffusion controlled rates to be competitive. The known self exchange rates between PtCl₄]²⁻ and PtCl₆]²⁻ are much too slow for this to be the reaction mechanism although Bercaw showed that with Pt^{II}-CH₃ species that the reactions can be faster.

In the Shilov system,¹⁶ Pt^{IV} is used as the stoichiometric oxidant. The proposed mechanism for this system is that Pt^{II} activates methane to yield a Pt^{II} methyl complex. This complex then reacts with the Pt^{II} via an inner-sphere electron transfer to give a Pt^{IV} methyl and non-methylated Pt^{II}. We recently reported the mechanism for the acid catalyzes methane uptake. In that study we showed that the platinum methyl complex **8** formed in the C-H activation is 17.7 kcal mol⁻¹ higher in energy than **2**. If there is a similar electron transfer between **4** and **8** it therefore needs to be very facile since the barrier will be added to the energy of **8**.

We have indeed found a facile an inner-sphere electron transfer transition state **9ts** from the reaction between **4** and **8** in which a sulphuric acid molecule had been dissociated. The free energy of **9ts** is calculated to be only 5.5 kcal mol⁻¹ relative to the methyl complex **8** and the Pt^{IV} complex **4**. Such low barrier indicates that the reaction is essentially diffusion controlled. The resulting complexes of the reaction is the organometallic Pt^{IV} methyl complex **10** and the non-methylated Pt^{II} complex **2**. The reaction is exergonic by 25.4 kcal mol⁻¹. The fact that the electron transfer is calculated to have such low barrier means that it is likely responsible for the reduction of the oxidized catalyst and regeneration of the C-H activation capable Pt^{II}, and at the same time it oxidizes the Pt^{II} methyl to Pt^{IV} methyl which can readily form the methyl bisulphate reductively.

It is interesting to note that this inner-sphere electron transfer is facilitated by the acid by protonation of the bisulphate leaving group, rather than chloride catalyzed as in the classical [Cl---Pt^{II}---Cl---Pt^{IV}---Cl] system.¹⁷ In the classical system, one could postulate that the pre-equilibrium reaction between [PtCl₄]²⁻ and Cl⁻ to generate [PtCl₅]³⁻ served to increase the nucleophilicity of the Pt^{II} center and that this facilitates the attack on the Cl center and the displacement of Pt^{II} and Cl⁻ from the Cl-Pt^{IV}-Cl complex. Since the energetic cost of generating Cl⁻ in concentrated sulphuric acid is prohibitively high, the activation and inner-sphere electron-transfer proceeds via a complementary pathway involving activation by protonation as opposed to Cl⁻ activation. Thus, in this case, rather than the Pt^{II} complex being activated to be a stronger nucleophile, the lowest energy pathway involves protonolysis of the X group of the Cl-Pt^{IV}-X ground state. This serves to increase the electrophilicity of the Cl atom of the Cl-Pt^{IV}-XH complex and also generates a more labile, HX leaving group in **6ts**. This illustrates the importance of the acid solvent

not only in the C-H activation even, but also in the oxidation and as will shown later, in the functionalization reactions.

Significantly, we find that trans to the chloride of **10** it is favourable to coordinate bisulphate while trans to the methyl group of **12** it is more favourable to solvate the bisulphate. The unfavourable coordination trans to the methyl group is likely due to a combination of the strong trans influence of the methyl group and the weakly coordinating properties of the bisulphate. Since the methyl group on **12** is electrophilic and leads to a more stable 4-coordinate Pt^{II} product on nucleophilic attack of HSO_4^- on the methyl group, the functionalization reaction proceeds from the 5-coordinate complex **12** versus the 6-coordinate **10**. The reorganization between **10** and **12** is calculated to have a barrier (**11ts**) of $14.0 \text{ kcal mol}^{-1}$ and is exergonic by $15.1 \text{ kcal mol}^{-1}$. Nucleophilic functionalization by a bisulphate on the methyl group occurs via **13ts**. The barrier was calculated to be $27.6 \text{ kcal mol}^{-1}$. Now the product have been generated and a Pt^{II} species **14** have been regenerated which can activate methane.

To conclude, our calculations have proposed to use a lower than the highest accessible oxidation state of the metal catalyst for reaction with methane in the case of the $(\text{bpym})\text{PtCl}_2/\text{H}_2\text{SO}_4$ system where methane CH activation is proposed to react with a Pt^{II} species rather than the thermodynamically more stable, higher oxidation state, $\text{Pt}(\text{IV})$. The C-H activation generates a $\text{Pt}^{\text{II}}\text{-Me}$ species, which is oxidized to a $\text{Pt}^{\text{IV}}\text{-Me}$ species. This complex is then readily undergoes reductive functionalization by nucleophilic substitution on the methyl group, to generate the product and regenerates the active, lower oxidation state catalytic species, $\text{Pt}(\text{II})$. For the mechanism where the catalyst is in the highest available oxidization state, it is likely to be more susceptible to poisoning by water or other coordinating molecules, since higher oxidation states are typically kinetically less labile due to the stronger ligand metal bond strengths. On the other hand, since the highest available oxidation state of the catalyst is the thermodynamically stable state, the catalyst will not be sensitive to deactivation through oxidation of the active species. For the mechanism where the active state is a lower oxidation state than is thermodynamically accessible. Since this lower oxidation state is less electron withdrawing than the higher oxidized states and forms weaker bonds to its ligands, it will likely be less sensitive to water poisoning and more kinetically labile. However, there is a risk that the active, reduced oxidation state catalyst will be deactivated by over oxidation reactions.

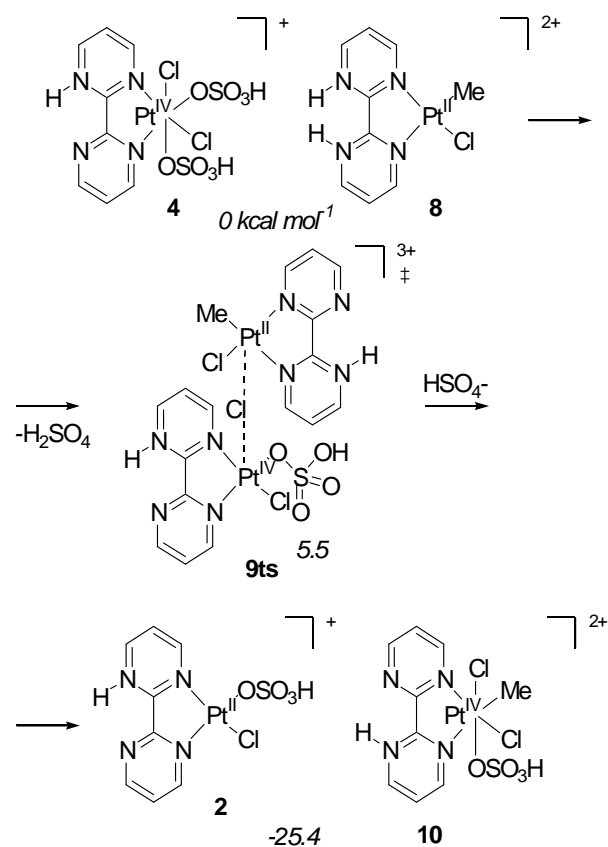


Figure 8.11: Inner-sphere electron transfer between non-methylated Pt^{IV} and methylated Pt^{II}. Relative G(500) in italics.

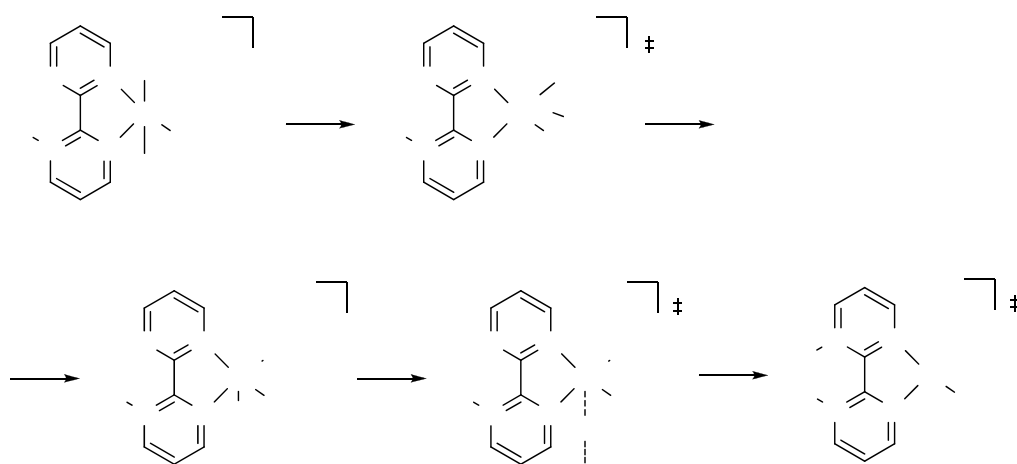
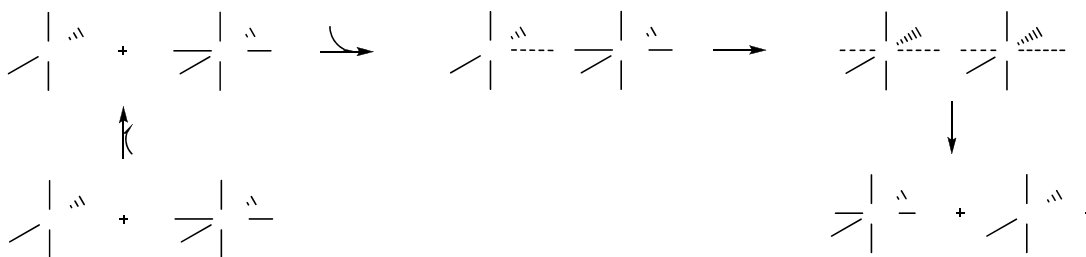


Figure 8.12: Nucleophilic functionalization of the methylated Pt^{IV} generates the methyl bisulfate product and regenerates the active Pt^{II} catalyst. Relative G(500) in italics.

8.5 THE OXIDATION STEP OF SHILOV CHEMISTRY WITH HIGHLY-CONCENTRATED [Cl⁻]

We used quantum chemical models to determine the rate-limiting factors in the class of reactions in which an Mⁿ-CH₃ intermediate is oxidized to Mⁿ⁺²-CH₃ by a metal halide. The oxidation step of the Shilov cycle, Pt^{IV}Cl₆²⁻ + Pt^{II}-CH₃ → Pt^{IV}-CH₃ + Pt^{II}Cl₄²⁻, serves as the reaction of interest. In light of the literature available treating this reaction and its role in our experimental work, we spent our primary effort developing detailed and validated models for this reaction. Such work aims at providing theoretical guidance for further search of alternative cheap oxidants. We mapped the free energy surface of the oxidation of Pt^{II}(CH₃)(Cl)₂(H₂O)¹⁻ by Pt^{IV}Cl₅(H₂O)¹⁻ to determine the relative contributions of electrostatic repulsion, redox potentials and entropy to the overall activation barrier. The number of chloride anions contained in the encounter complex was varied in order to understand the oxidation rate's dependence on [Cl⁻].

The oxidation reactions in aqueous solution were broken into stages. First we consider ligand substitution reactions (between water and chloride) by which higher-energy intermediates of the form Pt^{II}(CH₃)(Cl)_x(H₂O)_{3-x} and Pt^{IV}(Cl)_y(H₂O)_{6-y} may be generated from the most stable stoichiometries. A distribution of these species determined by reaction conditions is expected to exist. Second we consider the loose association of a Pt^{II}-CH₃ monomer with a Pt^{IV}-Cl monomer. To represent these encounter complexes (an assumed prerequisite of the oxidation reaction) we constrained the key platinum-chloride (Pt^{II}...Cl-Pt^{IV}) distance to 3.0 Å and relaxed all other coordinates. The choice of 3.0 Å is arbitrary but allows a qualitative decomposition of the reaction profile into stages. An additional water molecule is included in the encounter complexes to allow the Pt^{IV}-CH₃ product to assume an octahedral coordination environment. We included in each calculation an entropic penalty -TΔS = -(473K)(-15e.u.) = 7.1 kcal/mol, where 15 entropy units is typical for a reduction in molecularity by one. Finally, the transfer of Cl⁻ from the Pt^{IV} to the Pt^{II}-CH₃ center is examined. The topography of the energy surface for this step varies qualitatively with changes in stoichiometry, and since it is sensitive to four internal coordinates (the bond lengths along the H₂O...Pt^{II}...Cl...Pt^{IV}...L axis) locating well-defined minima and saddle points along the reaction coordinate was difficult. Employing a nudged-elastic band approach will aid locating transition states in this multidimensional space.



Scheme 1: Variable stoichiometries for oxidation of Pt^{II}-CH₃ by Pt^{IV}

Reactants

We find the most stable stoichiometry for the $\text{Pt}^{\text{II}}\text{-CH}_3$ and inorganic Pt^{IV} states at 1M $[\text{Cl}^-]$ to be $\text{Pt}^{\text{II}}(\text{CH}_3)(\text{Cl})_2(\text{H}_2\text{O})^{-1}$ and $\text{Pt}^{\text{IV}}(\text{Cl})_6^{-2}$, respectively. The stoichiometry of these species in the oxidation transition states may differ, since a more negative $\text{Pt}^{\text{II}}\text{-CH}_3$ may be more easily oxidized and a more positive Pt^{IV} may be a stronger oxidant. Replacing the water bound trans to the methyl group in **1** costs 4 kcal/mol at 1M $[\text{Cl}^-]$. To incorporate the concentration of free chloride, we adjust its free energy according the statistical mechanics correction $kT\ln([\text{Cl}^-]/[1\text{M}])$, using $T=473\text{K}$. Thus substitution of chloride into the coordination sphere is encouraged by higher chloride concentrations.

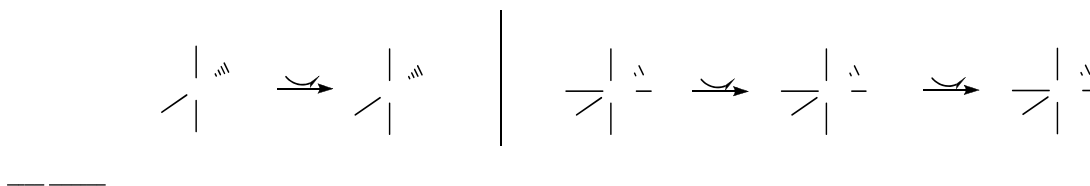


Figure 8.13: Free Energies of variously substituted reactant complexes in Shilov system

Encounter complexes:

1-C: $\text{Pt}^{\text{II}}(\text{CH}_3)(\text{Cl})_2(\text{H}_2\text{O}) \cdot \text{Pt}^{\text{IV}}(\text{Cl})_4(\text{H}_2\text{O})_2^{-1}$

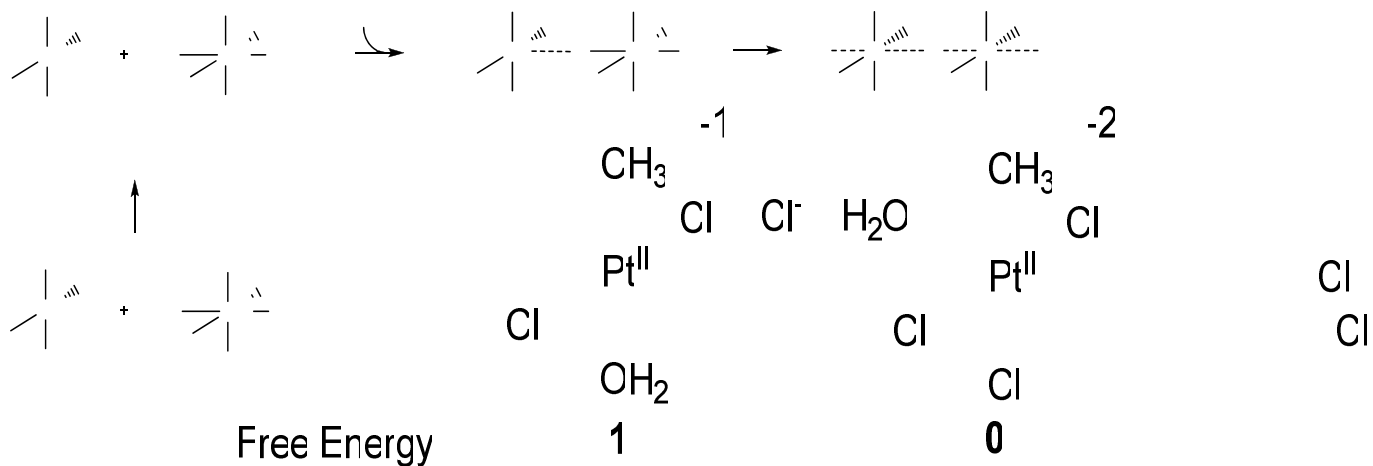


Figure 8.14: Energy barrier for formation of encounter complex $\text{Pt}^{\text{II}}(\text{CH}_3)(\text{Cl})_2(\text{H}_2\text{O}) \cdot \text{Pt}^{\text{IV}}(\text{Cl})_4(\text{H}_2\text{O})_2^{-1}$

1M $[\text{Cl}^-]$:	0.0 kcal/mol	4.0
5M $[\text{Cl}^-]$:	0.0	2.5

Substituting two chloride ligands of $\text{Pt}^{\text{IV}}\text{Cl}_6^{2-}$ with waters costs 13.5 kcal/mol, but results in a neutral Pt^{IV} and sets up a more exothermic oxidation. Complexation of **1** and **C**, as judged by the constrained complex, is then exothermic but disfavored due to

entropy. The oxidation reaction apparently proceeds from there without a barrier. Increased chloride concentration will disfavor the preequilibrium between **A** and **C**, inhibiting the reaction rate.

1-B: Pt^{II}(CH₃)(Cl)₂(H₂O) · Pt^{IV}(Cl)₅(H₂O)²⁻

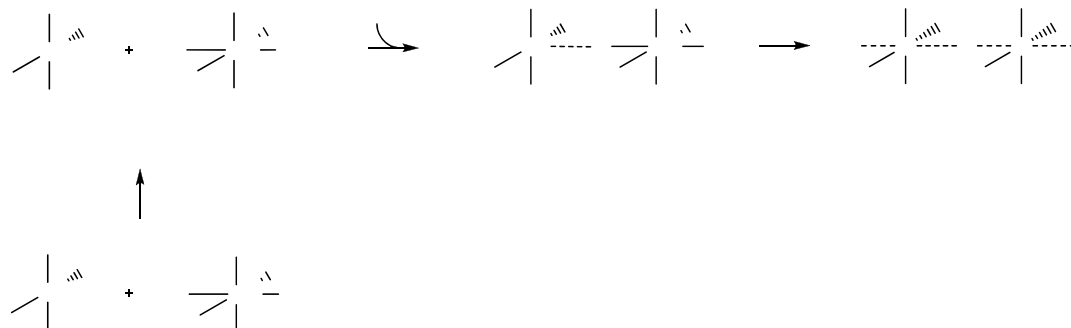


Figure 8.15: Energy barrier for formation of encounter complex Pt^{II}(CH₃)(Cl)₂(H₂O) · Pt^{IV}(Cl)₅(H₂O)²⁻

CH₃ -1 Cl -1 H₂O CH₃
Pt^{II} Pt^{IV} OH₂ Pt^{II}
Cl Cl Cl
OH₂ OH₂
1 3
5.2 (6.7)

Substituting one chloride ligand with water costs only 5.2 kcal/mol but precedes the complexation of two negatively charged species. Complexation is disfavored on both energetic and entropic grounds. A subsequent barrier exists and sampling of the free energy surface in this region suggests the barrier is a few kcal/mol above the constrained complex.

1-A: Pt^{II}(CH₃)(Cl)₂(H₂O) · Pt^{IV}(Cl)₆³⁻

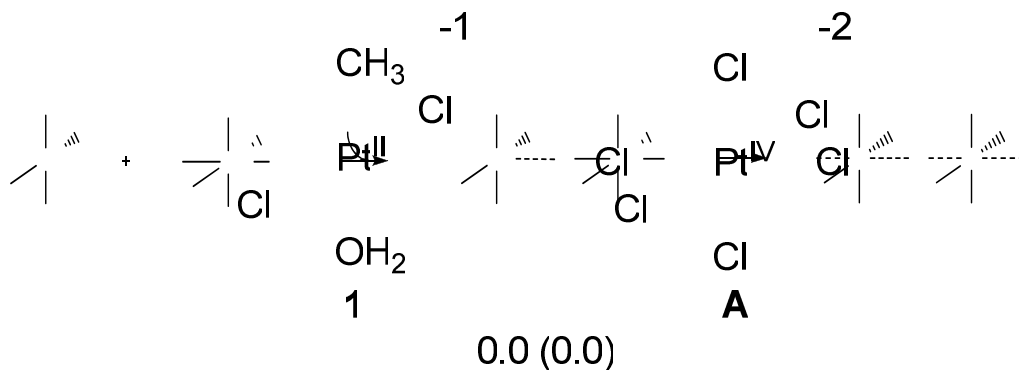


Figure 8.16: Energy barrier for formation of encounter complex Pt^{II}(CH₃)(Cl)₂(H₂O) · Pt^{IV}(Cl)₆²⁻

[Cl⁻] = 1M (5M)

In the oxidation of **1** by **A**, the complexation is the most endergonic in the series, forming a highly charged complex.

The energies of the constrained encounter complexes are remarkably similar, despite differences in composition and charge. Based on the given data it is reasonable that complex 1-B provides the lowest energy pathway to products at 1M [Cl⁻]. However, this pathway will suffer as the chloride concentration is increased, favoring both **0** to **1** and **A** to **B**. The increased negative charge on both reactants is expected to raise the energy of the encounter complexes, retarding oxidation rates.

Faster oxidation of Pt^{II}-CH₃ intermediates may be achieved if the oxidant is more positively charged at high chloride concentrations. This suggests the exploration of neutral chelating ligands on metals intended as oxidants. Such ligands are expected to inhibit CH activation, but they could possibly be chosen to preferentially bind to Cu or Fe.

CHAPTER NINE: PROPOSED FUTURE WORK

Upon the successful completion of this five-year project and corresponding to the current economy and energy crisis faced by the U.S., we have proposed a future research plan to further advance the development of the ionic liquid affiliated homogenous methane catalytic system towards final industrial commercialization. Described below is a three-year research plan given sufficient financial supports from the government and industrial partners. Successful completion of the tasks proposed below will lead this current technology to the **Technology Readiness Level 5** serving as a critical step for transferring the proposed research technology to practical industrial applications which can be of great benefits to the nation's economic strategy, energy crisis as well as environment protection.

Milestone 1 (Year 1): Design, screen and develop new catalytic systems for methane conversion with high yield (>90%) and high selectivity (>90%).

Subtask 1.1 Using molecular design technology to design and screen potential ionic liquid affiliated catalytic methane conversion systems

Our previous work has already provided some molecular level understanding of the chemistry involved in some Pt-based catalytic systems the PEER system, Catalytica system and the Shilov system. Powerful computational approaches based on QM, ReaxFF and MD have been developed to simulate certain chemistries involved in ionic liquids affiliated methane conversion systems. Therefore, in this stage, we will further extend our theoretical efforts on various possibility of combination of ionic liquids, catalysts, oxidants and reaction media to point out the possible systems for efficient methane conversion.

Subtask 1.2 Experimental test and evaluation of various catalytic systems guided by the theoretical predications

Experimental efforts will be taken on synthesizing necessary ionic liquids or catalysts, testing compatibility of designed system and evaluating the catalytic performance of some systems. For example, we are the first to observe the catalytic ability of Os(III) and Os(IV)-compounds on C-H activation of methane. Further search for compatible oxidants and reaction media might lead to an Os-based catalytic system for efficient methane conversion.

Subtask 1.3 Screen and identify the most promising systems with best conversion and selectivity

Integrating the computational and experimental findings, we will be able to screen and identify the most promising systems with best conversion and selectivity. The Virtual Rapid Prototyping (VRP) Method for fast screening of promising catalytic methane conversion systems will be further developed and enhanced. With such a VRP approach,

the cost and time required for developing a methane conversion system with desired performance will be significantly decreased.

Milestone 2 (Year 2): Optimize and improve selected catalyst systems for methane conversion

Subtask 2.1 Perform detailed chemistry analysis on reaction rate, selectivity and deactivation of selected catalytic system.

Upon reaching the first milestone, we will narrow down our theoretical and experimental efforts to the most promising systems. Further optimization will be based on indepth mechanistic understanding of the detailed chemistry influencing the performance (reaction rate, selectivity, deactivation, etc.) of the selected catalytic system.

Subtask 2.2 Optimize the catalytic system in terms of composition, reactor design, experimental protocols and conditions

As instructed by the indepth mechanistic understanding on the system performance, experimental work will be conducted systematically to achieve optimized composition, reactor design, experimental protocols and other experimental conditions (temperature, pressure, reactants mixing etc.).

Realization of both Milestones 1 and 2 sets its strong basis on our previously established theoretical (QM, MD, ReaxFF modeling; data base for molecular and other properties of ionic liquids, possible reaction pathway investigation of methane activation, oxidation and functionalization) and experimental (specially designed reactor and reaction protocol for testing various factors of catalytic methane conversion, characterization and analytic tools for quantitative and quantitative evaluations) approaches. Successful completion of the first two milestones will present us one or several optimized methane catalytic systems with high potentials for commercially viable applications.

Milestone 3 (Year 3): Scaling-up test and preliminary economic analysis

Subtask 3.1 Bench-scale reactor design and build-up

Subtask 3.2 Bench-scale testing

Subtask 3.3 Preliminary Economic Analysis

After discovering/identifying the best system and chemistry at the laboratory level, the next step will be bench-scale test to provide necessary data for justification of further pilot-scale test and economic feasibility analysis. This part serves as the critical transitional step between successful lab-chemistry to revolutionary technology which can be applied at an industrial scale and bring huge beneficial impacts to the nation's energy and economic security as well as the environment protection. This part of work will be conducted through closely collaboration with the industrial partners. In addition, our previous work have already identified some key factors for the bench-scale reactor design

including corrosion resistance, temperature and pressure control, system mixing, and in-situ reaction characterization and analysis.

We have established efficient laboratory-scale experimental apparatus and the accompanied analytical protocol for developing optimized methane partial oxidation systems. We have been able to conduct small scale experiments with 100% mass balance and excellent temperature. However, demonstration and further optimization of the selected systems requires a larger-scale reactor, which can load a relatively large amount of sample, optimize the performance of the selected systems and allow in situ experimental analysis.

Several key features needed for the bench scale reactor will include:

- (1) Relatively large sample capacity
- (2) Excellent corrosion resistance to conduct experiments under concentrate sulfuric acid, hydrochloric acid, or other strongly corrosive media
- (3) High pressure tolerance with in situ pressure monitor
- (4) Fast heating rate and precise temperature control
- (5) High speed reaction solution stirring to achieve good contact between the catalytic system and the methane gas
- (6) Capability of reaction equilibrium control for better product selectivity
- (7) In situ experimental analysis for better process control, system optimization and mechanistic investigation

Since it is known that Pt(II) is related to the C-H activation step and Pt(IV) is related to methane oxidation step, using in-situ UV-Vis could monitor oxidation states distribution the Pt(II)/Pt(IV) at deferent reaction stage which will provide very important message on catalyst and media system designing and controlling of reaction conditions. Also equally important is knowing of distribution of oxidation products and intermediates at all reaction stages (CH₃Cl, CH₃OH, HCOH, HCOOH, CO₂, etc.).

We propose to develop in-situ UV-vis spectroscopic method that could monitor the oxidation state changes of Pt (Pt^{II} ⇌ Pt^{IV}). The Pt^{IV} in ionic liquid should have absorption features at 360nm and 420nm¹¹, and we will use UV multimode fiber with special high temperature jacket to deliver Xe-lamp light sources to the reactor and collect the transmission also through multimode fiber. The reactor will be constructed with two Sapphire windows built in for the transmission measurement. The spectrometer detector and light source are located outside the oven. The schematic is given in Figure 9.1.

With the Sapphire windows built-in reactor, we will also be able to conduct Raman spectroscopy on certain product small molecules, e.g. CH₃OH, (CH₃)₂O, HCOOH and HCOH. We propose to use the 3rd harmonic of a pulsed Nd:YAG laser, i.e. 355nm, for the Raman excitation and also measuring the Pt concentration through its UV transmission measurement.

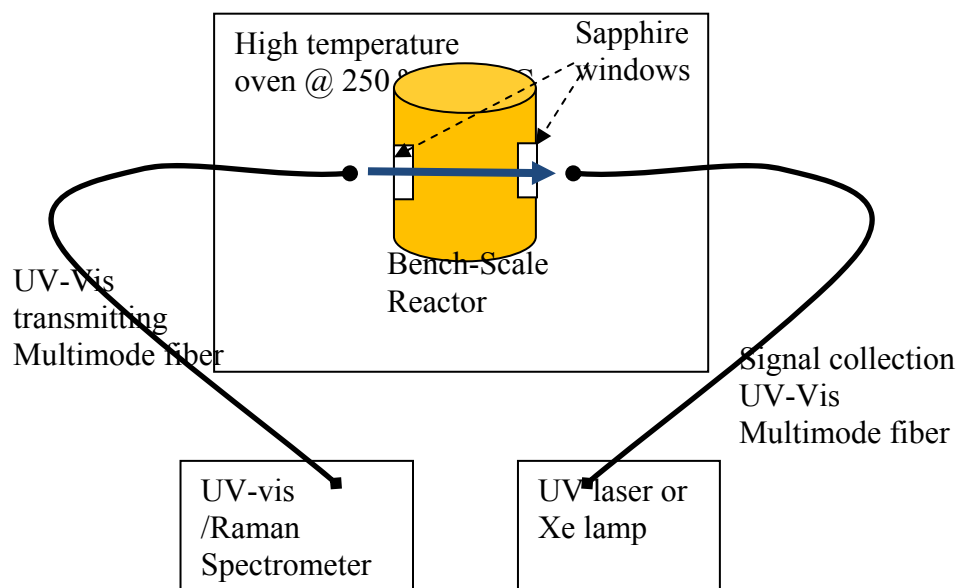


Figure 9.1: Schematic Diagram of *in situ* UV-vis spectroscopy to monitor the oxidation state change of Pt^{II} and Pt^{IV}

REFERENCES:

- ¹ R. A. Periana, D. J. Taube, S. Gamble, H. Taube, T. Satoh, and H. Fujii, "Platinum catalysts for the high-yield oxidation of methane to a methanol derivative," *Science*, **280**, 560-564, 1998
- ² (a) A. E. Shilov, and G. B. Shul'pin, *Activation and catalytic reactions of saturated hydrocarbons in the presence of metal complexes* (Kluwer Academic Publishers, Dordrecht, 2000); (b) R. J. Hodeges, D. E. Webster, and P. B. Wells, "The activation of Saturated hydrocarbons by transition-metal complexes in solution. Part I. Hydrogen-deuterium exchange in alkanes catalysed by potassium tetrachloroplatinate (II) in acetic acid," *J. Chem. Soc. (A)*, 3230-3238, 1971; (c) M. Muehlhofer, T. Strassner, and W. A. Herrmann, "New catalyst systems for the catalytic conversion of methane into methanol," *Angew. Chem. int. Ed.*, **41**, 1745-1747, 2002; (d) V. R. Ziatdinov, J. Oxgaard, O. A. Mironov, K. J. H. Young, W. A. Goddard III, and R. A. Periana, "Carboxylic solvents and O-donor effects on CH activation by Pt(II)," *J. Am. Chem. Soc.*, **128**, 7404-7405, 2006.
- ³ T. Gregory, P. Harper, R. S. Shinomoto, M. A. Deming and T. C. Flood, "Activation of Methane by the Reactive Intermediate Tris (trimethylphosphine) Osmium(0)", *J. Am. Chem. Soc.* **110**, pp 7915-16 (1988)
- ⁴ Gol'dshleger, N.F., Tyabin, M.B., Shilov, A.E. and Shteinman, A.A, *Russion J. Phys Chem.* **1969**, 43, 1222
- ⁵ Rudkov, E.S. and Shteinman, A.A., *Kinet. Katal.* **1973**, 13, 1346 (in Russian)
- ⁶ Becke, A. D., *J. Chem. Phys.* **1993**, 98, 5648.
- ⁷ Lee, C.; Yang, W.; Parr, R. G., *Phys. Rev. B.* **1988**, 37, 785.
- ⁸ Hay, P. J.; Wadt, W. R., *J. Chem. Phys.* **1985**, 82, 299.
- ⁹ (a) Krishnan, R.; Binkley, J. S.; Seeger, R.; Pople, J. A., *J. Chem. Phys.* **1980**, 72, 650. (b) Clark, T.; Chandrasekhar, J.; Schleyer, P. v. R., *J. Comput. Chem.* **1983**, 4, 294.
- ¹⁰ Zhao, Y.; Truhlar, D. G. *Acc. Chem. Res.* **2008**, 41, 157.
- ¹¹ (a) Marten, B.; Kim, K.; Cortis, C.; Friesner, R. A.; Murphy, R.; Ringnalda, M.; Sitkoff, D.; Honig, B., *J. Phys. Chem.* **1996**, 100, 9098. (b) Tannor, D. J.; Marten, B.; Murphy, R.; Friesner, R. A.; Sitkoff, D.; Nicholls, A.; Ringnalda, M.; Goddard, W. A.; Honig, B., *J. Am. Chem. Soc.* **1994**, 116, 11775.
- ¹² 6.0, J. Schrodinger, LLC: Portland, Oregon, 2005.
- ¹³ Tissandier, M. D.; Cowen, K. A.; Feng, W. Y.; Gundlach, E.; Cohen, M. H.; Earheart, A. D.; Coe, J. V.; Tuttle, T. R., *J. Phys. Chem. A* **1998**, 102, 7787.

¹⁴ Ross, R. B.; Powers, J. M.; Atashroo, T.; Ermler, W. C.; LaJohn, L. A.; Christiansen, P. A. *J. Chem. Phys.* **1990**, 93(9) 6654.

¹⁵ I. H. Hristov, T. Ziegler, *Organometallics* 2001, 22, 1668-1674. We believe that the major part of the discrepancy is due to the fact that we include the energy of generating SO₃ from H₂SO₄ or H₂S₂O₇, which are the more stable forms of SO₃ in sulphuric acid.

¹⁶a) N. F. Gol'dshleger, V. V. Es'kova, A. E. Shilov, A. A. Shteinman *Russ. J. Phys. Chem.* 1972, 46, 785-786. b) L. A. Kushch, V. V. Lavrushko, Y. S. Misharin, A. P. Moravsky, A. E. Shilov, *Nouveau Journal de Chimie* 1983, 7, 729-733.

¹⁷ R. G. Pearson, M. L. Morris, *F Basolo Disc. Faraday, Soc.* 1960, 29, 80-91.